University of Alberta

Sea Ice Data Assimilation for the Canadian East Coast

by

Anna Katavouta

A thesis submitted to the Faculty of Graduate Studies and Research
in partial fulfillment of the requirements for the degree of

Master of Science

Earth and Atmospheric Sciences

Fall 2010
Edmonton, Alberta

Examining Committee

Paul G. Myers, Earth and Atmospheric Sciences

Gerhard W. Reuter, Earth and Atmospheric Sciences

Faye Hicks, Civil and Environmental Engineering

Abstract

The sea ice fields produced by the NEMO sea ice/ocean coupled model's prognostic simulation drift from reality in the Labrador sea. Thus four additional data assimilation experiments were conducted in order to obtain satisfactory sea ice fields. In the first two experiments the model's sea ice concentration was pushed towards Canadian Ice Service fields using nudging. In the third and fourth experiment as the sea ice concentration was nudged, the sea ice thickness and the underlying ocean salinity and temperature are corrected, based on correlations between the sea ice concentration and the model tracers.

It was found that the simple nudging experiments produced sea ice fields close to reality. The experiments where corrections are applied to the underlying ocean salinity and temperature, produced sea ice concentration fields closer to the reality than the nudging experiment, by achieving a balance between the sea ice and the ocean fields.

Acknowledgments

I would first like to express my gratitude to my supervisor, Professor Paul G. Myers, for all his support, endless help and patience during the last two years. Most of all I will like to thank him for believing in me and giving me the opportunity to work on this project. I would also like to thank Dr. Arjen D. Terwisscha van Scheltinga for all the interesting discussions, ideas and help in various aspects during the conduction of this project. Big thanks to all the people that I shared the lab with: Colin More, Emily Collier, Ji Lei, John Wang, Laura Castro, Praveen Kuzhiyil Veluthedathe, Tamara Janes, Veronique Lago and Xianmin Hu. They made my days more cheerful but also helped me in every possible way, especially Xianmin. If he had not provided me his help, I would still be struggling to create various Matlab scripts. I also want to thank my friend Brendan M. Crozier for his help with the English language and for all the time that he spent to help me correct my English writing. Finally, I would like to thank all my family in Greece; especially my mother, Kleopatra Sarantakou, for believing in me and for supporting me both economically and emotionally.

Table of Contents

List of Tables

List of Figures

List of Symbols and Abbreviations

Symbols	Meaning
1-D	One dimension
A	Sea ice concentration Fraction
a	Albedo
a(t)	Expansion coefficient
AAD	Absolute average deviation
A^{vm}	Vertical eddy coefficient for momentum
A^{vS}	Vertical eddy coefficient for salinity
A^{vT}	Vertical eddy coefficient for temperature
B	Background error covariance
B_l	Heat budget of open ocean water
C_D	Drag coefficient
C_p	Specific heat capacity on constant pressure
D^S	Parameterization of small scale physics for salinity
D^T	Parameterization of small scale physics for temperature
D^U	Parameterization of small scale physics for momentum
e_b	Ocean bottom turbulent kinetic energy
EOF	Empirical orthogonal function
EMP	Evaporation minus precipitation minus rivers runoff plus the rate of change of sea ice thickness budget
F	Forcing terms
F	Coriolis acceleration
F_{cb}	Conductive heat flux inside the sea ice
F_{cs}	Conductive heat flux from the ocean to the sea ice
F_h	Sensible heat flux
F_{le}	Latent heat flux

F_{lw}	Downwelling longwave radiation
F_{sw}	Downwelling shortwave radiation
g	Gravitation acceleration for earth
H	Observation operator
h_i	Sea ice thickness
h_o	Thickness of newly formed sea ice
I	Penetrating downwelling solar radiation
i_o	Fraction of net shortwave radiation that penetrates sea ice or snow
k	Thermal conductivity of sea ice or snow
K	Nudging coefficient
L_i	Volumetric latent heat of fusion of sea ice
m	Mass
p	Pressure
P	Ice strength
Q	Heat flux
A.E	Absolute error
S	Salinity
T	Temperature
U	Velocity
U_h	Horizontal component of velocity
W	Weight
Z	Altitude
ε	Emissivity
$\acute{\varepsilon}$	Strain rate tensor
ζ	Bulk viscosities
η	Shear viscosities
λ	Longitude
ρ	Density
ρ_o	Reference density

σ	Stefan Boltzman constant
σ_T	Stress tensor
τ	Shear stress
φ	Latitude
Ω	Earth's angular velocity

CHAPTER 1

Introduction

In recent years there is an increasing need for quantification, understanding and prediction of the sea ice in the Northern Hemisphere polar and sub-polar regions, for both scientific and economic reasons. Projects, like the operational products of the Canadian Ice Service, aim to provide accurate sea ice information that result in economical and safety benefits for the Canadian East coast, but there is always the need for more accurate short term predictions of the sea ice concentration and state. Sea ice-ocean coupled numerical models are very promising forecasting tools for predictions of sea ice conditions, since the sea ice conditions are heavily influenced by the ocean. The issue that arises is the existence of errors in all of the models due to imperfect model physics and the limits of the models' resolutions. These model errors, in addition to the imperfections and errors in the observations that are used to initiate the models, lead to the drifting of the models' sea ice fields from reality. This is why the use of different data assimilation techniques is essential, since in data assimilation all the available information (for example observations) can be merged into the model to provide more accurate estimations and predictions of the sea ice conditions. The scientific studies of Caya et al., 2010 and of Lisaeter et al., 2003 demonstrated that the use of sea ice data assimilation in sea ice-ocean coupled models, can lead to great improvements on the models' resulting sea ice fields. This study focuses on the use of two data

assimilation techniques that are relatively easy to implement, in order to achieve sea ice fields closer to reality, in the region of the Labrador and Newfoundland shelves. The first technique is a simple sea ice nudging, where the model's sea ice concentration fields are corrected based only on their drift from the Canadian Ice Service (CIS) sea ice concentration fields. The second nudging experiment aims to achieve a balance between the sea ice and the ocean fields, in order to achieve better results. Thus as the sea ice concentration is nudged towards the CIS sea ice concentration fields, corrections are applied to the ocean salinity and temperature. Furthermore, in order to achieve better sea ice thickness fields, corrections are applied to the sea ice thicknesses. These corrections are based on covariances between the sea ice concentration and the model tracers (ice thickness, ocean salinity and ocean temperature). To find the covariances between the sea ice concentration and the tracers, the approach of Robert and Alves, 2005 is used, where it is presented that physically meaningful covariances can be obtained by applying random perturbation to the forcing field. In our case, we used the Empirical Orthogonal Functions (EOF's) method to create random perturbations in the atmospheric fields that are used to force an ensemble of simulation of our sea ice/ocean coupled model. The model used in this study is the NEMO (Nucleus for European Modelling of the Ocean) sea ice/ocean coupled model.

In the first chapter, some basic information about sea ice and the behavior of sea ice on the Labrador and Newfoundland shelves is briefly presented, together with a brief history and explanation of some data assimilation techniques. The details of the NEMO sea ice/ocean coupled model are discussed in chapter 2. In chapter 3, the results of the model prognostic simulation are evaluated. In chapter 4, the details and the results of two nudging experiments are presented. In the first nudging experiment, the nudging occurs every time step and in the second nudging experiment, the nudging occurs every five days. In chapter 5, two 1-D data assimilation experiments are presented, where, as the sea ice concentration is nudged, the sea ice thickness, the ocean salinity and the ocean temperature are corrected. In the first 1-D data assimilation experiment, the assimilation occurs every time step and in the second 1-D data assimilation experiment, the

assimilation occurs every five days. The second nudging experiment and the second 1-D data assimilation experiment are more realistic choices in comparison to the first experiments, since they give the opportunity for the model to freely evolve for five days, after the correction of the sea ice and ocean initial conditions though the nudging and the covariances. So through the second experiments, we essentially obtain 5 days advance forecasting. The first experiments, where the assimilation occurs every time step, are useful only for hindcasts, since the needed data is not available for the future. Finally, in chapter 6, the conclusions of this study are presented.

1.1 Sea Ice

1.1.1 General

Sea ice is frozen ocean water, formed in the polar and subpolar regions of both hemispheres. Sea ice is different from ice that forms from freshwater, with regards to its properties and its formation. A significant difference between freshwater and sea water is that the freezing point of sea water is lower than the freezing point of fresh water (0^oC for pure freshwater) due to the presence of salt. The temperature at which sea water freezes depends strongly on its salinity, the more saline the water the lower the freezing temperature (P. Wadhams, Ice in the Ocean, 2000).

Scientific studies focus on sea ice because of its influence on both climate and living beings. The presence of sea ice, can affect humans through navigation in the polar and subpolar seas and activities like hunting of seals or fishing. Also wildlife is affected by sea ice changes since some animals, like polar bears, live in Polar Regions and their survival depends on the presence of sea ice. Sea ice can affect global climatic conditions through its interaction with the atmosphere and the ocean. In order to understand how sea ice interacts and affects the climate, first we have to understand the physics of sea ice.

1.1.2 Processes

During autumn and winter, where the temperature of the air is lower than the temperature of the ocean surface, heat transfer from the ocean to the atmosphere occurs (sensible heat transfer). Thus the temperature of the ocean's surface water decreases due heat loss. Since the surface sea water becomes colder, its density increases and the denser water starts to sink being replaced by warmer underlying water, which will then cool and repeat the cycle. For typical ocean salinities there is no threshold temperature where further cooling will cause the sea water to become less dense, like in the case of freshwater (for example in lakes at $4^{o}C$). The above might lead us to believe that the whole ocean water column would have to reach the freezing point for the initiation of ice formation. In reality, since the sea surface layer is separated from the underlying water by the pycnocline (a region with a big density gradient), only the surface layer water needs to reach the freezing temperature to initiate the formation of ice. Once the sea ice forms, it acts as an insulator between the ocean and the atmosphere, reducing the rate of the heat transfer and slowing the ice growth as the thickness of the ice increases. Another factor that can increase the insulating effect of the ice is the accumulation of snow above it, which causes even more delay in the growth of sea ice (Wadhams, 2000).

During summer and spring, when the solar radiation reaching the surface of the earth increases, the melting of the ice is initiated. Even if sea ice has a much higher albedo and thus absorbs less and reflects more solar radiation than the open water, the energy provided to the sea ice is enough to initiate melting. The first sign of melting is small puddles of water on the surface of the sea ice. These puddles of water, by having lower albedo than sea ice, will absorb even more solar energy and further increase the melting of the underlying sea ice. In fact, the contact of the water in the puddles with the warm summer air will accelerate the melting of the surrounding sea ice even more due to the heat transfer from the air to the water inside the puddles. Finally the melting rate can also be increased by the drift of sea ice towards warmer waters (Canadian Ice Service).

If the sea ice is not attached to the land (coast), the sea ice will not always stay in its place of formation, instead it will drift. Two main factors can initiate and affect the motion of sea ice, the wind and the ocean currents. The wind causes the motion of sea ice through frictional drag, acting on the ice surface. The stronger the wind, the faster sea ice moves and typically, if no other forces act on the sea ice, an open pack of ice will move with a speed of approximate 2% the wind speed (Canadian Ice Service). Since we are dealing with friction, one can understand that ice packs with rougher surfaces move faster. In the existence of an ocean current we have sea water in motion and as the sea water moves, it carries the sea ice along. The higher the velocity of a current, the faster sea ice moves. Since the velocity of currents decrease with depth, the greater the depth of a sea ice pack, the slower its motion. Other, not so profound, factors can affect the sea ice motion, like the Coriolis force and the sea surface height slopes as the sea ice packs will move from the high sea surface level towards the low sea surface level (Wadhams, 2000).

1.1.3 Formation

When the top layer of the ocean reaches the freezing point, small needle-like crystals start forming. These crystal forms are called frazil ice and they consist of nearly fresh water since during their formation salt is rejected into the ocean. In calm ocean conditions, the needle-like ice crystals combine by freezing together creating a thin crust of ice called Nilas. Nilas surface is matte and its thickness does not exceed 10cm. Next Nilas grows thicker at the bottom through a process called congelation growth. On the other hand, in a rough ocean frazil ice is accumulated, with the help of winds and the ocean waves, into circular forms of ice called “pancake ice” (Wadhams, 2000). With time, these “pancakes” bond together into a more solid form. In both cases (calm and rough ocean), the sea ice continues to grow and becomes thicker during the winter, with the sea ice product of one winter being called as “first year ice”. During summer, sea ice starts melting; the ice formed during the past winter, that does not melt totally, and

instead survives until the next winter, is called “old year ice”. If the sea ice survives for more years then it called “multiyear ice” (Canadian Ice Service).

1.1.4 Salinity-Brine

During the formation of sea ice, as the water freezes, it expels salt into the underlying ocean; as a result the surrounding water salinity increases. In contrast, when sea ice melts (temperature of sea ice is raised above freezing point), fresh water is provided to the surrounding ocean, make it less saline. Not all the salt from the formation of sea ice is provided immediately to the ocean. As the ice crystals are forming, the salt that is expelled is accumulated into small drops called brine. When the ice crystals combine, brine is trapped into cracks between the crystals. Since brine is more saline, it requires a lower temperature to freeze thus it remains in liquid form in these cracks until it drains out and air replaces it (Wadhams, 2000).

1.1.5 Global Climate

Sea ice affects global climate as much as it is affected by it. Sea ice and the atmosphere are closely connected and influence each other. Sea ice has a high albedo and thus it helps keep the polar regions, like the Arctic, cold by reflecting more sun light back into space. If climate change induces sea ice melting through warming, the albedo of the polar region will become lower and thus more heat will be absorbed by the planet. This will lead to further melting of the sea ice, which amplifies the warming. This climate feedback mechanism is known as snow/ice albedo feedback and it can eventually alter atmospheric circulation (Wadhams, 2000). Furthermore, in the polar regions, sea ice works as an insulator between the atmosphere and the ocean, preventing the heat from the warmer ocean from escaping towards the cooler atmosphere. If climate changes cause the sea ice to become very thin or melt, heat exchange between the ocean and the atmosphere becomes possible and thus the atmosphere can absorb heat from the ocean. The absorption of heat will result in a rising of the temperature of the atmosphere. This will result in further melting of the ice.

The ocean is also affected by sea ice through fresh water or brine release, associated with melting and freezing processes. Sea ice drifts from the Arctic into the North Atlantic, by melting it releases freshwater to the surface layer. The excessive melting of ice in high latitudes will result in the release of excessive amounts of freshwater, which, as it is less dense than saline water, does not sink but instead stays at the top of the ocean. This can lead to the suppression of convection and thus the suppression of deep water formation. Hence the large scale ocean circulation, driven by global density gradients created by surface heat and freshwater fluxes (thermohaline circulation), which contribute to a proper temperature balance around the earth, may be impacted (Aagaard, 1989).

1.2 Canadian East Coast (below 60^{o}N)

1.2.1 Labrador and Newfoundland Shelves

The Labrador and Newfoundland shelves are located on the west border of the Atlantic Ocean, from approximate 60^{o} North to 45^{o} North latitude (Figure 1.1). These shelves are generally very shallow in contrast to the very deep interior of the Labrador Sea. Sea ice is a major feature along the Labrador and Newfoundland shelves and greatly affects the climatic conditions and the marine life of the region. Although results from Myers, 2005 shows that there is a limited exchange of freshwater between the Labrador shelf and the interior of the Labrador Sea, the melting of sea ice in the region could still have a small influence on the deep water formation, in the interior of Labrador sea by providing a additional fresh water to the surface layer of the central Labrador Sea

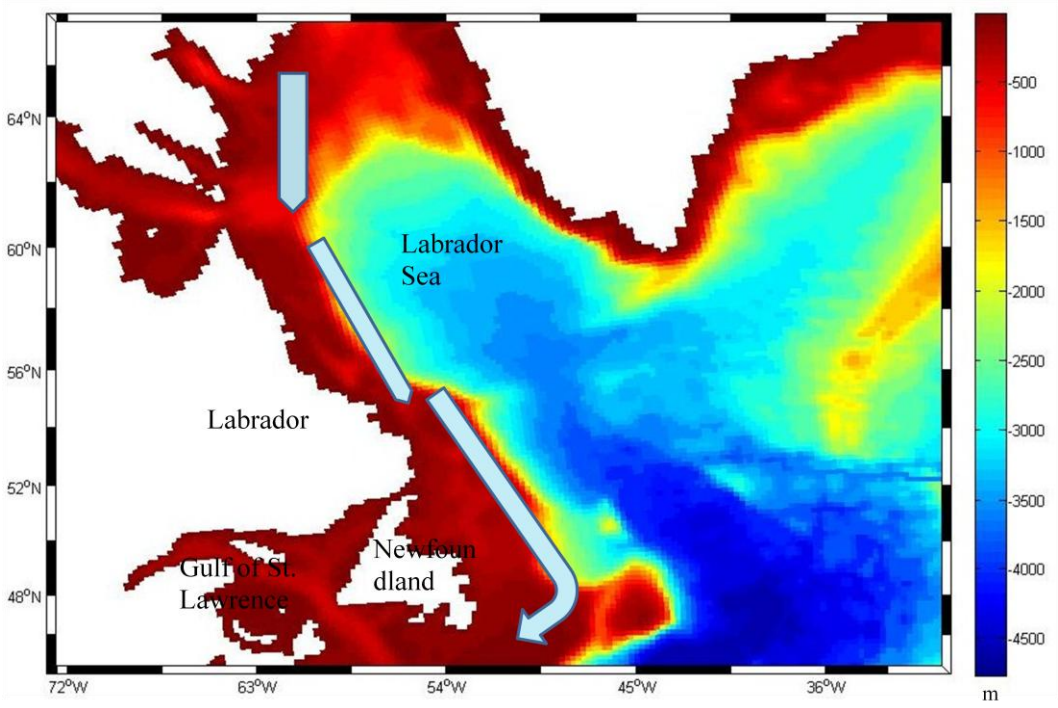

Figure 1.1: The Labrador and Newfoundland shelves. The shelf branch of the Labrador Current is represented by light blue arrows.

1.1.2 Sea Ice in the Region

Along the Labrador and the Newfoundland shelves, the Labrador Current (Figure 1.1) flows with a maximum surface speed of around 0.5 m/s and has a width of 50km (Ikeda, 1989). The Labrador Current water originates, mainly, from the Arctic. The Arctic water is fresh and cold due to the large inflow of freshwater from large river systems and thus the Labrador Current water is also fresh and cold. This cold and fresh water is separated by a strong shelf break front (the front where the relative shallow shelves end and the basin becomes deep) from the warmer and more saline waters offshore; thus ice only exists along the coast and it is rarely found in the interior of the Labrador Sea. Some sea ice drifts, from the Arctic, through Davis Strait, along the Labrador shelf with the help of the Labrador Current, and some sea ice is formed locally on the Labrador shelf due to the cold and dry winds that blow above the region. The ice drifts further south with the help of the Labrador Current and the strong northwesterly winds blowing

along the coast. In an average year, sea ice appears in December, drifts southward towards the Newfoundland shelf and reaches its maximum extent by March. Melting usually begins in April and the sea ice disappears completely by the end of June (Canadian Ice Service). This seasonal cycle can be shown in Figure 1.2

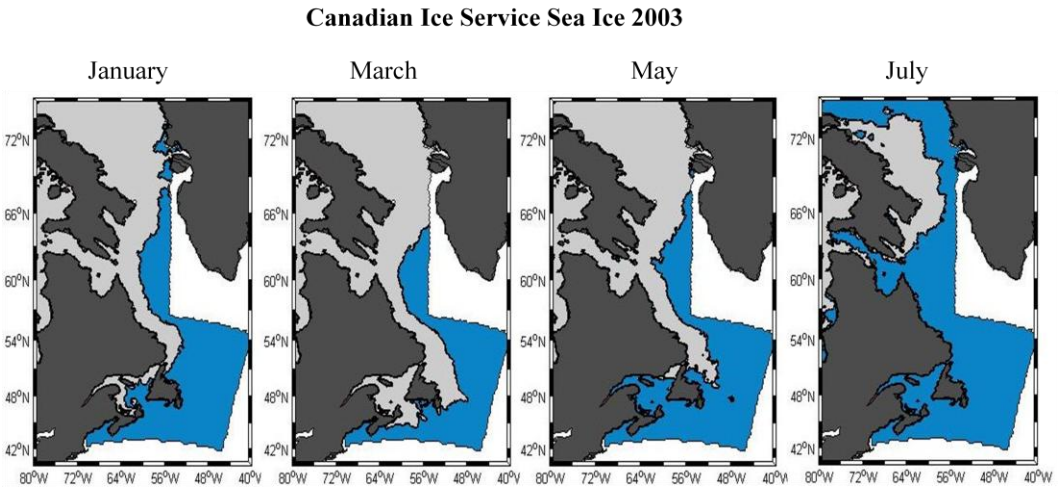

Figure 1.2: Sea ice edges produced from the Canadian Ice Service data for January, March, May and July of 2003.The white colour indicates that there is no available data for these regions.

1.1.3 Reasons for Studying this Region

As we already stated, sea ice is a significant component of the climatic system of the area. Knowledge about sea ice, in the Labrador and Newfoundland region, is vital for navigation since ice can be hazardous to ship activity as well as to offshore resource exploitation structures, and therefore it is essential to know where and how thick the sea ice is. For an economy partially based on fishing, as the one of the Labrador and Newfoundland regions, we can understand how important the knowledge about the conditions of sea ice are, since they affect the phytoplankton and zooplankton distribution and thus the fish distribution. Another reason that makes this region so interesting is the fact that sea ice disappears completely in the summer. Thus different issues and procedures must be taken into account when we study it in comparison to places where ice never melts (like Arctic) and where most of previous studies focus.

1.3 Data Assimilation

1.3.1 Forecasting

Forecasting is usually used in the geophysical sciences to predict the state of a system (e.g. atmosphere and ocean) at some time in the future. Generally two methods are used for forecasting, the empirical approach and the dynamic approach. The empirical approach is based on the analysis of historical data and the occurrence of similar situations. The dynamic approach is based upon equations that predict the evolution of a system. In practice, the dynamic approach is based on computer modeling and called numerical prediction. The forecast is computed with the help of mathematical equations describing the physics and the dynamics of a system. Ocean and sea ice models have been used generally to simulate and predict the properties of ocean and sea ice, respectively. Since sea ice and ocean properties are closely linked and can influence each other, ocean and ice models can be combined together (coupled ocean/sea ice models) in order to achieve better forecasting of both the sea ice and the ocean. Thus ocean/sea ice coupled models have been developed and used in areas where the presence of the ice is noticeable, like the east coast of Canada (Ikeda, 1989).

1.3.2 Application

To run and produce a forecast, models must start from an initial state based on observations. To reduce uncertainties in the model it is essential to have an initial model state as close as possible to reality. The discontinuities that can occur in the observations, the lack of data and the errors that exist even in the most modern observation tools, are responsible for the drift of the model simulations from reality. This is where data assimilation comes into play, making the first appearance in meteorology about 50 years ago, where all the available observations, for a time period, are merged into the model and, through reanalysis, better initial conditions are prepared. As in meteorology, data assimilation is applied in oceanography for the same purpose. Moreover, data assimilation can be used for the improvement of boundary conditions and, to

some extent, to compensate for imperfect model physics or inadequate model resolution in order to provide estimates in agreement with nature (Lisaeter, 2003).

Data assimilation progresses in analysis cycles. In every cycle the observations of a current state of a system are combined with the forecast of this system, in order to balance the uncertainties in the forecast and the errors of the observations, and produce a more accurate reanalysis. Then the model progresses in time and its results become the forecast for the next cycle and the procedure repeats.

1.3.3 History

The use of data assimilation began first in meteorology due to the availability of measurements for atmospheric properties. In oceanography due to the scarcity of observations for ocean properties, data assimilation became vital later, with the development of satellites and projects that provide high density and more accurate observations.

The first step towards data assimilation was the objective analysis introduced by Panofsky (1949) and modified further by Cressman (1954, evolution of his technique in 1959). In the Cressman analysis the corrections of the initial forecasting of every gridpoint (background field), are based on a weighted combination of the differences between the observed values and the predicted values, within a radius of influence. The weight of each difference depends only on the distance between the background gridpoint and the position of the observation. This method was evolutionary in comparison to the previous methods of analysis (subjective analysis) where the forecast corrections were based on individual opinions. The mathematic formulation of a simple Cressman analysis is:

$$\boldsymbol{x}_a(j) = \boldsymbol{x}_b(j) + \frac{\sum_i^n w(i,j) * [\boldsymbol{y}(i) - \boldsymbol{x}_b(i)]}{\sum_i^n w(i,j)} \quad eq\ 1.3.1$$

$$w(i,j) = \begin{cases} \frac{R^2 - d_{i,j}^2}{R^2 + d_{i,j}^2} & for\ R \geq d_{i,j} \\ 0 & for\ R < d_{i,j} \end{cases} \quad eq\ 1.3.2$$

Where in $x_a(j)$ denotes the analyzed model state at grid point j, $x_b(j)$ denotes the background model state at grid point j, y(i) denotes the observation vector at the point i where the observation took place, $x_b(i)$ is the background state interpolated to point i, w(i,j) denotes the weight function, R is a constant which represent the influence radius and $d_{i,j}$ represents the distance between the grid point j and the observation point i.

The big breakthrough in data assimilation came from Gandin (1963) and the introduction of a statistical approach, referred to as optimal (or statistical) interpolation. The weights used in optimal interpolation are related correctly to the observation errors and they are also related with the background errors. Thus in this method the background fields are used as source of information and not only as an initial state. The analysis equation has the below form:

$$\boldsymbol{x}_a = \boldsymbol{x}_b + \boldsymbol{W}[\boldsymbol{y} - H(\boldsymbol{x}_b)] \quad eq\ 1.3.3$$

Where x_a and x_b denote the analyzed and background model state correspondingly, y represents the observations, H is the observation operator which maps from the analysis space to the observation space and **W** is the optimal weighted matrix (is explained in eq 1.3.4) .This equation says that the analysis is obtained by adding a correction term to the background field. This equation can be regarded as a list of scalar analysis equations, one per model variable.

$$\boldsymbol{W} = \boldsymbol{B}\boldsymbol{H}^T(\boldsymbol{H}\boldsymbol{B}\boldsymbol{H}^T + \boldsymbol{R})^{-1} \quad eq\ 1.3.4$$

Where **B** denotes the background errors covariances (the background errors denote the difference between the background field, just before the analysis, from the true state), **R** the observation errors covariances (the observation errors denote errors in the observations, representativeness errors and errors in the design of the

operator H), **H** and $\mathbf{H}^{T}$ represent the linearalized observation operator and its transpose. (More information about covariances in Appendix B).

In recent years (after 1990) variational analysis methods have become more popular. The basic idea behind these methods is the use of observation to correct the least accurate points of the model without allowing the modification of the most accurate points. These methods have the advantage of higher accuracy but they have a higher computational cost, in comparison with the optimal analysis methods. The variational methods work by looking for the analysis field ($x_{a)}$ that minimizes a cost function. The mathematical form of this cost function is:

$$J(x) = (\boldsymbol{x} - \boldsymbol{x}_b)^T \boldsymbol{B}^{-1}(\boldsymbol{x} - \boldsymbol{x}_b) + [\boldsymbol{y} - H(\boldsymbol{x})]^T \boldsymbol{R}^{-1}[\boldsymbol{y} - H(\boldsymbol{x})] \quad eq\ 1.3.5$$

$$\boldsymbol{x}_a = Arg\min(J) \quad eq\ 1.3.6$$

Where J(x) called cost function of the variational analysis and x denotes the model state and vector.

CHAPTER 2

Model Details

Sea ice interaction with the ocean can influence both the ocean and the sea ice properties. Thus a coupled model with two components, one for the sea ice and one for the ocean, can be beneficial for hindcasting and forecasting both the sea ice and the ocean. In our study we used the NEMO (Nucleus for European Modelling of the Ocean) version 2.3 sea ice/ocean coupled model with OPA (Ocean General Circulation model, version 9) as the oceanic component and LIM version 2 (Louvain-la-Neuve sea Ice Model, version 2) as the sea ice component. In this chapter the details of the OPA model are based on the OPA 8.1 Reference manual, Madec et al., 1998, and the details for the LIM model are based on the study of Fichefet and Morales Maqueda, "Sensitivity of a global sea ice model to the treatment of the ice thermodynamics and dynamics", 1997.

2.1 OPA model

2.1.1 Primitive Equations

The ocean can be described through equations used in fluid dynamic. In order to be able to solve these equations the following assumptions have to be made (OPA 8.1 Reference manual, NEMO ocean engine):

1. Spherical Earth approximation: The geopotential surfaces are assumed to be spheres so that the gravity (local vertical) is assumed to be parallel to the earth radius.
2. Thin shell approximation: The ocean depth can be assumed small enough in comparison with the earth's radius, that can be neglected. This means that throughout the depth of the ocean (from the bottom to the surface) g (earth's gravitational acceleration) is treated as constant.
3. Turbulence closure hypothesis: The unresolved processes by the model's resolution, (turbulent fluxes, small scale processes) are represented entirely in terms of large scale patterns through parameterization resolved by the model's resolution.
4. Boussinesq approximation: The Ocean's density variations are small enough to be neglected except in the buoyancy term. Therefore the term δρ (density difference) is neglected in the Navier-Stokes equation (eq. 2.1.1) and in the continuity equation (eq. 2.1.3) leading to the incompressible form of the equation $\nabla \boldsymbol{U}=0$, where $\boldsymbol{U}$ indicates the velocity of the fluid flow.
5. Incompressibility hypothesis: The divergence of velocity of the fluid flow is zero. A good assumption for the Ocean, where the velocity of water is smaller than 1500 m/s (speed of sound in water).
6. Hydrostatic Hypothesis: The vertical momentum equation is reduced to an equation where the buoyancy force is balanced by the vertical pressure gradient. This assumption is not valid for small scale (smaller than the ocean depth) processes. Since the ocean width is much greater than its depth the assumptions is generally valid for large-scale circulation.

Using the above assumptions we obtain the following six equations correspondingly: the momentum balance (eq. 2.1.1), hydrostatic equilibrium (eq. 2.1.2), the incompressibility equation (eq. 2.1.3), heat conservation (eq.2.1.4), salt conservation (eq. 2.1.5) and an equation of state (2.1.6). The equations are represented in a coordinate system with an orthogonal set of unit vectors ($\boldsymbol{i},\boldsymbol{j},\boldsymbol{k}$),

where $\boldsymbol{k}$ is the local upward vector and $\boldsymbol{i}$,$\boldsymbol{j}$ are horizontal with $\boldsymbol{i}$ directed to the North and $\boldsymbol{j}$ directed to the East:

$$\frac{\partial \boldsymbol{U}_h}{\partial t} = -[(\nabla \times \boldsymbol{U}) \times \boldsymbol{U} + \frac{1}{2}\nabla(\boldsymbol{U^2})]_h - f\boldsymbol{k} \times \boldsymbol{U}_h - \frac{1}{\rho_o}\nabla_h p + \boldsymbol{D^U} + \boldsymbol{F^U} \quad eq\ 2.1.1$$

$$\frac{\partial p}{\partial z} = -\rho g \qquad eq\ 2.1.2$$

$$\nabla \boldsymbol{U} = 0 \qquad eq\ 2.1.3$$

$$\frac{\partial T}{\partial t} = -\nabla(T\boldsymbol{U}) + D^T + F^T \quad eq\ 2.1.4$$

$$\frac{\partial S}{\partial t} = -\nabla(S\boldsymbol{U}) + D^S + F^S \quad eq\ 2.1.5$$

$$\rho = \rho(T, S, p) \qquad eq\ 2.1.6$$

Where $\boldsymbol{U}$ is the velocity composed of a horizontal vector component ($\boldsymbol{U}_h$) and a vertical vector component ($w\boldsymbol{k}$), T is the temperature of the ocean, S the salinity of the ocean, ρ the density and ρ_o a reference density of the ocean, g the gravitation acceleration, p the pressure and $f=2\boldsymbol{\Omega k}$ the Coriolis acceleration ($\boldsymbol{\Omega}$ is the Earth's angular velocity vector). Where $\boldsymbol{F}^U$, F^T, F^S are forcing terms and $\boldsymbol{D}^U$, D^T and D^S are the parameterizations of small scale physics for momentum, temperature and salinity correspondingly.

In many ocean circulation applications there is the need for specifically increasing model resolution in regions where the dynamics are enhanced (i.e. ocean fronts, boundary currents, surface layer). Also it is convenient to use a lateral boundary-following coordinate system for better representation of coastal dynamics. For the above reasons, and to solve the problem associated with the presence of a singular point at the North Pole that arises from the use of the common geographical coordinate system, a curvilinear geopotential coordinate system is used (three dimensional orthogonal grids on a sphere). All of the equations used by the model are transformed to the above coordinate system and then numerically solved using

finite difference schemes (further details in appendix C). The ocean model uses a C grid arrangement (further details in appendix C).

2.1.2 Subgrid Physics

The small scale motions (turbulence) cannot be captured by the large model resolution; thus the turbulence motions are not solved explicit but always parameterized (subgrid scale physics $\boldsymbol{D^U}$, D^T and D^S). Due to the strong anisotropy between the vertical and the lateral motion, the subgrid scale physics are divided into lateral and vertical parts. The vertical turbulent fluxes are assumed to depend on the gradients of large scale quantities and thus the resulting vertical momentum and tracer diffusive operators are given as:

$$\boldsymbol{D^{vU}} = \frac{\partial}{\partial z}\left(A^{vm}\frac{\partial \boldsymbol{U}_h}{\partial z}\right) \quad eq\ 2.1.7$$

$$D^{vT} = \frac{\partial}{\partial z}\left(A^{vT}\frac{\partial T}{\partial z}\right) \quad eq\ 2.1.8$$

$$D^{vS} = \frac{\partial}{\partial z}\left(A^{vS}\frac{\partial S}{\partial z}\right) \quad eq\ 2.1.9$$

Where A^{vm}, A^{vT} and A^{vS} denote the vertical eddy coefficients for momentum, temperature and salinity, representatively; which are computed from a 1.5 turbulent closure model based on a prognostic equation for the turbulent kinetic energy and a closure assumption for the turbulent length scale. (More information about the turbulent kinetic closure scheme can be found in the OPA 8.1 Reference manual, NEMO ocean engine).

The lateral tracer mixing is dependent on the large scale gradients of the tracers along isopycnals (surfaces of constant density), in addition an eddy induced advective term that follows a spatially varying GM parameterization, is added (Gent and McWilliam, 1990, Visbeck et al., 1997). More elaborate details on the sub-grid physics and its equations can be found in the OPA 8.1 Reference manual, NEMO ocean engine.

2.1.3 Ocean Boundaries

The ocean exchanges fluxes with the atmosphere, solid earth and sea ice. These fluxes are exchanged at the interface (boundary) of the ocean with the rest of the earth system components and presented briefly as (OPA 8.1 Reference manual, NEMO ocean engine):

- Coast/land-ocean interface: The major exchange of flux that can be taken into account is the freshwater provision to the ocean, though river discharges. This freshwater supply can locally alter the surface salinity of the ocean and it is usually specified as a freshwater flux at the air-sea interface in the vicinity of the river mouths.
- Solid earth-ocean interface: The model neglects heat and salt exchange between the ocean and its bottom. Since there is no flow in or out of solid boundaries, the ocean's velocity at the bottom is parallel to the solid boundaries. On the other hand, the ocean exchanges momentum with the solid boundaries through friction and since this is a small scale process it needs to be parameterized in terms of turbulent fluxes through bottom or lateral boundary conditions. In our case the non-linear (quadratic) bottom friction option available in OPA model was used, which in the curvilinear geopotential coordinate system has the form:

$$\boldsymbol{F}_{bottom} = \frac{A^{vm}}{e_3}\frac{\partial \boldsymbol{U}_h}{\partial k} = C_D\sqrt{u_b^2 + v_b^2 + e_b}\,\boldsymbol{U}_h^b \qquad eq\ 2.1.10$$

  Where $\boldsymbol{U}_h{}^b=(u_b,v_b)$ denotes the horizontal velocity of the bottom ocean layer, C_D denotes a drag coefficient, A^{vm} the vertical eddy coefficient for momentum and e_b denotes a bottom turbulent kinetic energy due to tides and other short time scale currents.
- Atmosphere-ocean interface: Heat, momentum (wind stress) and freshwater (Precipitation-Evaporation) is exchanged between the atmosphere and the ocean. The surface boundary condition on momentum is given by the stress exerted by the winds in the curvilinear geopotential coordinate system as:

$$\left|\frac{A^{vm}}{e_3}\frac{\partial \boldsymbol{U}_h}{\partial k}\right|_{z=0} = \frac{(\tau_u, \tau_v)}{\rho_o} \qquad eq\ 2.1.11$$

Where (τ_u, τ_v) are the two components of the wind stress vector.

The surface boundary condition for heat and freshwater fluxes is given in the curvilinear geopotential coordinate system as:

$$\left|\frac{A^{vT}}{e_3}\frac{\partial T}{\partial k}\right|_{z=0} = \frac{Q}{\rho_o C_P} \qquad eq\ 2.1.12$$

$$\left|\frac{A^{vS}}{e_3}\frac{\partial S}{\partial k}\right|_{z=0} = EMP|S|_{z=0} \quad eq\ 2.1.13$$

Where *EMP* is the evaporation minus precipitation, minus the river runoff, plus the rate of change of the sea ice thickness budget, Q is the non-penetrative part of the net surface heat flux and C*p* is the specific heat capacity at constant pressure.

The penetration of solar radiation into the ocean, introduces a new term in the equation 2.1.4 (time evolution of temperature):

$$\frac{\partial T}{\partial t} = \cdots + \frac{1}{\rho_o C_P e_3}\frac{\partial I}{\partial k} \qquad eq\ 2.1.14$$

Where *I* denotes the downward penetrating solar radiation.

- Sea ice-ocean interface: Ocean and sea ice exchange freshwater, momentum, heat and salt. We discuss these exchanges further in section 2.3.

2.2 LIM model

LIM (version 2) is a simple 3-layer (one for snow, two for ice) model which includes thermodynamic and dynamic processes. Ice is assumed to behave as a two dimensional viscous plastic (VP) continuum. The model was developed by Fichefet and Morales Maqeuda in 1997, and thus the description of the LIM model, in this study, is based on their study.

2.2.1 Thermodynamics

First let us focus on the vertical growth and decay of the sea ice due to thermodynamic processes. The sea ice is assumed to be a horizontal homogenous slab within the ice-covered part of each grid cell, extending in two layers of equal thickness. Above the sea ice, in a third layer, snow may accumulate if the temperature is below the freezing point. The temperature of sea ice and snow are controlled by the following one dimensional heat diffusion equation:

$$\rho_i c_p \frac{\partial T_i}{\partial t} = G(h_e) k \frac{\partial^2 T_i}{\partial z^2} \quad eq\ 2.2.1$$

Where T_i is the temperature, ρ_i represents the density, c_p denotes the specific heat and k represents the thermal conductivity of sea ice or snow. $G(h_e)$ is a correction function that takes into account the varying thickness contribution of ice and snow to heat conduction and depends on the conductivity of ice and snow. Consult Fichefet and Morales Maqeuda, 1997 for further details.

At the surface of the snow ice system a balance of fluxes is supposed to exist so that the energy changes are equal to zero:

$$(1 - i_o)(1 - a_{su})F_{sw} + \varepsilon_{su}F_{lw} - \varepsilon_{su}\sigma T_{su}^4 + F_h + F_{le} + F_{cs} = 0 \qquad eq\ 2.2.2$$

Where F_{sw} denotes the incoming (downwelling) shortwave radiation, a_{su} denotes the albedo of the surface layer, i_o is the fraction of the net shortwave radiation that penetrates sea ice/snow, F_{lw} is the incoming (downwelling) longwave radiation, σ is the Stefan-Boltzman constant, ε_{su} is the emissivity of the surface layer, F_h denotes the sensible heat flux, F_{le} denotes the latent heat flux and F_{cs} is the conductive heat flux coming from below the surface. The calculations for latent heat and sensible heat are computed following the standard bulk formulation ($F_{le}=\rho_a c_p C_D V_{srf}(q_{10}-q_{srf})$ and $F_{cs}=\rho_a c_p C_D V_{srf}(T_{10}-T_{srf})$ where ρ_a is the air density, C_D a drag coefficient V_{srf} the surface wind, q_{10} and q_{srf} the 10 meters and the surface specific humidity, T_{10}-T_{srf} the 10 meters and the surface temperature). The fluxes towards the surface are assumed positive while the fluxes outwards from

the surface are negative. If the surface temperature is above the melting point and sea ice/snow is still present, the temperature will be held at the melting point and the excess of energy will be balanced by being used for melting sea ice or snow.

If the snow weight is large enough to force the lower boundary of the snow layer to sink, sea water will penetrate the snow and freeze there. The result will be ice formed from mixed snow/sea water. This formation is taken into account by the model through the changes of snow and ice thickness associated with this snow ice formation.

The mechanism of "brine damping" is incorporated into the model based on the approach of Semtner (1976). In this approach the solar energy that is absorbed inside the ice is stored in a heat reservoir which represents internal meltwater. The energy from this reservoir keeps the top layer ice temperature from dropping below the freezing point; this procedure is equivalent to the release of heat through refreezing of the internal brine pockets. The heat reservoir is restricted to 50% of the energy needed to melt the whole ice sheet. When this limit is reached, further solar radiation absorbed inside the ice contributes to the ice melting.

Any imbalance between the conductive heat flux inside the ice (F_{cb}) and the heat flux from the ocean to the ice (F_w) is balanced by an increase or decrease of the ice thickness:

$$\left(\frac{\partial h_i}{\partial t}\right)_{ice} = \frac{F_{cb} - F_w}{L_i} \quad eq\ 2.2.3$$

Where L_i denotes the volumetric latent heat of fusion of sea ice.

The above discussion focused on the vertically growth and decay of sea ice, but sea ice can grow and decay laterally, as well. Let us thus examine how the LIM model handles the lateral decrease or increase of ice. We define A, the sea ice concentration, as the fraction of a grid cell area covered by sea ice. Changes to A depend on the heat budget of the open water area B_l. For negative B_l, the change (increase) in ice concentration is given by the following equation:

$$\left(\frac{\partial A}{\partial t}\right)_{increase} = \sqrt{1-A^2}\,\frac{(1-A)B_l}{L_i h_o} \quad eq\ 2.2.4$$

Where h_o represents the thickness of newly formed sea ice. The term $(1\text{-}A^2)^{1/2}$ distributes the energy between lateral and vertical growth so only a fraction ($(1\text{-}A^2)^{1/2}$) contributes to the increase in ice concentration. The remaining fraction leads to an increase of preexisting sea ice thickness.

It is assumed that a sea ice concentration decrease is caused by the vertical melting of thin ice. Assuming that the sea ice is uniformly distributed between 0 and $2h_i$ (where h_i denotes sea ice thickness) and that the melting rate does not depend on the local sea ice thickness, reduction of ice concentration caused by vertical melting is given by:

$$\left(\frac{\partial A}{\partial t}\right)_{decrease} = \frac{A}{2h_i}\left\{-\left(\frac{\partial h_i}{\partial t}\right)_{increase-decrease}\right\} for\ ice\ decreasing$$
$$> ice\ increasing\ else\ \left(\frac{\partial A}{\partial t}\right)_{decrease} = 0 \quad eq\ 2.2.5$$

2.2.2 Dynamics

The sea ice drifts with velocity $\boldsymbol{u}$ which is determined from the momentum balance equation. For the momentum balance equation, sea ice is considered to be a two dimensional continuum in dynamic interaction with the atmosphere and the ocean (the advection of momentum is neglected):

$$m\frac{\partial \boldsymbol{u}}{\partial t} = -mf\boldsymbol{k}\times\boldsymbol{u} + \boldsymbol{\tau}_{ai} + \boldsymbol{\tau}_{wi} - mg\boldsymbol{\nabla}n + \boldsymbol{F} \quad eq\ 2.2.6$$

Where m is the mass of the snow-sea ice per unit area and $\boldsymbol{u}$ is the velocity of sea ice per unit area. The first term represents the Coriolis force with f denoting the Coriolis parameter and $\boldsymbol{k}$ the upwards unit vector. $\boldsymbol{\tau}_{ai}$ and $\boldsymbol{\tau}_{wi}$ denotes the drag due to air and water respectively, in units of force per unit area (stress). The third term represents the gravitational force due to the horizontal gradient of the ocean surface dynamic height (n). $\boldsymbol{F}$ denotes the force per unit area due to variations in

internal ice stress and is computed based on the viscous-plastic constitutive law proposed by Hibler, 1979. $\boldsymbol{F}$ can be rewritten as:

$$\boldsymbol{F} = \nabla\sigma_T \qquad eq\ 2.2.7$$

Where σ_T is a two dimensional stress tensor (σ_{ij}). Sea ice is assumed to have a viscous-plastic constitutive law:

$$\sigma_T = 2\eta\dot{\varepsilon} + \left[(\zeta - \eta)T(\dot{\varepsilon}) - \frac{P}{2}\right]I \quad eq\ 2.2.8$$

Where η,ζ are shear and bulk viscosities, respectively, $\dot{\varepsilon}$ is the strain rate tensor, $T(\dot{\varepsilon})$ is the trace of $\dot{\varepsilon}$, P is the ice strength and I is the two dimensional unity tensor. For further details consult the study of Hibler, 1979 and the associate study of Zhang and Hibler, 1997.

Local changes, in the physical fields that are advected (sea ice concentration, snow and sea ice volume per unit area, sea ice and snow enthalpy per unit area, the latent heat inside the brine reservoir per unit area), are computed from a general conservation law:

$$\frac{\partial\Psi}{\partial t} = -\boldsymbol{\nabla}(\boldsymbol{u}\Psi) + D\nabla^2\Psi + S_\Psi \quad eq\ 2.2.9$$

Where Ψ denotes the advected physical field, S_Ψ denotes the rate of change of Ψ due to thermodynamics and D denotes a horizontal diffusivity and has constant value inside the ice pack and zero value at the ice edge. D is used for numerical reasons, to avoid non-linear instabilities arising from the coupling of ice dynamics and transport.

The equations of transport and motion of sea ice are transformed to the same curvilinear geopotential coordinates system used for the ocean model. The ice model equations are solved numerically, as in the ocean model, by using finite difference schemes (further details in appendix C). The sea ice model uses a B grid arrangement (further details in appendix C).

2.3 Sea ice/Ocean Coupled Model

2.3.1 Model Details

The sea ice ocean coupled model details are based on the studies of Timmerman et al., 2005 and Goose and Fichefet, 1999. Sea ice exchanges heat, salt, freshwater and momentum with the ocean and since it lays at the surface boundary of the ocean, it controls the solar radiation that penetrates the ocean. In our coupled model solar radiation penetrates the ocean surface following an exponential extinction profile. The momentum exchange is taken into account through the ocean/sea ice stress (τ_{wi}):

$$\tau_{wi} = \rho_o c_{wi} |\boldsymbol{u}_w - \boldsymbol{u}_i| (\boldsymbol{u}_w - \boldsymbol{u}_i) \quad eq\ 2.3.1$$

Where $\boldsymbol{u}_i$ and $\boldsymbol{u}_w$ are the ice velocity and the ocean surface velocity respectively, ρ_o is a reference seawater density and c_{wi} is a drag coefficient.

The sensible heat from the ocean to the ice (F_{wl}) is given by the following equation:

$$F_{wl} = \rho_o c_{pw} c_h u_* (T_w - T_{freez}) \quad eq\ 2.3.2$$

Here c_{pw} represents the specific heat of sea water, c_h is a coefficient, u_* is the friction velocity, T_w denotes the surface sea water temperature and T_{freez} denotes the seawater freezing point.

The mass exchange between the sea ice component and the ocean component of the coupled model is represented by a salt exchange (F_{salt}):

$$F_{salt} = S_w \left(\frac{\partial m_s}{\partial t}\right) + (S_w - S_i) \left(\frac{\partial m_i}{\partial t}\right) \quad eq\ 2.3.3$$

Where S_w and S_i are the seawater reference salinity and the sea ice salinity (assumed to be constant) respectively, m_s and m_i are the mass of snow and ice per unit area. The first term on the right represents the freshwater provided to the

ocean by the melting of the snow and the second term on the right represents the brine rejection or freshwater flux from ice freezing or melting, respectively.

2.3.2 Configuration and Forcing

The North Atlantic/ Nordic seas NATL4 regional configuration developed by the European DRAKKAR collaboration (The DRAKKAR group) is used to perform our simulations. The domain extends from 20^{o}S to 80^{o}N (Figure 2.1) and the South and North boundaries are closed buffers. The configuration has a horizontal resolution of ¼^{o} (27.75 km at the equator and 13.8 km at 60^{o}N) and 46 vertical levels, with the vertical grid spacing increasing from 6 meters at the surface to 250 meters at the bottom. The ocean model barotropic time step is 90s and the ocean model baroclinic time step is 2400s. The ocean model is coupled bidirectionally to the sea ice model every 6 time steps.

For the Atmospheric forcing fields we use the CORE (Common Ocean-ice Reference Experiments) forcing data set (Griffies et al., 2004). CORE provides monthly rain and snow, daily shortwave and longwave radiation and temperature, humidity, zonal and meridional wind velocities at 10 meters every 6 hours. For our simulations we use the years 2002-2005.

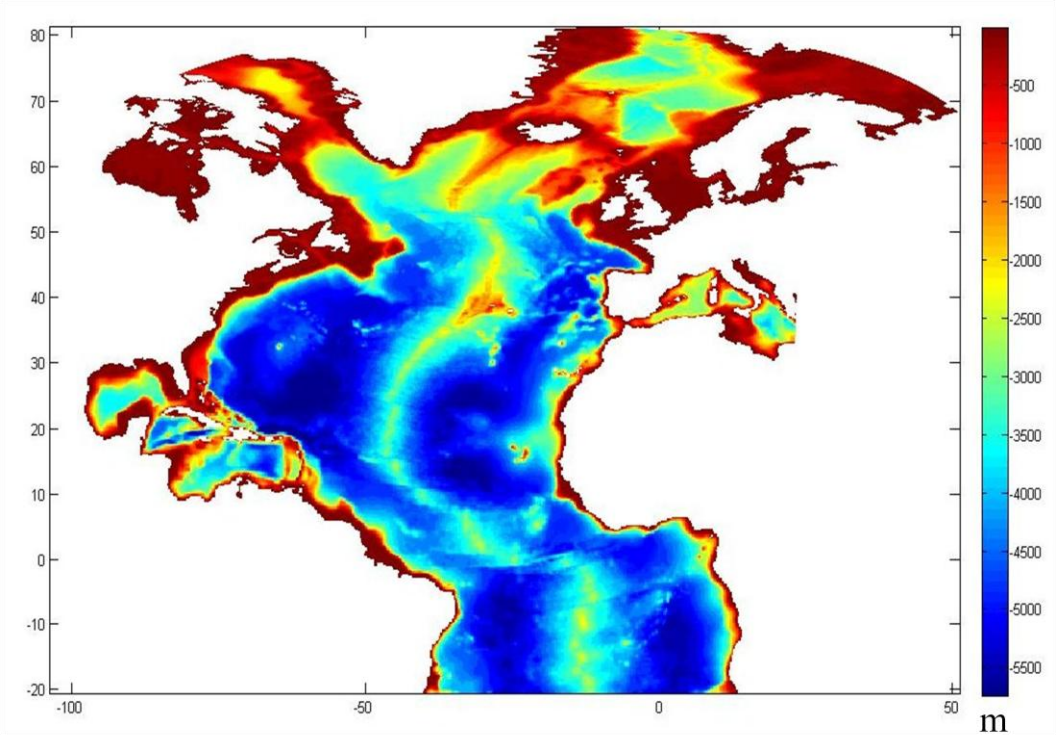

Figure 2.1: Bathymetry of the NATL4 configuration domain.

2.4 Sea Ice Data for Validation and Assimilation

For validation of the sea ice results by the model and for assimilation of the sea ice we are using weekly regional sea ice charts produced by the Canadian Ice Service (CIS). These ice charts contain information for sea ice concentration and the stage of development of sea ice (Canadian Ice Service digital charts database, Working with the gridded data, NETCDF and TEXT formats release V. 10, 2005). These fields are produced by the Canadian Ice Service, by using all the information available at a time (surface observations, aerial reconnaissance and satellite imagery) combined with information from previous charts, nowcasting and the general expertise of ice forecasters (T. Carrieres, 2000).

CHAPTER 3

Model's Prognostic Simulation

Our study focuses on sea ice, thus in this chapter we are going to explore the sea ice results from the model's free simulation (free-run). To determine how close the ice fields produced by the model are to reality, we are comparing them with ice fields produced by the Canadian Ice Service. To be able to compare ice fields produced by the model (sea ice edge, sea ice concentration, sea ice covered area, sea ice thickness etc.) with ice fields produced by the Canadian Ice Service (CIS), we interpolate in space all of the ice fields produced by the Canadian Ice Service (CIS) so that their resolution will match the resolution of the model results. From now on we are going to refer to the sea ice fields produced by the Canadian Ice Service as CIS.

3.1 Sea Ice Edge

The sea ice edges are defined by a sea ice concentration of 15%, a value commonly used to define the sea ice edge in many studies (e.g. Fichefet and Morales Maqeuda, 1997). For the Labrador and Newfoundland region during the years 2002 (high ice period) and 2004 (low ice period), the CIS sea ice edges are represented by black lines and the model's sea ice edges by red lines in Figures 3.1 and 3.2, respectively. The light gray colour indicates regions covered by sea ice according to the CIS and the white colour indicates region where there are no available CIS sea ice charts.

3.1.1 Year 2002

In Figure 3.1 the sea ice edges produced by the model, along the Labrador and Newfounland shelves, are almost identical to the CIS sea ice edges for February and March, the months of maximum sea ice advance and growth. The same seems to be the case during July and June when the sea ice quickly melts and retreats to northern latitudes. On the other hand, during January, when the sea ice growth and advection towards the south is rapid, sea ice produced by the model extends further south than the sea ice observed in the CIS data. The exact opposite happens during April and May, the months of the initiation of ice melting. During this time period the ice edge produced by the model is constrained further north than the CIS sea ice edge, indicating that the model sea ice melts faster during these two spring months. For the years 2003 and 2005, the model seems to have the same behavior (not shown).

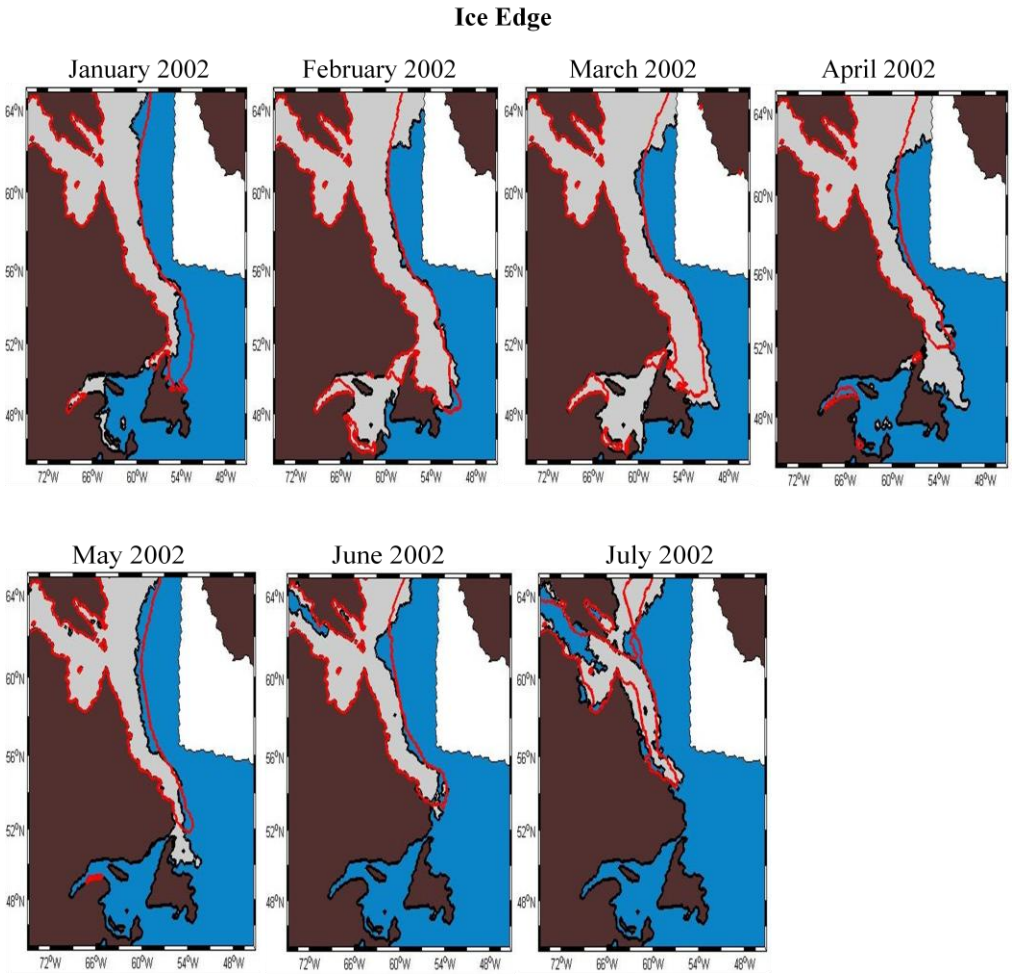

Figure 3.1: Monthly differences between the sea ice edges resulting from the model (red line) and the sea ice edges produced by the Canadian Ice Service (CIS) (black line) for the year 2002. Where the gray colour indicates regions covered by sea ice according to the CIS, and where the white region outside our domain indicates that there are no CIS ice charts available for this region.

3.1.2 Year 2004

In Figure 3.2 the monthly differences between the ice edges produced by the model and the CIS sea ice edges for the year 2004 are similar to the ones for the year 2002. The two exceptions are during February and July, where the model's sea ice appears to extend further south in comparison to the CIS sea ice. This is probably due to the fact that 2004 was a very low sea ice year, thus during the winter the growth and the advection of sea ice towards the south was slow and

delayed and during the spring the melting of sea ice was fast. Therefore, for 2004 the model cannot capture the low growth rate and fast melting of sea ice.

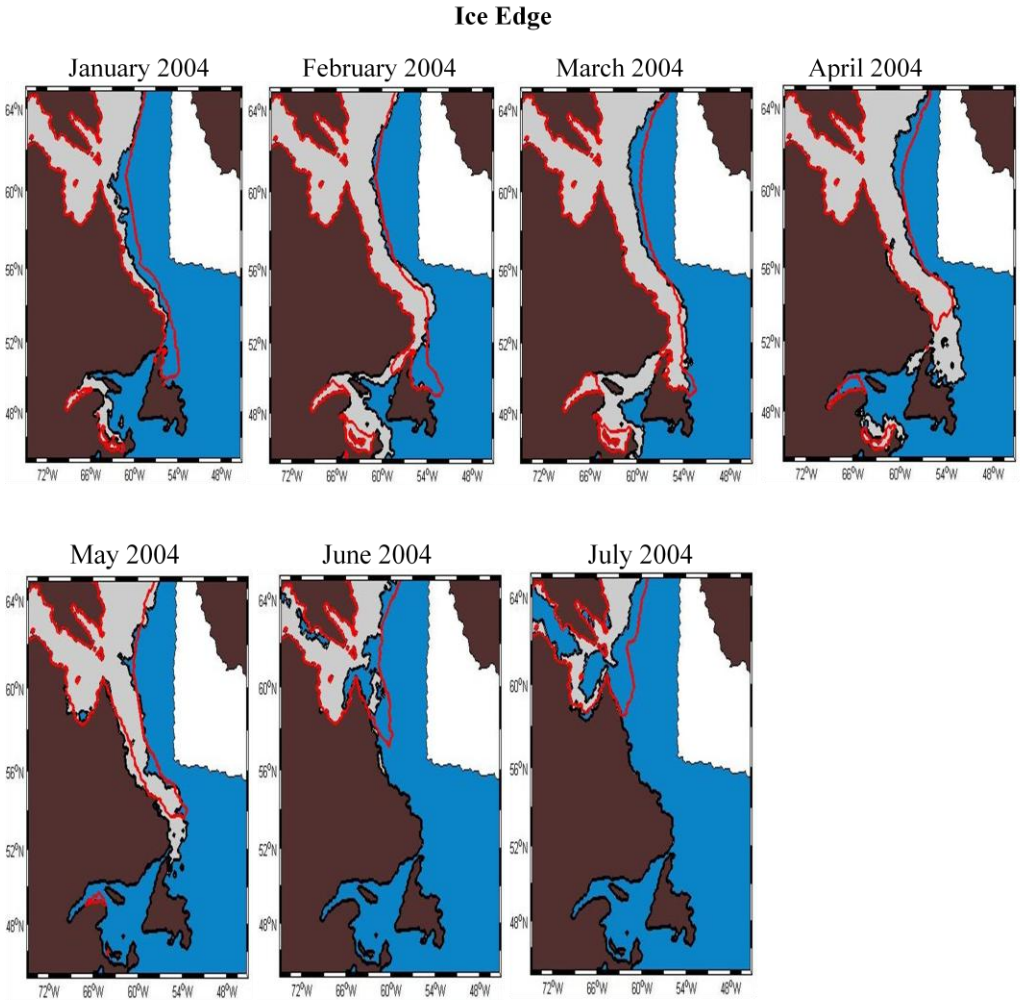

Figure 3.2: Monthly differences between the sea ice edges resulting from the model (red line) and the sea ice edges produced by the Canadian Ice Service (CIS) (black line) for the year 2004. Where the gray colour indicates regions covered by sea ice according to the CIS, and where the white region outside our domain indicates that there are no CIS ice charts available for this region

3.1.3 Overall Model Sea Ice Edge

The model simulation generally produced reasonable sea ice edges in all months; however, many discrepancies from reality (CIS sea ice edges) remain. A closer look at both Figures 3.1 and 3.2 reveals that in the Gulf of Saint Lawrence the

model generally underestimates the sea ice coverage; this is also the case for 2003 and 2005 (not shown). The resolution of the model and fact that it is configured for basin scale simulations, make it difficult to obtain good result in limited coastal regions.

3.2 Sea Ice Concentration

To explore how well the model represents sea ice concentrations off the Canadian East coast, we compare the model's results with CIS sea ice concentration fields. The sea ice concentrations produced by the model, the CIS sea ice concentrations and their differences are presented for 3 months (January, March, May) of the years 2002 and 2004 in Figures 3.3 and 3.4, respectively. For the images where the differences are presented, positive values indicate that the model overestimates the sea ice concentration and negative values indicate that the model underestimates the sea ice concentration.

3.2.1 Year 2002

The model overestimates sea ice concentration along the offshore Labrador shelf edge and underestimates sea ice concentration along the Labrador shelf coast, during the entire year of 2002, Figure 3.3 (only January, March and May are presented). Figure 3.3 shows that the largest discrepancies between sea ice concentration fields produced by the model and CIS sea ice concentration fields, occur in January, where the model overestimates sea ice concentration for the majority of the Labrador shelf. This indicates that the model's sea ice growth and advection towards the south is more rapid than reality during January. The opposite is the case for March, where the model is not able to capture the fast sea ice growth and advection towards the south, and thus the model underestimates the sea ice concentration on the Newfoundland shelf. The model overestimates sea ice concentration along the north Labrador shelf break. This indicates that there are higher discrepancies between the model and the CIS sea ice fields, closer to where the sea ice edge lies in the north of Labrador sea.

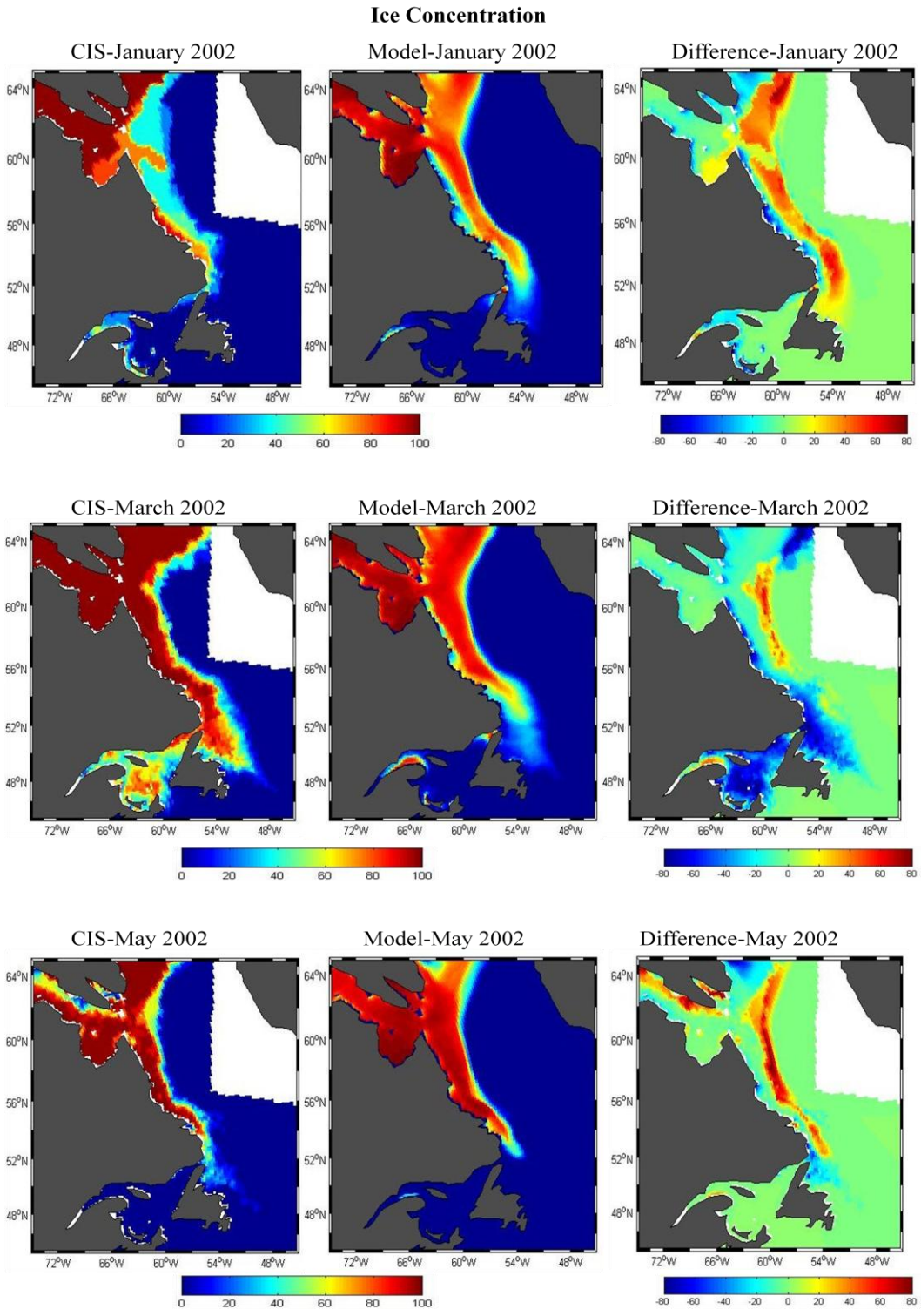

Figure 3.3: The CIS Sea ice concentrations (left), the sea concentrations produced by the model (middle) and the differences between these two (right) are presented for January, March and May of 2002.

3.2.2 Year 2004

During the year 2004 and 2002 the model behaves similar, Figure 3.4 (only January, March and May are presented). Again January is the month showing the largest overestimation of model sea ice concentrations. By comparing Figure 3.4 and Figure 3.3, it is apparent that along the Newfoundland shelf, the model is in better agreement with the CIS, during the March of 2004 than during the March of 2002. This was expected since 2004 was a low sea ice year and thus the growth and the advection of the ice towards south was limited. Therefore the model is able to simulate the sea ice concentrations with a higher degree of accuracy for the month of March, the month of maximum growth and advection of sea ice towards the south.

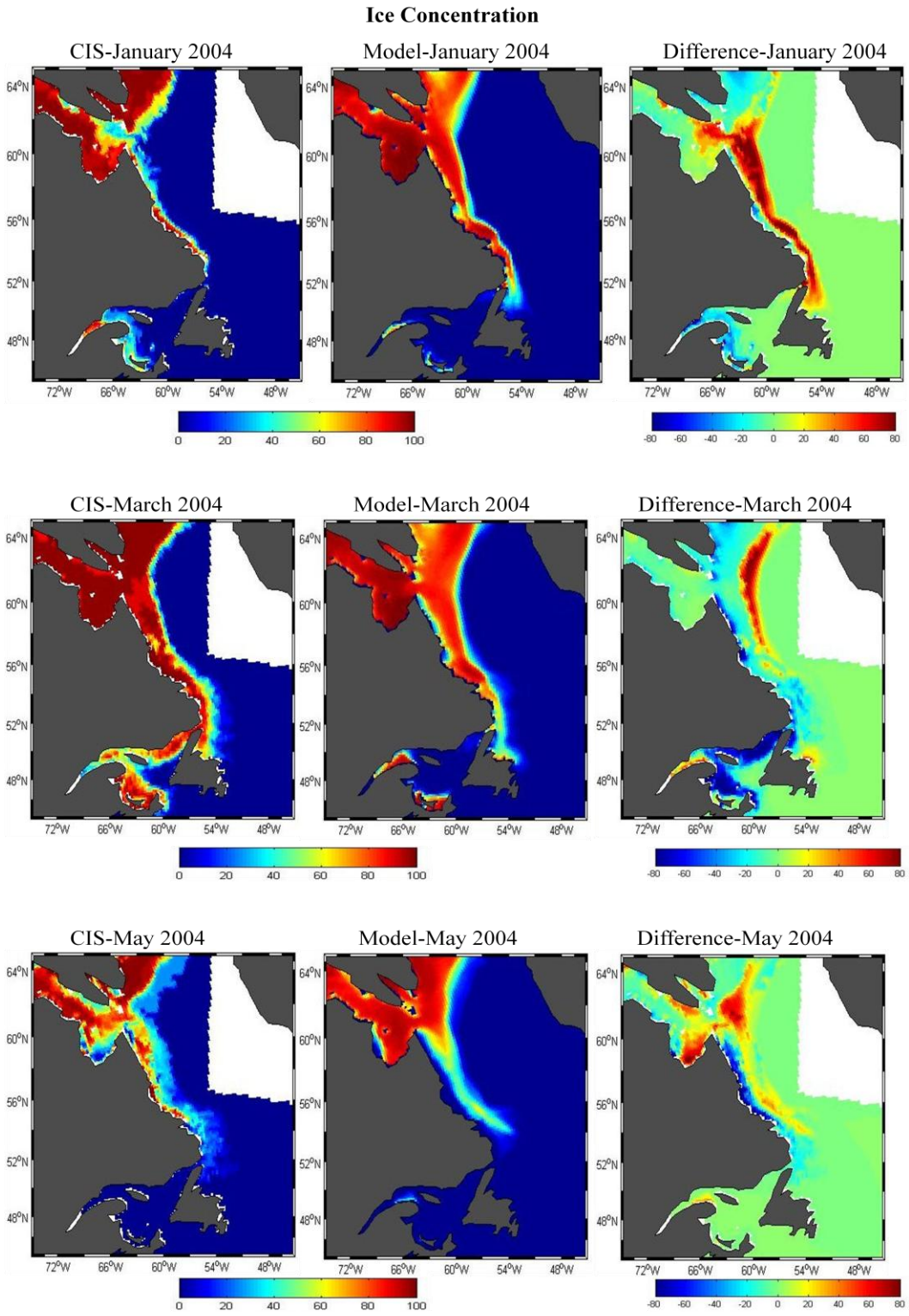

Figure 3.4: The CIS Sea ice concentrations (left), the sea ice concentrations produced by the model (middle) and the differences between the two (right) are presented for January, March and May of 2004.

3.2.3 Overall Model Sea ice Concentration

Generally, the model showed discrepancies from the reality during all the years which were simulated, 2002, 2003, 2004 and 2005 (2003 and 2005 not shown). The results of the model indicate that to some extend the model is able to capture the sea ice concentration seasonal cycle but still is not able to accurate represent the sea ice concentration during each month.

3.3 Sea Ice Covered Area

The sea ice covered area is computed as the summation of the area occupied by each grid cell, multiplied by the sea ice concentration fraction for that grid cell. The time series for the sea ice covered area, between the years 2002 to 2005, for the Labrador and Newfoundland shelves (area highlighted in green), are shown in Figure 3.5. The sea ice covered area resulting from the CIS sea ice fields is represented in black and the sea ice covered area resulting from our model is represented in red.

Figure 3.5 shows that the model produces a sea ice seasonal cycle which corresponds to reality; sea ice appears during late November/early December then continues to grow and expand towards the south until the middle of spring when it starts retreating, and disappears completely by the end of July. Figure 3.5 also indicates that, although the model produced the lowest sea ice covered area for the year 2004 (year of lowest sea ice), the model seems to be unable to capture the big differences between high and low sea ice years. During most months of all the years, the model is not capable of producing as large a sea ice covered area as the one produced from the Canadian Ice service. Thus interannual variability is significantly underestimated (although the general difference between high and low ice years is qualitatively simulated).

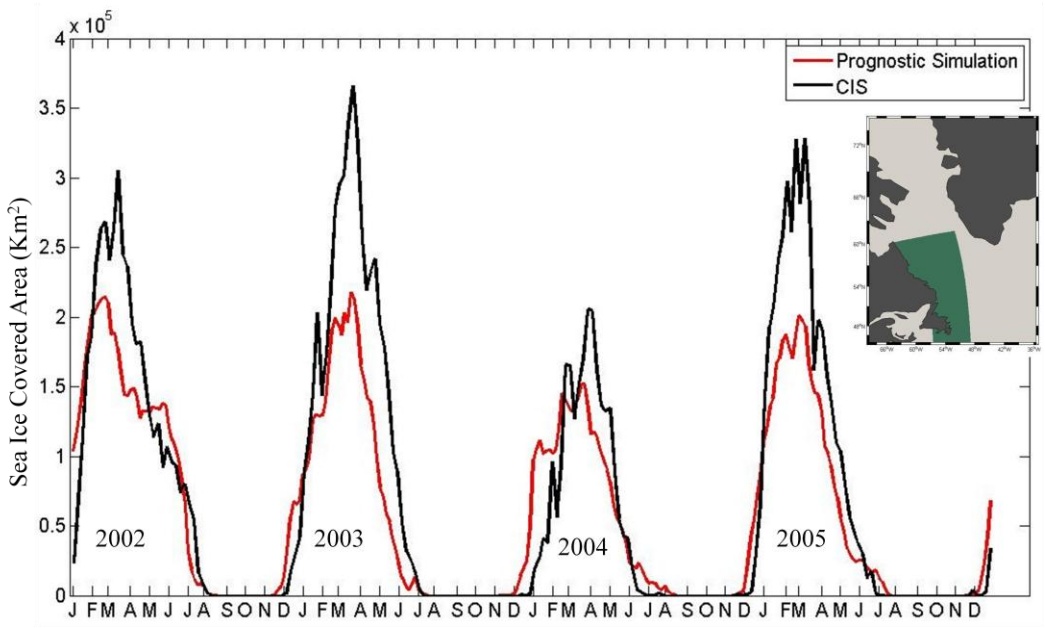

Figure 3.5: Time series of the sea ice covered area. Sea ice covered area produced by the model is represented with red and sea ice covered area produced by the CIS is represented with black. Both are computed for the region highlighted in green in the inset.

Figure 3.6 represents the monthly averaged difference over the 4 years (2002-2005) between the CIS sea ice covered area and the model's sea ice covered area. It reveals that generally the sea ice covered area produced by the model is underestimated. The only exception is during December and January, when sea ice covered area produced by the model is overestimated. This indicates that during this period the model's sea ice growth is too fast.

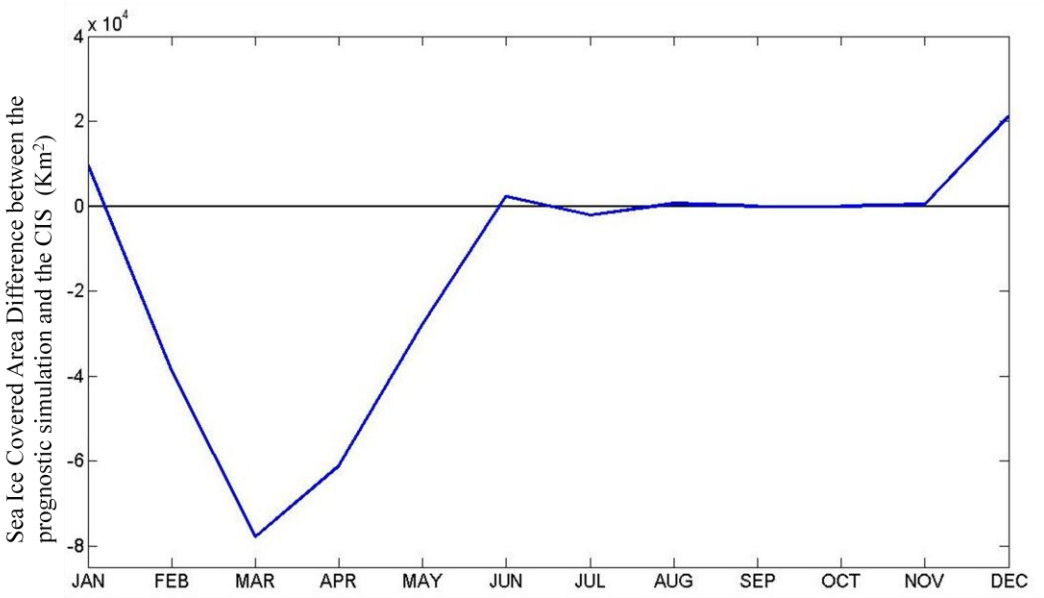

Figure 3.6: Monthly averaged time series of the difference between the sea ice covered area produced by the model and the sea ice covered area produced by the CIS. Values above zero indicate that the model overestimates the sea ice covered area and below zero that the model underestimates sea ice covered area.

3.4 Sea Ice Thickness

The only available information that can be used to compare and validate the model's sea ice thickness results is the categorization of sea ice into four categories by the CIS:

Table 3.4: The sea ice thicknesses that correspond to each stage of development.

Stage of development	Ice thickness range
New ice or nilas	<0.1 meters
Young ice	0.1-0.3 meters
First year ice	0.3-2.0 meters
Old ice*	>2.0 meters

**On the Labrador and Newfoundland shelves the sea ice melts every summer making the presence of old sea ice impossible. Thus when we refer to sea ice*

thickness above 2 meters we do not mean old sea ice just sea ice with ice thickness above 2 meters.

By using the above categories we can roughly examine how well the sea ice thickness is simulated by our model. Only figures for 2002 are presented but the rest of the years behave similarly. Figure 3.7 shows that in March and May the sea ice thickness produced by the model is roughly in agreement with the CIS sea ice thickness; this is the same case for April, June and July (not shown). For December and January (only January is shown) the model indicates presence of first year sea ice (sea ice thickness 0.3-2.0 meters) in southern regions where the CIS indicates young ice (sea ice thickness 0.1-0.3 meters). The above results support the conclusion from the previous sections of Chapter 3, that the model sea ice grows and extends to the south faster than it should during December and January.

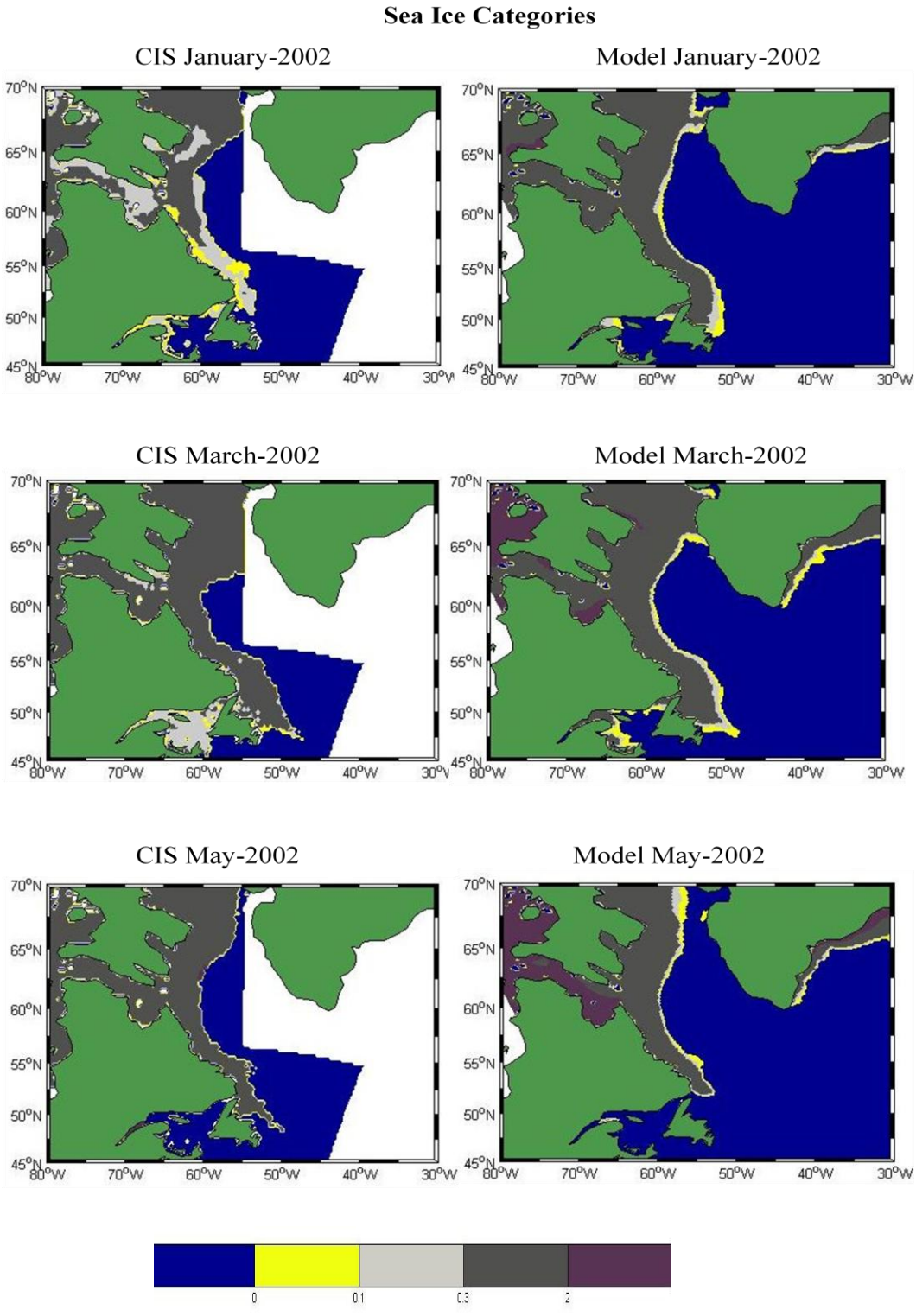

Figure 3.7: CIS Sea Ice thickness categories are presented on the left and sea ice thickness categories produced by the model are presented on the right, for the year 2002.

3.5 Overall Behavior of the Sea Ice/Ocean Coupled Model

The sea ice fields produced by the model have many discrepancies from the CIS sea ice fields in terms of sea ice edge, sea ice concentration, sea ice covered area and sea ice thickness. More realistic model sea ice fields are always desirable. A way to improve the model sea ice results is by merging available observations or information of sea ice into the model. In our case, sea ice concentration fields produced by the Canadian Ice Service are assimilated into our model. In the following chapters the different data assimilation techniques that were used and the improvements on model sea ice fields obtained through data assimilation are presented.

CHAPTER 4

Nudging Experiments

In chapter 3, it was presented that our model results, as concerns sea ice, are far from perfect. To improve the model results, a simple data assimilation method called Newtonian relaxation, or nudging, was used. In this chapter, the details of the Newtonian relaxation method and the improvements in the model results through Newtonian relaxation are discussed.

4.1 Newtonian Relaxation (Nudging) Method Details

4.1.1 Theoretical Background

In nudging, the model is pushed gently towards observed values by adding an additional term to the model's prognostic equation. This term is proportional to the difference between some field constructed based on all the available information (observations, nowcasting etc.), and the model's predicted values. The above can be described by the following equation:

$$\frac{\partial x}{\partial t} = F(x,t) + K * (x_{obs} - x) \quad eq\ 4.1.1$$

Where $K*(x_{obs}-x)$ represents the nudging term that is added to the prognostic equation, x_{obs} represents the observation of the parameter that need to be assimilated, K is called the nudging coefficient and K^{-1} represent the relaxation

time. The choice of value for *K* is dependent on how strong one needs the Newtonian relaxation to be, but caution should be used as if value K is set too high, the nudging term will dominate the prognostic equation. Such strong nudging will also damp the model's interannual variability.

4.1.2 Sea Ice Concentration Nudging

In this study, the sea ice concentration fields are nudged towards the sea ice concentration fields produced by the Canadian Ice Service (CIS). The nudging term is added to the equations *2.2.4* and *2.2.5*, which control the evolution of the sea ice concentration. Two additional experiments have been made and the details are of those experiments are presented below:

Table 4.1: The two nudging experiments details:

Experiment	**Years of Simulation**	**Nudging Coefficient**	**Assimilation Time Step**
Continuous nudging	2002-2005	1/(5*86400) s^{-1}	Model's time step
Forecast nudging	first 6 months of 2002	1/(sea ice model's time steps) s^{-1}	5 days

The nudging coefficient is chosen to be 1/(5*86400) s^{-1} (86400s=1 day) for the continuous nudging experiment. This small coefficient is efficient, since we want to add small corrections every time step so that the nudging will not be dominant. The use of this coefficient is explained as if by applying these small corrections in every model's time step, it will take 5 days time period in order the model sea ice concentration fields to become equal with the CIS sea ice fields. On the other hand, for the forecast nudging experiment, the nudging coefficient is chosen as 1/(sea ice model's time steps) s^1 making the nudging very strong when it occurs. Since the nudging occurs instantaneously every five days, we impose all the corrections instantaneously in a single time step, changing the model's sea ice concentration field to become equal with the CIS sea ice concentration field, in

this time step. Thus we provide initial correct conditions for the model's free evolution during the following 5 days.

4.2 Continuous Nudging Experiment Model Results (Nudging occurs every model's Time Step)

4.2.1 Sea Ice Edge

In Figure 4.1 the CIS sea ice edges, the sea ice edges resulting from the prognostic simulation (free-run) and the sea ice edges resulting from the continuous nudging experiment are presented with black, red and green lines respectively, for the years 2002 and 2004. It is clear that the discrepancies between the CIS sea ice edges and the model's free-run sea ice edges become smaller through nudging and in some cases are almost eliminated. The sea ice edges resulting from continuous nudging lie somewhere between the CIS sea ice edges and the model's free run sea ice edges.

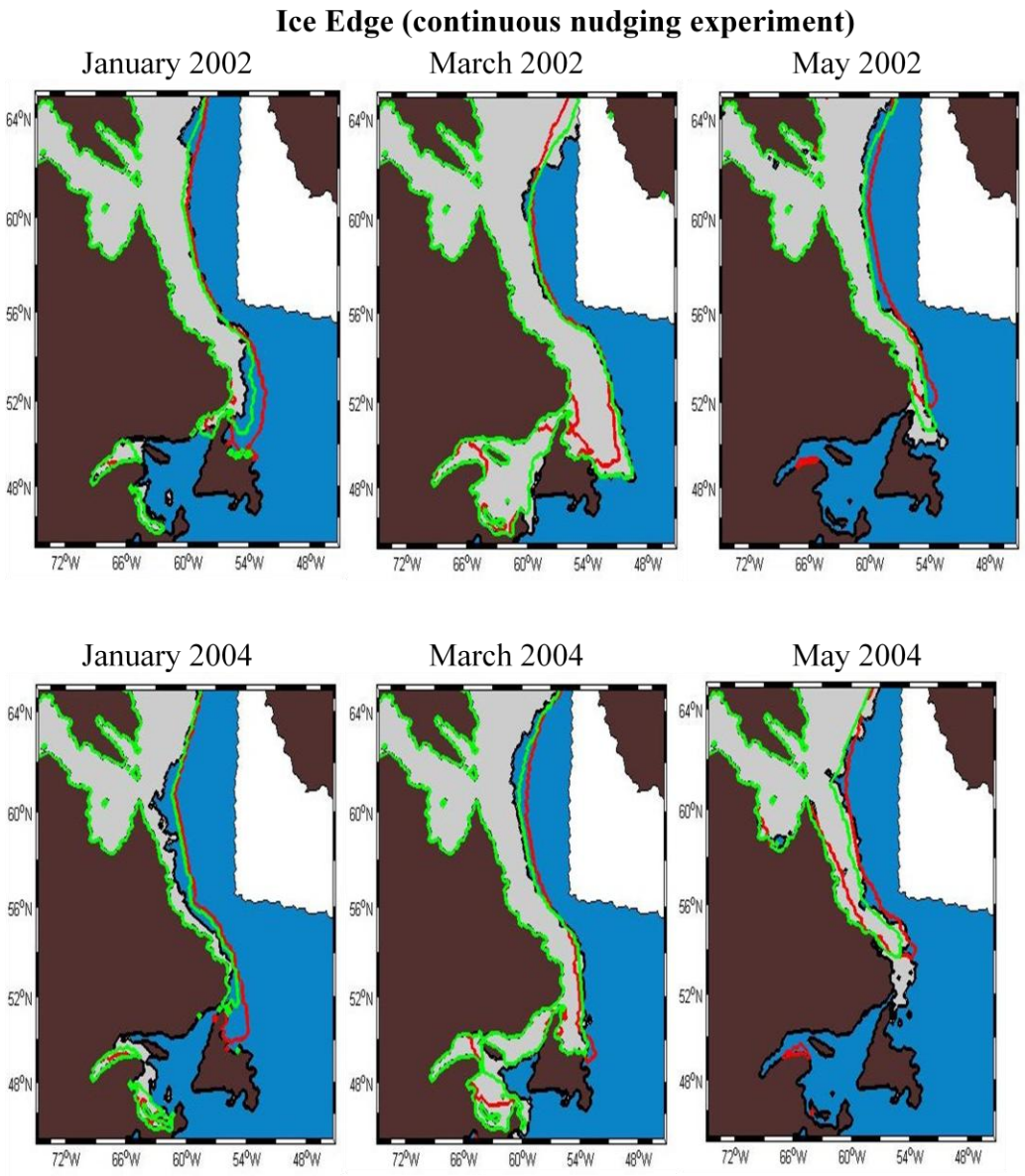

Figure 4.1: The sea ice edges resulting from the model's free run (red line), the sea ice edges resulting from the continuous nudging experiment (green line) and the sea ice edges defined by the Canadian Ice Service (CIS) (black line) are presented for January, March and May of 2002 and 2004. The gray colour represents the region that the CIS indicates as covered by sea ice and the white colour indicates where there are no CIS sea ice charts available.

4.2.2 Sea Ice Concentration

Figure 4.2 and 4.3 shows the sea ice concentrations resulting from the continuous nudging experiment, the sea ice concentration differences between the CIS and the model's prognostic simulation and the sea ice concentration differences between the CIS and the continuous nudging experiment for the years 2002 and 2004, respectively. For the figures where the differences are presented, positive values indicate that the model overestimates the sea ice concentration, and negative values indicate that the model underestimates the sea ice concentration. It is revealed, by comparing the sea ice concentration differences between the model's prognostic simulation and the CIS and the sea ice concentration differences between the continuous nudging experiment and the CIS, that the large sea ice concentration differences between the model's prognostic simulation and the CIS tend to become smaller through nudging, for all the months in all the years of our simulation.

For January of 2002 and 2004, on the Labrador and Newfoundland shelves, the sea ice concentration is overestimated by the continuous nudging experiment. This overestimation (reaching as high as 40%) is smaller than the overestimation of the sea ice concentration by the model's prognostic simulation (reaching as high as 60% for 2002 and as high as 80% for 2004). On the Newfoundland shelf, the improvements in sea ice concentration are very noticeable due to the fact that in this region the nudging causes the sea ice disappearance in areas where they were indicated as "ice-free" from the model's prognostic simulation but as covered by sea ice by the CIS (this can be seen in Figure 4.1). This is the same case for the Gulf of Saint Lawrence.

For March of 2002, the sea ice concentration is still about 20% overestimated by the nudging experiment, along the North Labrador shelf break. This is an improvement, since in this area the model's prognostic simulation overestimates sea ice concentration by almost 40%. The improvements through nudging are more noticeable in the Newfoundland shelf. There the continuous nudging experiment is around 20% closer to the CIS than the model's prognostic

simulation. In the offshore region of the Newfoundland shelf these discrepancies from the CIS are eliminated though nudging. For March of 2004, the nudging improves the sea ice concentration by as much as 20%, along the North Labrador shelf break. In the Newfoundland shelf and in the Labrador coast, the discrepancies with the CIS tend to be eliminated through nudging. For both March of 2002 and 2004, in the Gulf of Saint Lawrence, nudging leads to the appearance of sea ice in areas indicated as "ice-free" by the model's prognostic simulation. This leads to the better agreement of the nudging experiment with the CIS.

For May of 2002, the model's prognostic simulation results in a sea ice concentration overestimation that reaches 70%, along the Labrador shelf break. This overestimation is reduced to around 20% and in some areas is eliminated, through the continuous nudging. For May of 2004, in the Labrador shelf coast, the sea ice concentration differs by 40% and more, between the prognostic simulation and the CIS, and is reduced to 20% through nudging. For the Labrador shelf, the prognostic simulation's 20% overestimation is almost eliminated though nudging and closer to the shelf break, the nudging experiment results instead in a small underestimation of the sea ice concentration. This change is due to the fact that, as seen in figure 4.1, the prognostic simulation's sea ice edges are lying further offshore than the CIS sea ice edges, for the Labrador shelf. On the other hand the continuous nudging experiment's sea ice edges are lying further inshore than the CIS sea ice edges. For March of 2002 and 2004 there are no sea ice concentration differences between the nudging experiment and the CIS fields, in the Gulf of Saint Lawrence. This is associated with the disappearance of sea ice, through nudging, from the areas where sea ice existed in the prognostic simulation.

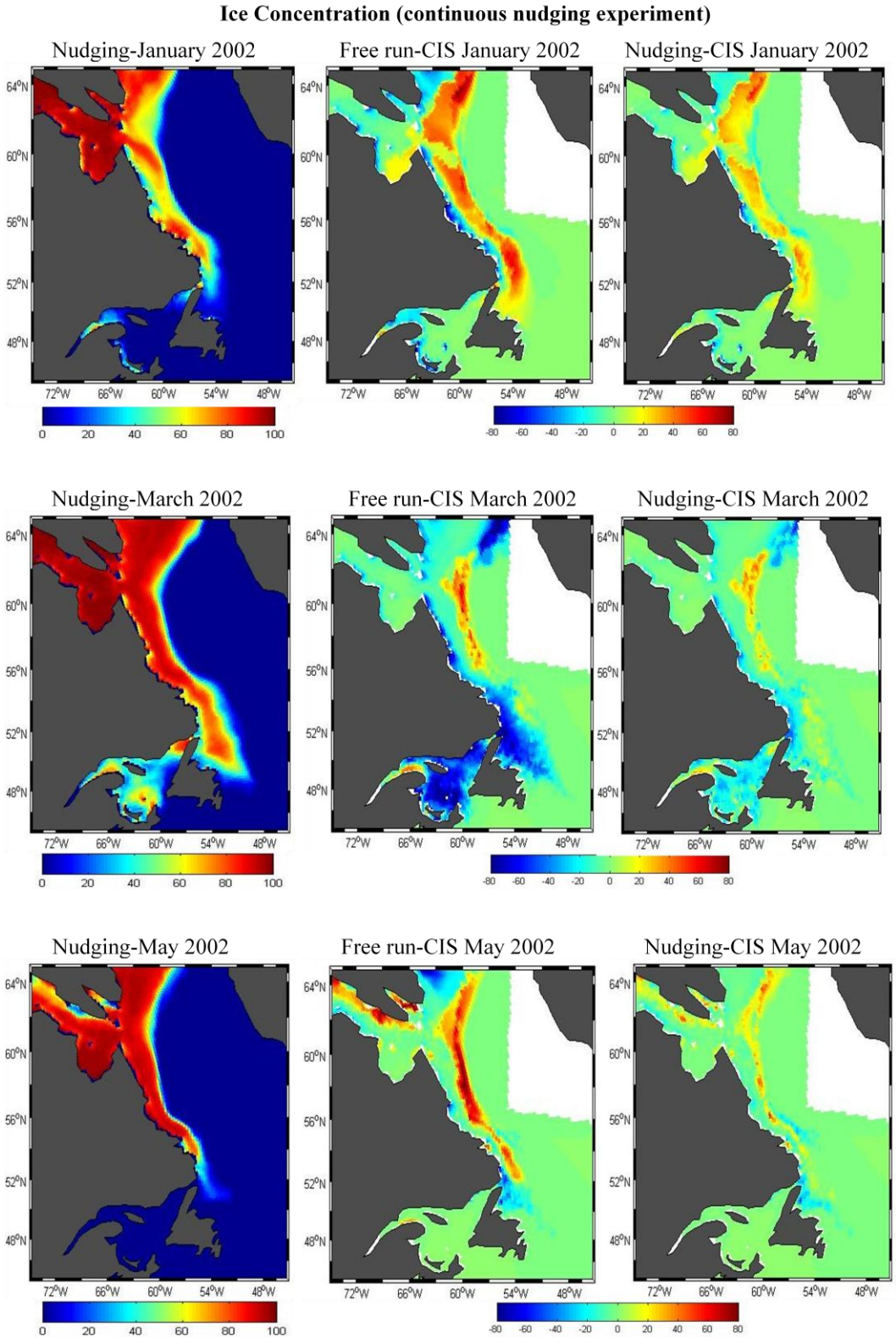

Figure 4.2: The sea ice concentrations that result from the continuous nudging experiment (on the left), the sea ice concentration differences between the CIS

and the model's prognostic simulation (in the middle) and the sea ice concentration differences between the CIS and the continuous nudging experiment (on the right) are presented for January, March and May of 2002.

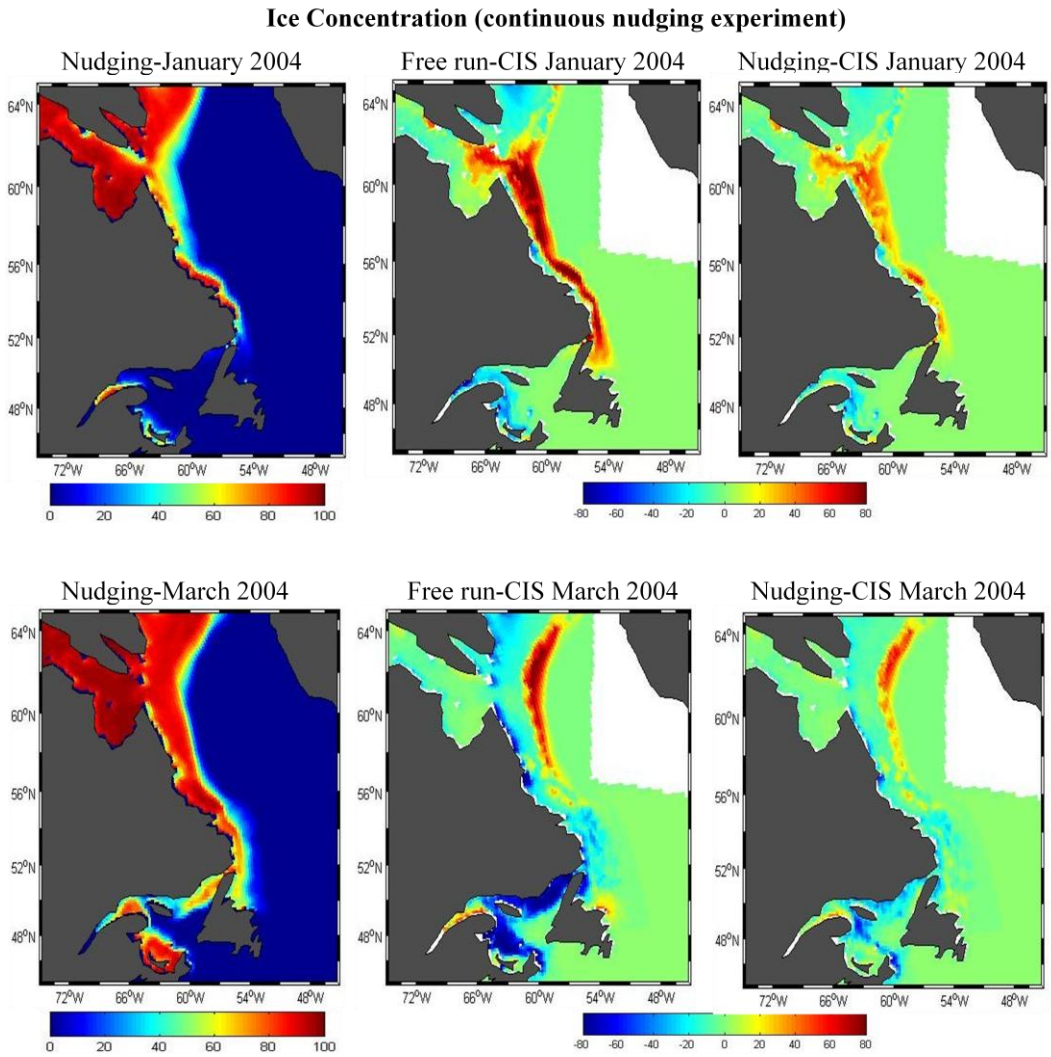

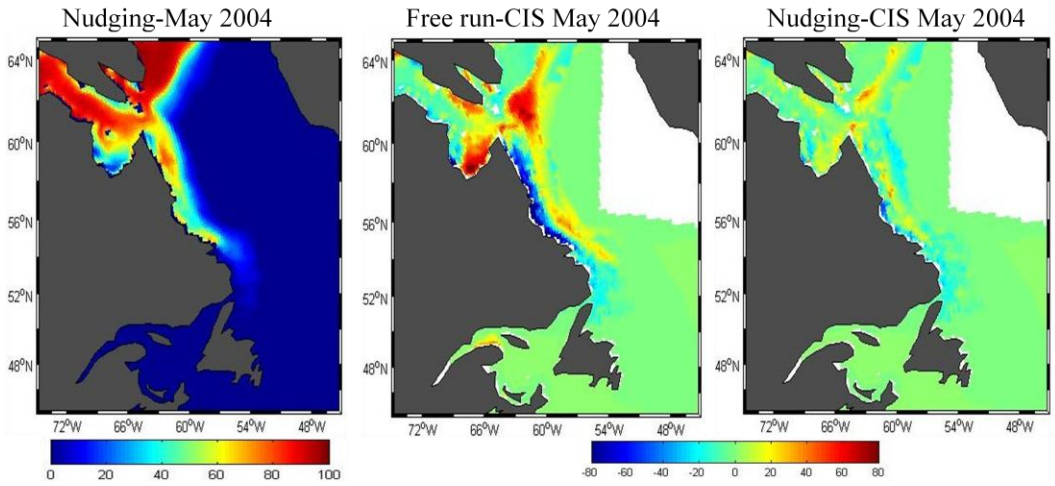

Figure 4.3: The sea ice concentrations that result from the continuous nudging experiment (on the left), the sea ice concentration differences between the CIS and the model's prognostic simulation (in the middle) and the sea ice concentration differences between the CIS and the continuous nudging experiment (on the right) are presented for January, March and May of 2004.

4.2.3 Sea Ice Covered Area

The time series for the sea ice covered area between the years 2002 and 2005, computed for the area highlight in green in the inset, is presented is Figure 4.4. Figure 4.4 shows that the large differences in sea ice covered area between the CIS and the model's prognostic simulation (free run) tend to be eliminated through nudging. For the time period of maximum sea ice covered area (around March), the nudging brings very big changes to the model sea ice covered area for all the years expect 2004. These changes are as large as $0.6*10^5$ km^2 for 2002, $1.5*10^5$ km^2 for 2003 and $1*10^5$ km^2 for 2005. For 2004, the changes around March are not as high ($0.2*10^5$ km^2). This is due to the fact that in the nudging experiment the big differences between the high and the low sea ice years have been captured. In contrast, the model's prognostic simulation was unable to capture these differences and thus resulted in a similar sea ice covered area for all of the years. During the beginning of sea ice appearance in the area (December-January), in the nudging experiment the sea ice growth seems to be too fast but not as fast as the prognostic simulation sea ice growth. This is more visible in

January of 2004, where the nudging experiment indicates almost $0.5*10^5$ km^2 lower sea ice covered area than the model's prognostic simulation. Finally, the sea ice covered area that results from the nudging experiment is in very good agreement with the CIS sea ice covered area, for all of the 2002-2005 period.

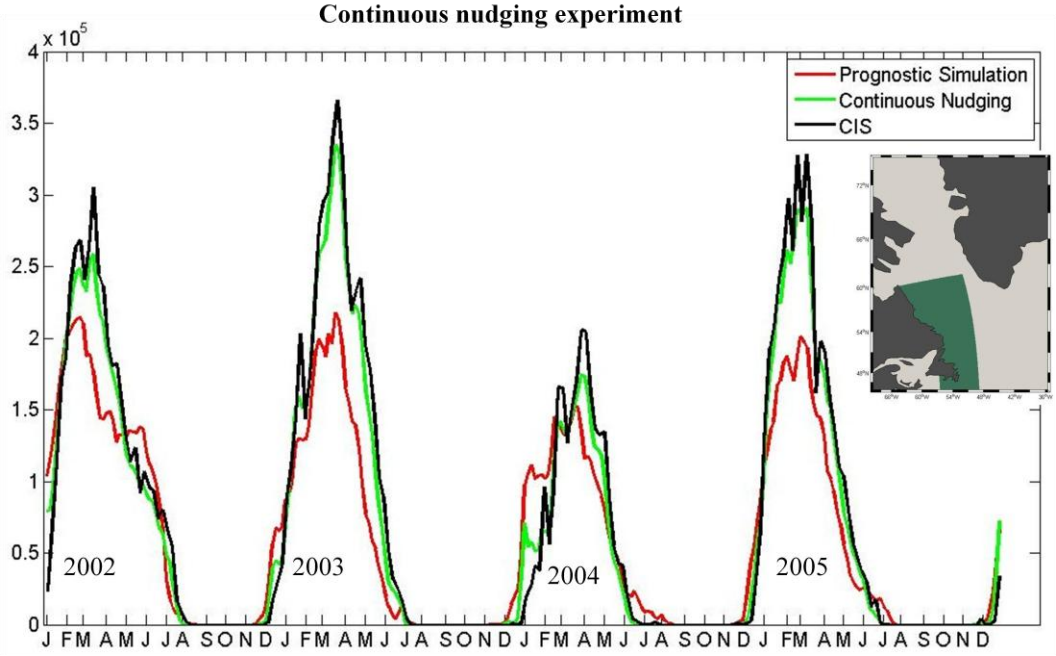

Figure 4.4: Time series of the sea ice covered area. The sea ice covered area produced by the model's free run is represented with red, the sea ice covered area that results from the continuous nudging experiment is represented with green and the sea ice covered area produced by the CIS is represented with black. All the sea ice covered areas are computed for the region highlighted in green in the inset.

4.2.4 Sea Ice Thickness

Figure 4.5 reveals that the nudging experiment brings differences to the model sea ice thickness. For the figures where the differences are presented, positive values indicate that the model's prognostic simulation results in lower sea ice thickness values than the nudging experiment and negative values indicate that the model's prognostic simulation results in higher sea ice thickness values than the nudging experiment. For January, the differences in sea ice thickness reach 40 cm (around

4%), with the nudging experiment resulting in generally lower sea ice thicknesses for the Labrador and Newfoundland shelf breaks. The same is the case for March and May, with the nudging experiment resulting in generally lower sea ice thicknesses for the Labrador shelf break but higher sea ice thicknesses for the rest of the domain. This was expected since, except for January, the model's prognostic simulation seems to underestimate the sea ice concentrations in the Labrador shelf coast and the Newfoundland shelf. Thus for these areas, the sea ice concentrations are increased through nudging, in order to agree with the CIS values. This leads to the increase of the sea ice thicknesses (as much as 1 meter). The opposite happens along the Labrador shelf break. In addition, the differences of sea ice thickness in South areas (for example the Gulf of Saint Laurence during March) are relative big, since these areas were indicated as sea ice free by the model's prognostic simulation, and thus only through nudging does sea ice appears there. The validation of the sea ice thickness is difficult due to the lack of CIS sea ice thickness fields. It is not shown, but the stage of development fields' comparison between the continuous nudging and the CIS (Figure 3.7) reveals that they are in reasonable agreement.

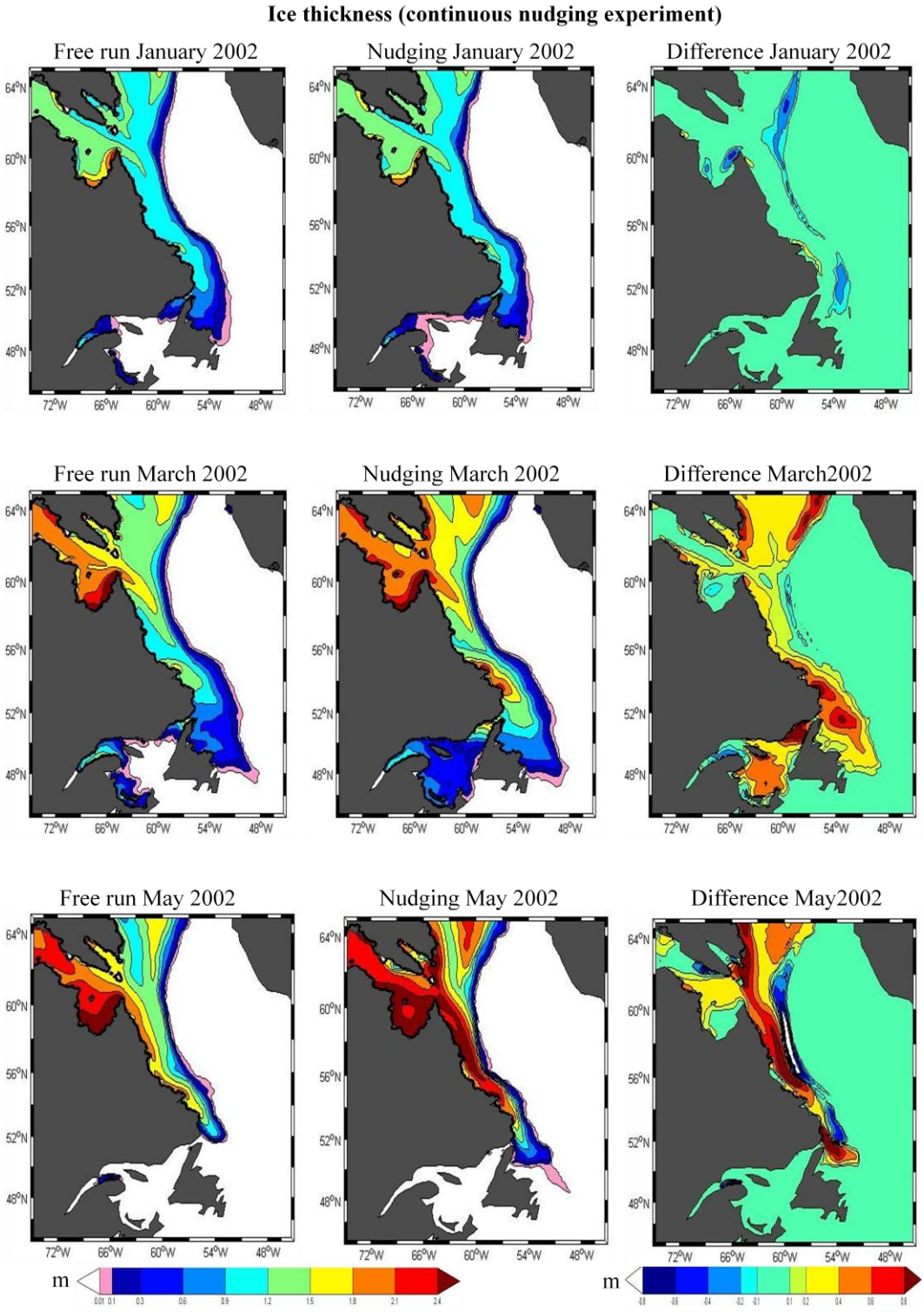

Figure 4.5: The sea ice thicknesses that result from the continuous nudging experiment, the sea ice thicknesses that result from the model's prognostic

simulation (free run) and their differences are presented for January, March and May of 2002.

4.2.5 Ocean Heat and Freshwater Contents

During nudging, the ocean state is indirectly modified through coupled sea ice/ocean model physics. Thus the resulting ocean salinity and temperature of the nudging experiment are different from the model's prognostic simulations, in the areas where the nudging had an effect. The ocean salinity and temperature are affected more near the surface of the ocean. The differences decrease as the depth increases, until at large depths there is no effect. These differences in temperature and salinity lead to differences in the heat and freshwater content of the ocean. In Figures 4.6 and 4.7 the continuous nudging experiment heat and freshwater contents, calculated for the upper 17 meters of the ocean are presented. For the freshwater content calculations, a reference salinity of 34.8 PSU (Myers, 2005) was used.

In January and March, the continuous nudging experiment heat content gains between 0.015 to 0.02 terajoules along the Labrador shelf break. In March, the continuous nudging experiment results in lower temperatures than the prognostic simulation, in the North of the region, on the Newfoundland shelf and in the Gulf of St. Lawrence. This leads to heat content losses of 0.06 terajoules, 0.0.3 terajoules and more than 0.06 terajoules, respectively. The differences in the heat content are generally in agreement with the sea ice edge differences (Figure 4.1). This indicates that the heat content changes (temperature changes) are associated with appearance or disappearance of the sea ice and not with sea ice concentration differences alone.

In January and March, on the Labrador shelf, the nudging experiment salinity increases of 0.2 to 0.5 PSU leads to a 5 to 50 m^3 decrease in the freshwater content. The big freshwater content increase (larger than 100 m^3), in the Gulf of Saint Lawrence, is associated with the appearance of sea ice through nudging. The freshwater content (salinity) seems to be more sensitive to sea ice concentration

changes than the heat content. Thus differences in freshwater content occur in areas where the sea ice concentration was altered through nudging.

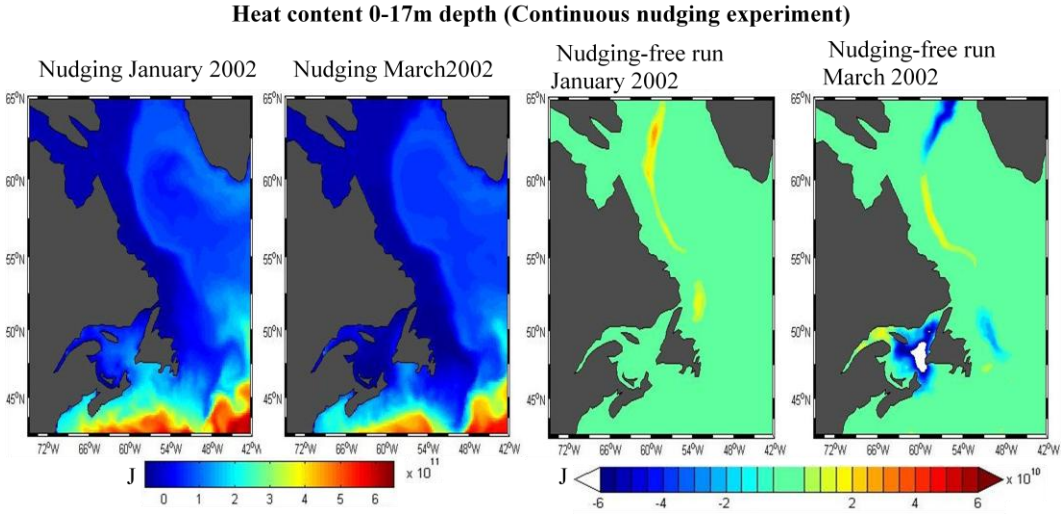

Figure 4.6: The heat content of the 17 upper meters of the ocean resulting by the continuous nudging experiment and the differences between the continuous nudging experiment and the model's prognostic simulation are presented for January and March of 2002.

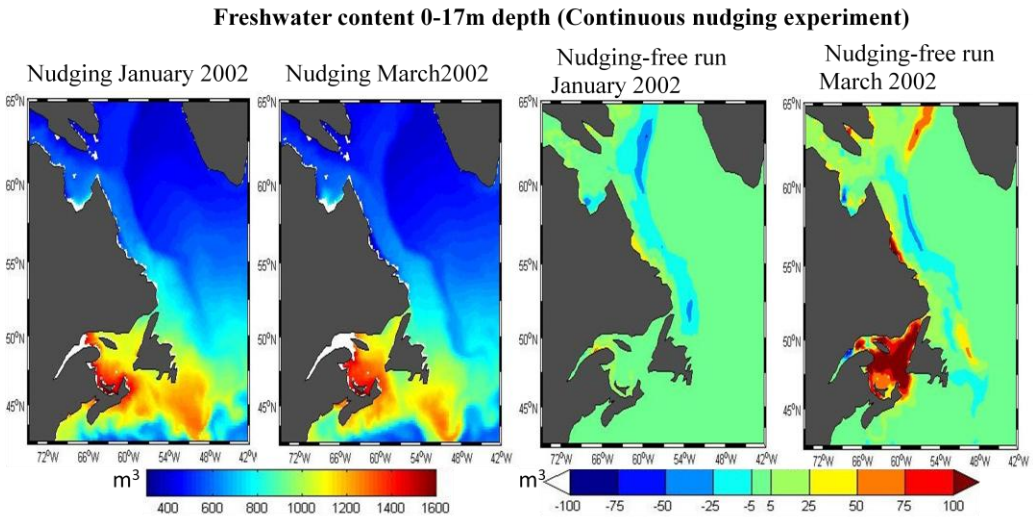

Figure 4.7: The freshwater content of the 17 upper meters of the ocean resulting by the continuous nudging experiment and the differences between the continuous

nudging experiment and the model's prognostic simulation are presented for January and March of 2002.

4.3 Forecast Nudging Experiment Model Results (Nudging Occurs Every 5 days)

The impact of the forecast nudging on the sea ice and ocean fields is overall of the same nature as the continuous nudging. This is the reason why the results of the forecast nudging are presented briefly, just to point out the similarities and the differences with the continuous nudging. Similarities are expected since in both experiments the sea ice concentration fields are nudged towards the CIS sea ice concentration fields. Due to the different nudging coefficients and the different time scale of nudging occurrence, the two experiments have small differences in the sea ice concentration fields. These differences are reflected in the sea ice thickness fields and in the ocean fields through the model physics.

4.3.1 Sea Ice Edge

Figure 4.8 demonstrates that the sea ice edges resulting from the two nudging experiments are almost identical (the yellow line overlaps the green line). As in the continuous nudging, in the forecast nudging the sea ice edges differences, between the CIS and the prognostic simulation, tend to be eliminated. A closer view of Figure 4.8 reveals that the forecast nudging sea ice edges are slightly closer to the reality (CIS) than the continuous nudging. The reasons for this will be discussed later in section 4.4.

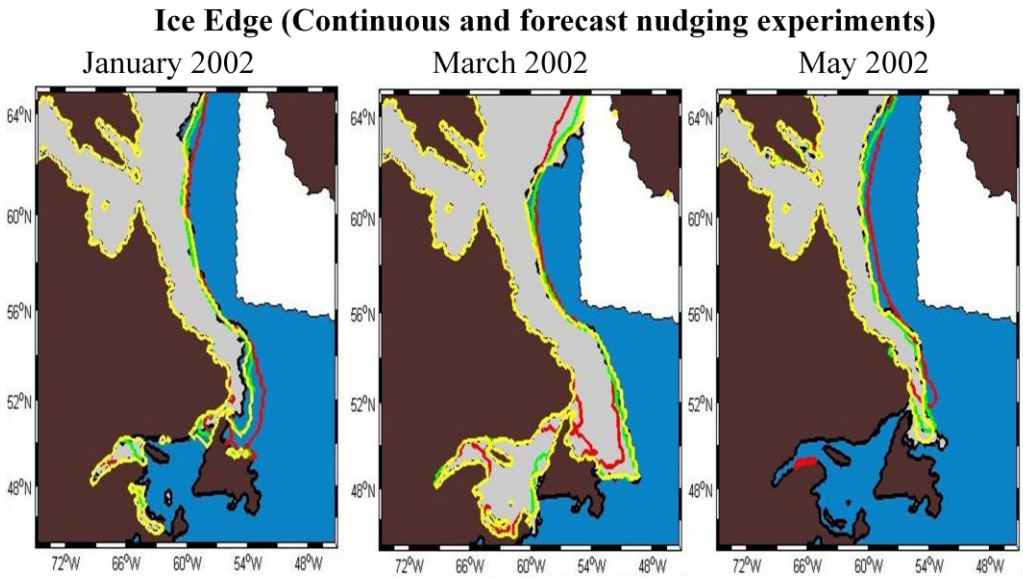

Figure 4.8: The sea ice edges resulting from the model's free run (red line), the sea ice edges resulting from the continuous nudging experiment (green line), the sea ice edges resulting from the forecast nudging experiment (yellow line) and the sea ice edges produced by the Canadian Ice Service (CIS) (black line) are presented for January, March and May of 2002. Where the gray colour represents the region that the CIS indicates as covered by sea ice and where the white colour indicates that there are no CIS sea ice charts available.

4.3.2 Sea Ice Concentration

Figure 4.9 reveals that, as in the case of the continuous nudging experiment, the sea ice concentration differences between the model's prognostic simulation (free run) and the CIS, tend to be eliminated through the forecast nudging. In January 2002, the forecast nudging experiment produces a 10% to 20% lower sea ice concentration than the continuous nudging experiment, in the interior of the Labrador shelf and around 10% higher sea ice concentration along the Labrador shelf break, the Labrador coast and the west Gulf of Saint Lawrence. In March 2002, the forecast nudging experiment produces around 20% to 30% lower sea ice concentration than the continuous nudging experiment in the North Labrador shelf break and around 10% to 20% higher sea ice concentration in the South Labrador and Newfoundland shelves. In the Gulf of Saint Lawrence the differences

between the two nudging experiments vary between -30% to +30%. In May 2002, the forecast nudging experiment produces a 10% to 20% lower sea ice concentration than the continuous nudging experiment in the North Labrador shelf break and a 10% to 20% higher sea ice concentration in the Labrador shelf break between 53^{o} and 56^{o} latitude and the Newfoundland east coast. These differences lead to a better agreement of the forecast nudging experiment with the CIS, than the continuous nudging experiment (comparison of Figures 4.2 and 4.9). This is associated with the continuouser nudging coefficient that was used in the forecast nudging experiment; this is explained further in sub chapter 4.4. Although, the sea ice concentration differences are smaller in the case of the forecast experiment, it is noticeable that the areas where the differences occur are almost the same in both of the experiments. This is the case for all of the first six months of 2002. The reason is that in both of the experiments the same areas are affected. These are the areas where the prognostic simulation sea ice drifts from the CIS values. Thus the only difference lies in the degree to which these areas are affected by the two nudging experiments.

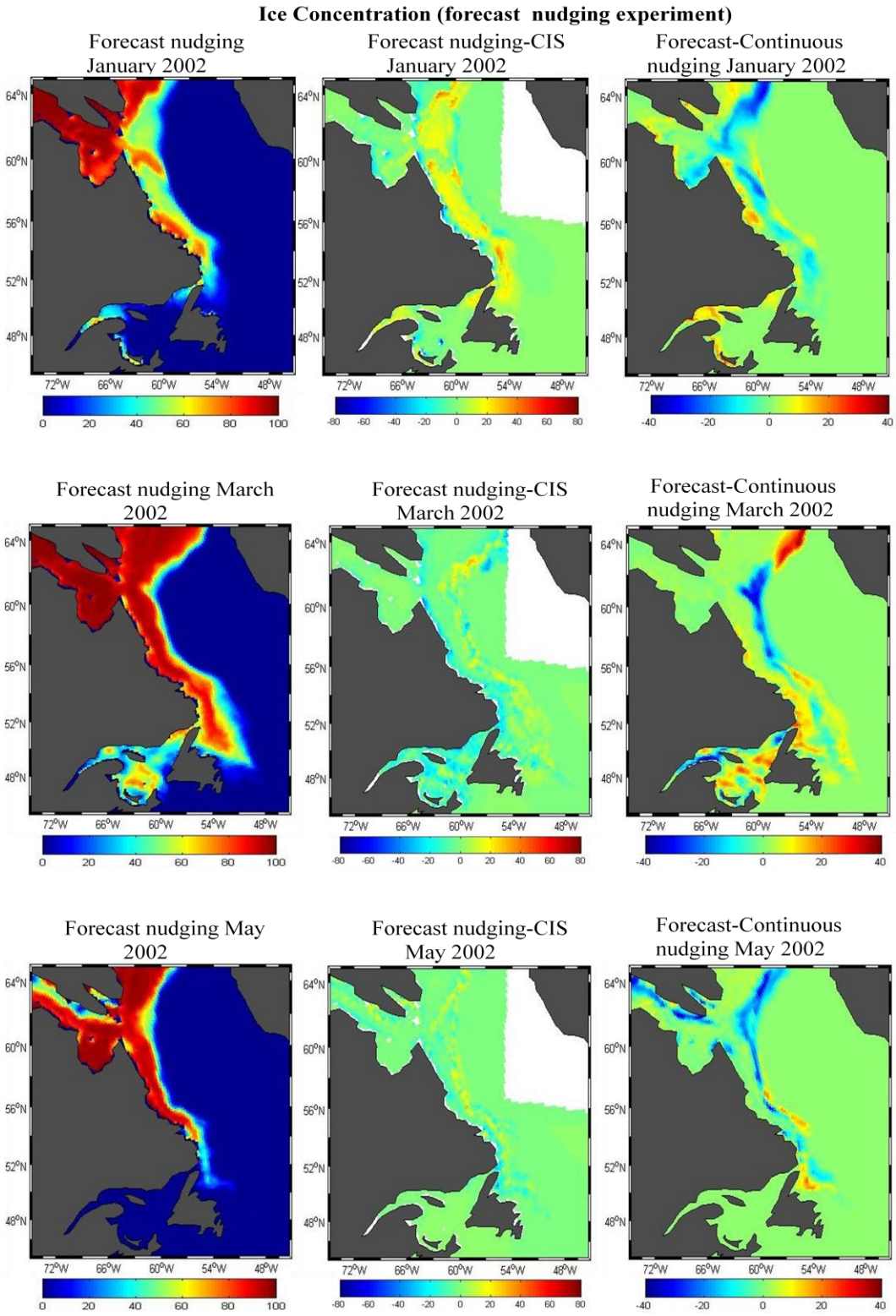

Figure 4.9: The sea ice concentration results from the forecast nudging experiment (on the left), the sea ice concentration differences between the

forecast nudging experiment and the CIS (in the middle) and the sea ice concentration differences between the forecast and the continuous nudging experiments (on the right) are presented for January, March and May of 2002.

4.3.3 Sea Ice Covered Area

Figure 4.10 shows that the sea ice covered area resulting from the forecast nudging experiment, is generally in good agreement with the CIS sea ice covered area. Sea ice covered area resulting from the forecast experiment appears to be really close to the sea ice covered area resulting from the continuous nudging experiment. The only noticeable difference between these two is the fluctuations of the sea ice covered area resulting from the forecast experiment. These fluctuations are due to the fact that in the forecast nudging experiment, nudging occurs every five days. This means that the sea ice concentration is pulled towards the CIS sea ice fields and then the model evolves undisturbed for 5 days until it is momentary pulled again towards the CIS sea ice fields. Thus these fluctuations represent the drift of the sea ice covered area away from the CIS values. The fluctuations reach $1*10^5$ km^2 in the time period of maximum drift of the model prognostic simulation (around March).

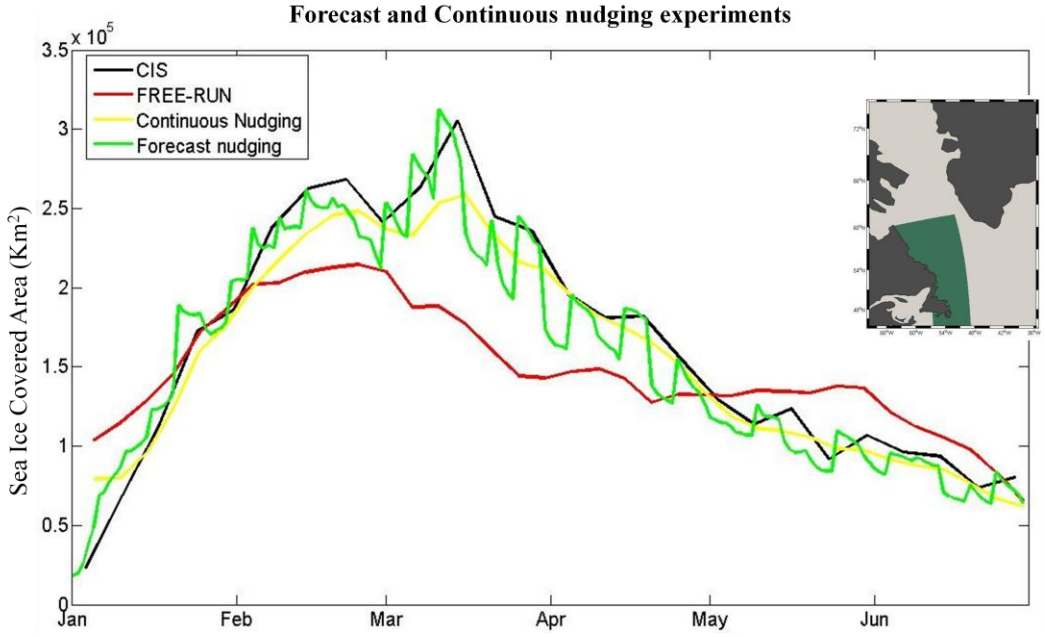

Figure 4.10: The time series of the sea ice covered area for the first 6 months of 2002. The sea ice covered area produced by the model's free run is represented with red, the sea ice covered area produced by the CIS is represented with black, the sea ice covered area resulting from the continuous nudging experiment is represented with yellow and the sea ice covered area resulting from the forecast nudging experiment is represented with green. All of the sea ice covered areas are computed for the region highlighted in green in the inset.

4.2.4 Sea Ice Thickness

Figure 4.11 reveals that the forecast nudging experiment produces ice thickness fields of similar structure to the ones produced by the continuous nudging experiment but with some profound differences. The right pictures of Figure 4.11, reveals that for January 2002, the forecast nudging experiment produces up to 30 cm thinner sea ice than the continuous nudging experiment in the offshore Labrador and Newfoundland shelves. This reflects the fact that in January, the forecast nudging experiment produces lower sea ice concentrations than the continuous nudging experiment for these areas. For March of 2002, along the North Labrador and Newfoundland shelves offshore edge, the forecast nudging

experiment results in a 20 cm to 40 cm sea ice thickness decrease in comparison with the continuous nudging experiment, and around a 20 cm sea ice thickness increase, along the Labrador coast. For May 2002, the forecast nudging experiment results in higher sea ice thicknesses along the Labrador coast and lower sea ice thicknesses offshore of the Labrador and the Newfoundland shelves (the magnitude of these differences varies continuously from 10 to 60 cm). The above differences are associated with the sea ice concentration differences and, as it will be seen in the next sub chapter, with ocean temperature differences (heat content figure 4.12).

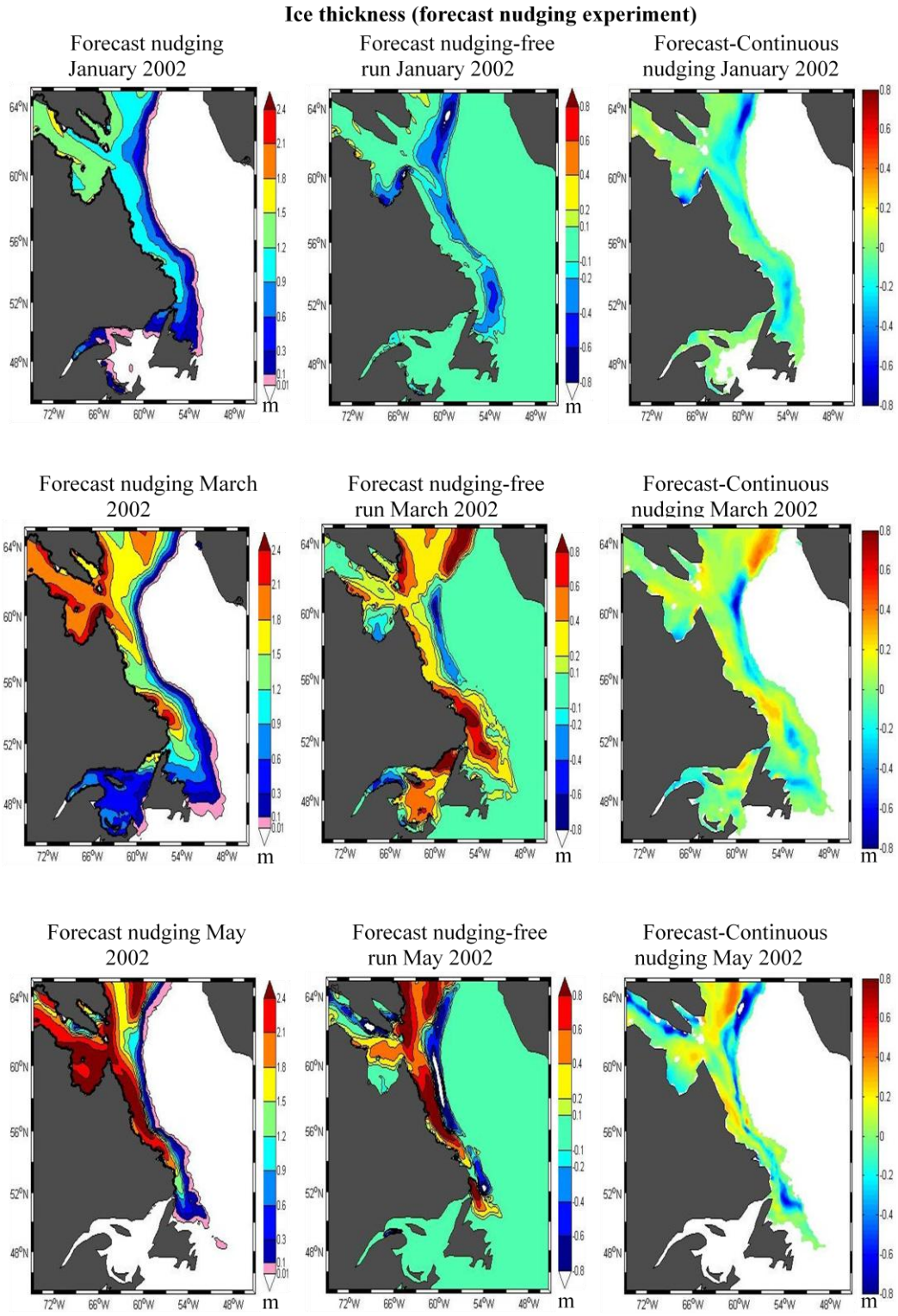

Figure 4.11: The sea ice thickness results from the forecast nudging experiment (on the left), the sea ice thickness differences between the continuous nudging

experiment and the free run (in the middle) and the sea ice thickness differences between the forecast nudging experiment and the free run (on the left) are presented for January, March and May of 2002.

4.3.5 Ocean Heat and Freshwater Content

The effect of the sea ice concentration nudging, when the nudging occurs every five days, on the ocean's temperature and salinity, is similar to the effect when the nudging occurs every model time step. It is visible, in Figure 4.12, that in January the forecast nudging results in a very small increase in heat content, of a magnitude of 0.01 terajoules, from the continuous nudging experiment. In March, the forecast nudging experiment results in lower heat content values by 0.03 terajoules, for the North of the region, and by 0.01 to 0.02 terajoules, along the Newfoundland shelf break, and higher heat content values by 0.01-0.03 terajoules, for the Labrador shelf break. In January, there is a decrease in the forecast nudging experiment freshwater content values (around 10 m^3) along the Labrador shelf break and an increase of the same magnitude, along the Labrador coast (around 55^o latitude) and the Gulf of Saint Lawrence . For March, along the Labrador shelf the forecast nudging experiment freshwater content values decreases by 10 to 50 m^3, and increases by 10 to 50 m^3 along the Newfoundland shelf and the Labrador coast. The heat and freshwater content differences between the two nudging experiments correspond to the differences in the sea ice concentration fields. A comparison between Figures 4.11, 4.12 and 4.13 reveals that the sea ice thickness differences between the two nudging experiments are associated with the heat and freshwater content differences. This is reasonable, since they are connected and influence each other through the model's physics.

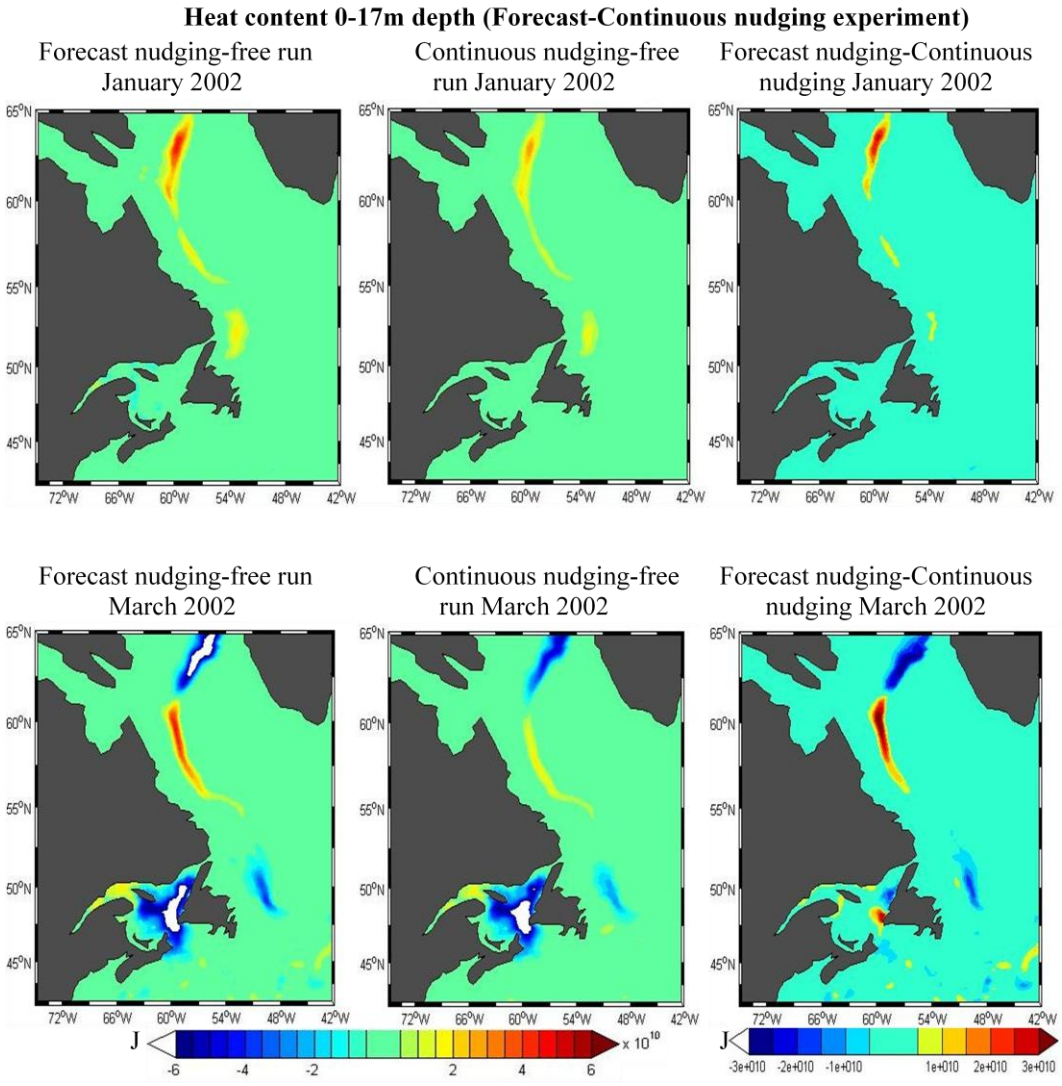

Figure 4.12: The ocean heat content differences for the first 17meters between the forecast nudging experiment and the prognostic simulation (on the left), the continuous nudging experiment and the prognostic simulation (in the middle) and the forecast and continuous nudging experiment (on the right) are presented for January and March of 2002.

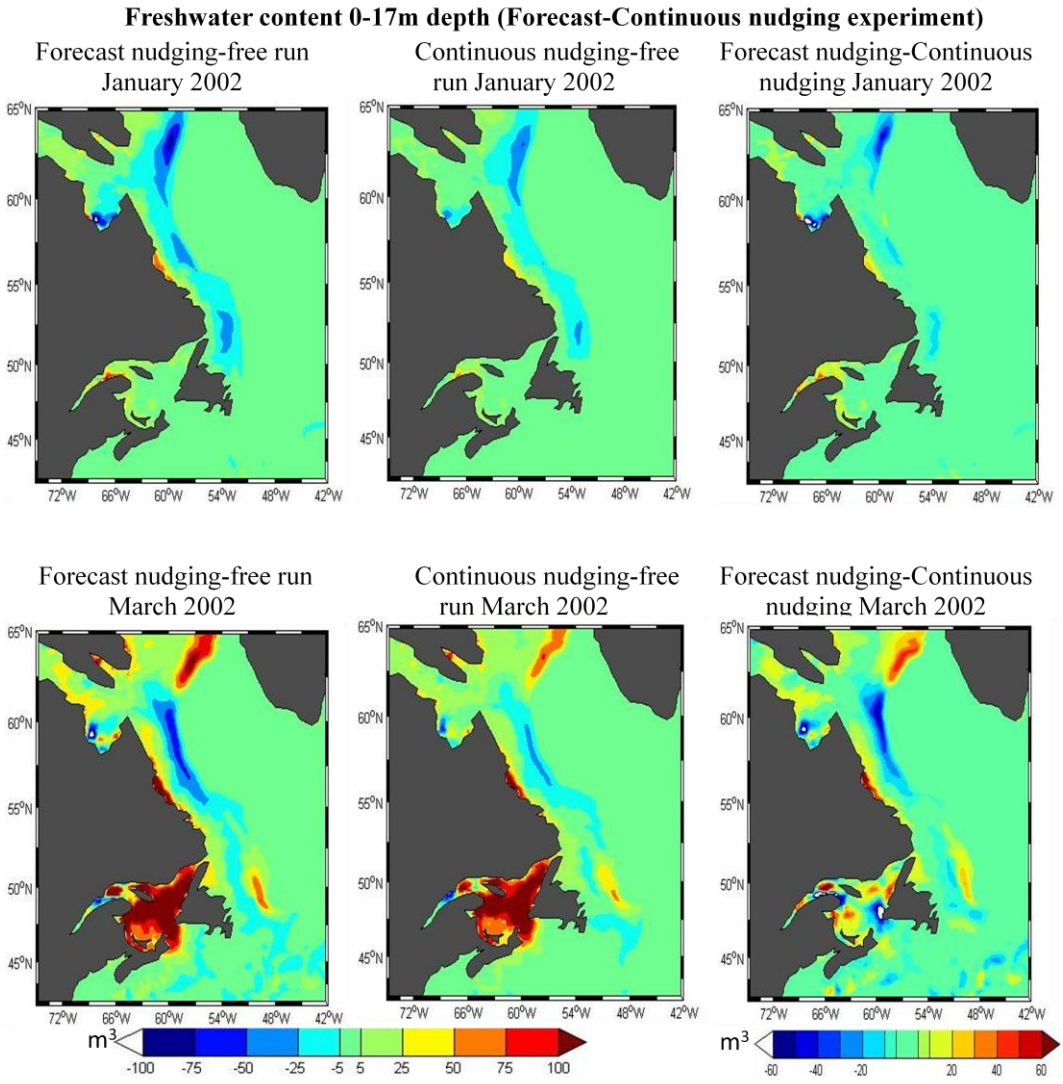

Figure 4.13: The ocean freshwater content differences for the first 17meters between the forecast nudging experiment and the prognostic simulation (on the left), the continuous nudging experiment and the prognostic simulation (in the middle) and the forecast and continuous nudging experiment (on the right) are presented for January and March of 2002.

4.4 Evaluation of the Two Nudging Experiments

This chapter confirms that the two nudging experiments bring desirable changes to the sea ice concentration fields. The differences in the sea ice fields and ocean fields between the two nudging experiments are due to the different nudging

coefficients and the fact that in the forecast experiment the nudging occurs every 5 days, allowing a 5 day time period of model free evolution. In more detail the differences are the following:

- The forecast nudging experiment's monthly sea ice concentration fields and sea ice edges are in better agreement with the CIS than the continuous nudging experiment (Figure 4.8 and 4.9). This is due to the use of a large coefficient every 5 days to push instantaneously the sea ice concentration fields to become the same as the CIS fields.
- The forecast nudging experiment sea ice covered area is in better agreement with the CIS for the days that the nudging occurred (every 5 days) than the continuous nudging experiment. The fluctuations in Figure 4.10 reveal that the forecast nudging experiment sea ice covered area drifts away from the CIS during the days where the model evolves freely (period between the nudging occurrences).
- The sea ice covered area fluctuations (Figure 4.10) indicate that the forecast nudging experiment's daily sea ice concentration fields are in less agreement with the CIS than the continuous nudging experiment, during the free evolution of the model (5 days). This is hidden in the monthly average fields.
- The sea ice thickness differences between the forecast nudging experiment and the prognostic simulation are larger than the sea ice thickness differences between the continuous nudging experiment and the prognostic simulation (Figure 4.11). This is associated with the fact that the sea ice concentration, the ocean salinity and the ocean temperature differences between the forecast nudging experiment and the prognostic simulation are larger.
- The ocean heat and freshwater content differences between the forecast nudging experiment and the prognostic simulation are larger than those between the continuous nudging experiment and the prognostic simulation. This is due to the initial sea ice conditions (sea ice

concentration becomes the same as the CIS sea ice concentration) before the 5 days of free evolution of the ocean state, in the forecast nudging experiment.

In both nudging experiments the sea ice thickness and the ocean state is indirectly modified through the coupled sea ice/ocean model's physics. Since nudging is an artificial non-physical approach of correcting a field by merging available information, the modifications that nudging brings in other fields are not always representative of the reality. For example adding, artificially, sea ice in a region with warm waters will not be efficient; on the other hand, the further addition of more sea ice can result in changes in the underlying water temperature that may not correspond to the reality. Thus it would be efficient to be able to connect and correct the underlying ocean properties (salinity and temperature) as the sea ice concentration is changing, in order to be consistent and maintain the balance between the sea ice and ocean fields. A way to be able to achieve these corrections is explored in the next chapter.

CHAPTER 5

1-D Data Assimilation Experiments

For the purpose of this chapter, two 1-D data assimilation experiments were conducted. In these experiments, as the model's sea ice concentration is nudged towards the CIS sea ice concentrations fields, the sea ice thickness and the underlying ocean salinity and temperature are corrected at each grid point and at each depth, based on their correlations with the sea ice concentration. The correlations are obtained by using a ten member ensemble with perturbation to the forcing fields. The main interest of the study is on winter (January, February and March) 2002, thus the two 1-D data assimilation experiments results are presented only for this season of 2002. In chapter 5, the method that has been used to obtain these correlations and the results of the two 1-D data assimilation experiments are discussed.

5.1 Method to Obtain Correlations between Sea Ice Concentration and Tracers

5.1.1 Random Perturbations to the Atmospheric Forcing Fields

The procedure discussed in this section was conducted for one reason, to allow us to look at the whole set of the ten member ensemble model results and be able to relate the sea ice concentration with the sea ice thickness, ocean salinity and

ocean temperature fields. In order to create perturbation to the atmospheric forcing fields, Empirical Orthogonal Functions (EOFs, further details in appendix D) are used (O. Alves & C. Robert, 2005). The perturbations for each forcing field are constructed by randomly weighting and combining the first fifty leading EOFs, of each forcing field and their expansion coefficients (details in appendix D):

$$Perturbation_i(x,y,t) = \sum_{i=1}^{10}\sum_{j=1}^{50} W_{i,j} * EOF_j(x,y) * a_j(t) \quad eq.\,5.1.1$$

In equation 5.1.1, *Perturbation* denotes the perturbations of each field and *i* denotes the number of the ensemble member (1 to 10). $W_{i,j}$ is a weight randomly chosen from a Gaussian distribution with mean zero, a different random number is used for each EOF and each ensemble member. An example of the perturbation that is created is shown in figure 5.1, where the longwave radiation perturbation is presented for January 1st, for the 3rd ensemble member, for the year of 2002. Then these perturbations are added to the corresponding atmospheric forcing field and the result is a ten member ensemble of perturbed atmospheric forcing fields (precipitation, snow, longwave radiation, shortwave radiation, temperature, humidity, meridional wind velocity, zonal wind velocity).

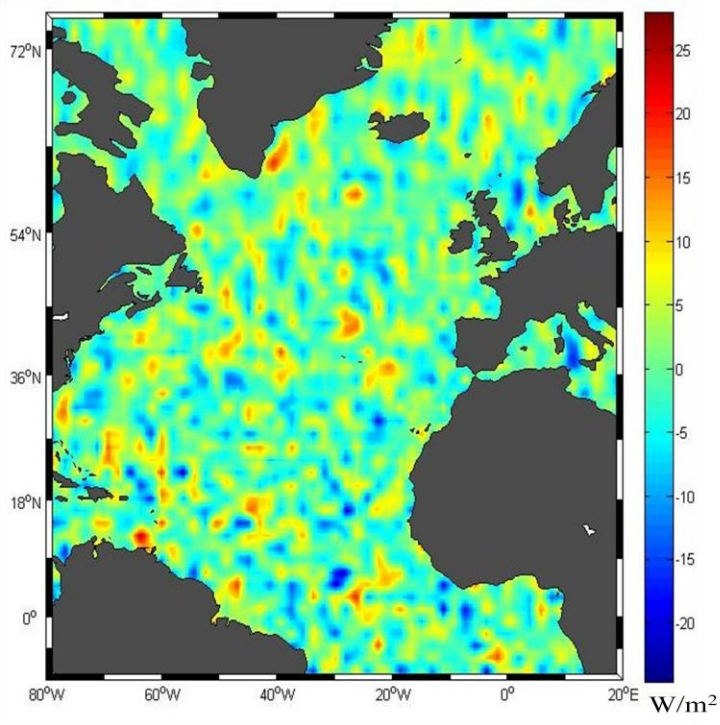

Figure 5.1: Longwave radiation perturbation for the 1st of January, for the 3rd ensemble member, for the year of 2002.

The ten member ensemble perturbed atmospheric fields have been used to force the model for the first fifteen days of January of 2002. The result is ten versions of the model simulation, each with slight differences in the sea ice and the ocean fields. To have a better view of the fields produced by the above procedure, the ten member ensemble model results average absolute deviation from the model prognostic simulation, for the first 15 days of January, are presented in Figure 5.2. These average absolute deviations were computed following the below equation

$$AAD = \frac{1}{10}\sum_{i=1}^{10} |x_i - X| \quad eq.5.1.2$$

Where x_i represents the ten member ensemble model results and X represents the prognostic simulation model results.

The average sea ice concentration deviations from the prognostic simulation reach as high as 6%. These deviations vary strongly, with the south of the Labrador

shelf experiencing the bigger deviations. The deviations reach the highest values near the shore around 54^{o} latitude and in the Strait of Belle Isle (Labrador Strait). This can be explained, since in these two areas the variations of sea ice concentration can be heavily influences by winds due to the topography. Thus small changes in the wind direction and strength can cause big changes in the sea ice concentration of these regions. The large sea ice concentration deviations near the North Labrador shelf break (between 3 and 5 %), lie between the transitions of prognostic sea ice concentrations from 50% to 70%. In this area, where the sea ice concentration growth slope is steep, small atmospheric changes (for example changes in wind direction and strength) can lead to significant changes in the sea ice concentration.

Figure 5.2 reveals that the largest sea ice thickness deviations lie along the sea ice edges. This was expected since the sea ice edge thickness is very sensitive to atmospheric conditions and sea ice edge position. The large sea ice thickness deviations (6cm) near the North Labrador coast, are associated with the influence of the atmospheric conditions on the outflow of sea ice through Hudson Strait. Finally, the large deviations in the South Labrador shelf are again associated with the heavy influence of winds on this area.

Ocean temperature deviations, associated with the sea ice, exist only along sea ice edges reaching 0.16 ^{o}C. This was expected since the atmosphere has little influence on the ocean temperature when the ocean is covered by sea ice. Thus only near the sea ice edges, where the insulating effect of the sea ice is small (since there the sea ice concentration and the sea ice thickness is small), can the atmospheric conditions influence the ocean temperature. Ocean salinity deviations are also larger (as large as 0.07 PSU) along the sea ice edges, somewhat for the same reasons. Salinity is more sensitive to sea ice formation or melting processes than the temperature, thus the sea ice deviations do not exist only in the Labrador shelf break but spread into the Labrador shelf. This indicates that the salinity deviations are also associated with the sea ice changes caused by the perturbed atmospheric conditions.

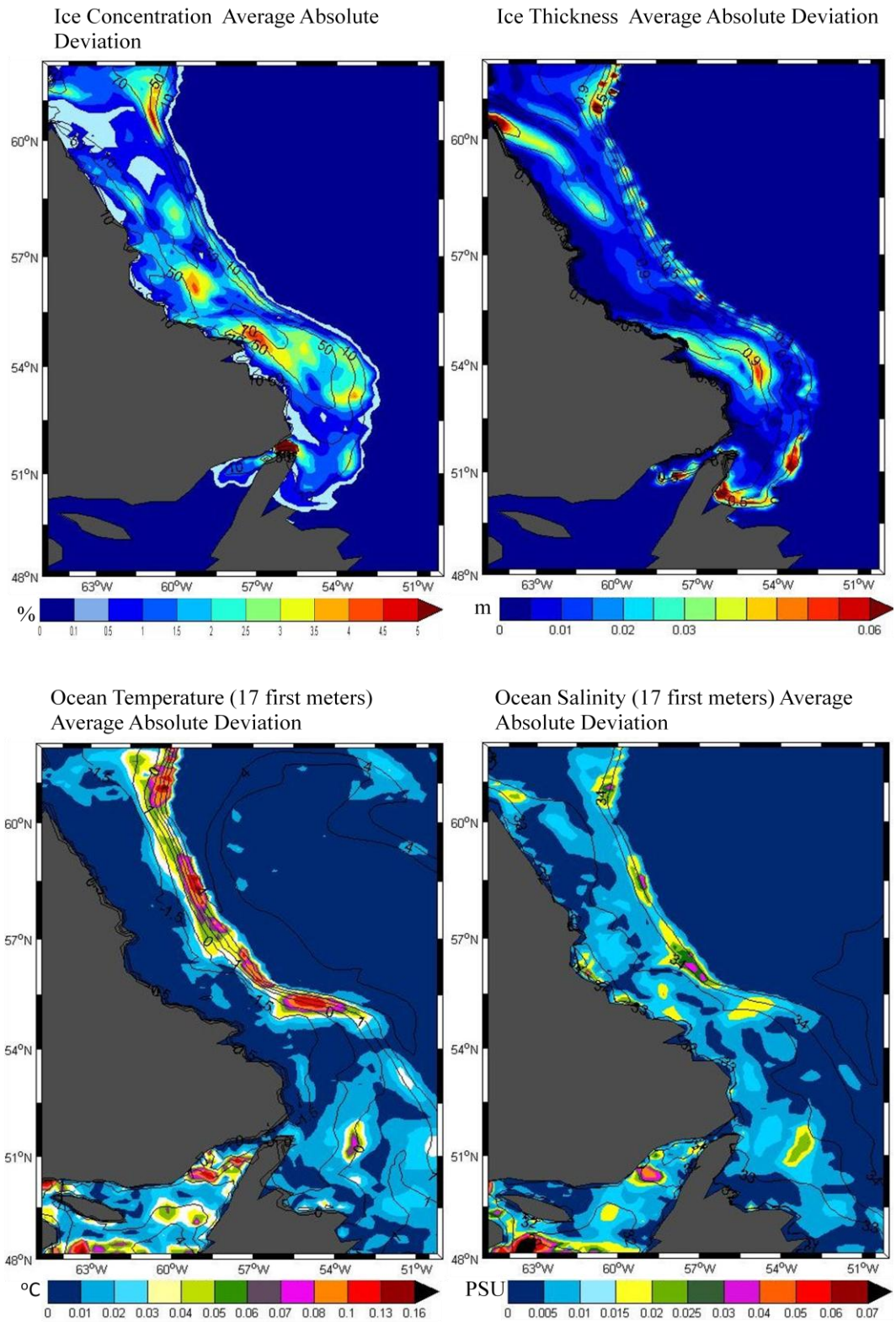

Figure 5.2: The ten member ensemble resulting sea ice concentration, sea ice thickness, ocean salinity (for the first 17 meters) and ocean temperature (for the

first 17 meters) average absolute deviations from the prognostic simulation fields are presented for the first 15 days of January of 2002. The contour lines indicate the prognostic simulation values of each field. Attention should be paid to the nonlinearity of the colourbar.

5.1.2 Correlations between Sea Ice Concentration and Tracers

Based on the ten version model results obtain following the procedure described in section 5.1.1, the cross-covariances (Appendix B) between sea ice concentration and sea ice thickness, ocean salinity and ocean temperature fields were calculated, at each grid cell and at each depth. The covariates between one grid cell's fields and another's grid cell fields were ignored. An alternative approach would be to choose a radius of influence around each grid cell to calculate the covariances inside this radius of influence. But the approach of cross-covariances calculated at each grid cell can be considered as the first step that someone must follow in order to move to more complicated methods. Thus in this study we decided to use cross-covariances calculated only within each grid cell.

The covariances between the sea ice concentration and sea ice thickness, ocean salinity and ocean temperature, for the year of 2002, are presented in Figure 5.3, 5.4 and 5.5, respectively. Figure 5.3 reveals that the covariances between the sea ice concentration and the sea ice thickness are in the majority positive, with the negative covariances generally of low value, which is mostly the case since higher sea ice concentration usually is associated with thicker sea ice.

From Figure 5.4 one can see that the majority of sea ice concentration-ocean temperature covariances (for the first 17 meters) are mostly negative (higher water temperature-lower sea ice); this is consistent with other studies (Lisaeter et al., Caya et al.). For sea ice concentration-ocean salinity covariances (for the first 17 meters) Figure 5.5 shows that the values are mostly negative, this is consistent again with other studies (Lisaeter et al., Caya et al.) and reflects the fact that in the Labrador and Newfoundland shelves, in the period of late winter and early spring,

advection effects dominate the thermodynamic effects. For an explanation of the negative sea ice concentration-ocean salinity covariance, consider the case where as the sea ice progress southwards it meets warmer waters and melts, leading to cooling and freshening of the underlying surface waters; more sea ice transport will result in the cooling of the waters and further transport into the region will lead to an increase of the sea ice concentration. So the result of the above situation is a reduction of the ocean surface salinity corresponding to sea ice concentration increasing. Such an area is near the Labrador coast around 54^{o} North, where sea ice is locally formed along the coast and is immobilized. Thus sea ice moves from the North to this area, where it meets warmer waters and starts melting and releasing freshwater as the winds drives it towards the barrier of immobilized sea ice. Eventually the newly transported sea ice freezes together with the immobilized sea ice; this is an example of how a sea ice concentration increase can lead to an ocean salinity decrease. Positive cross-covariances between the sea ice concentration and the ocean salinity indicate that the thermodynamics effects dominate over advection effects. Such an area is the Strait of Belle Isle, where there is no significant transport of sea ice from the North. The sea ice concentration covariances with the ocean salinity and temperature become weaker with depth and below around 200 meters are equal to zero.

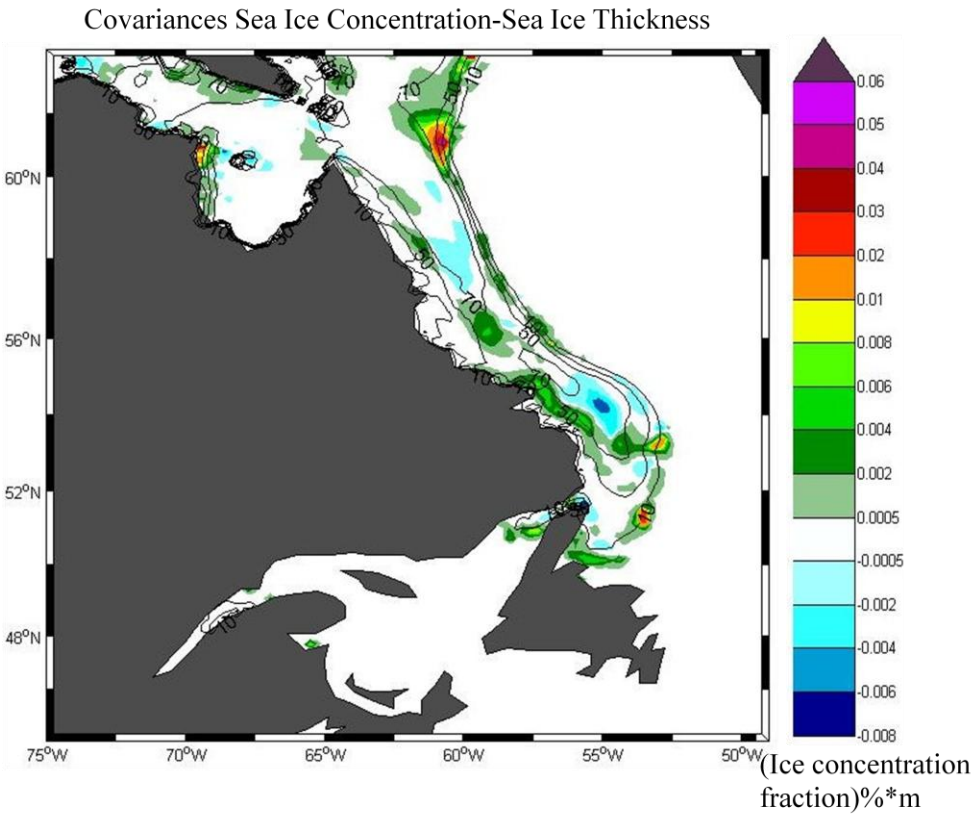

Figure 5.3: The sea ice concentration-sea ice thickness covariances. The contours represent the sea ice ocean concentrations. Attention should be paid to the non-linearity of the colourbar.

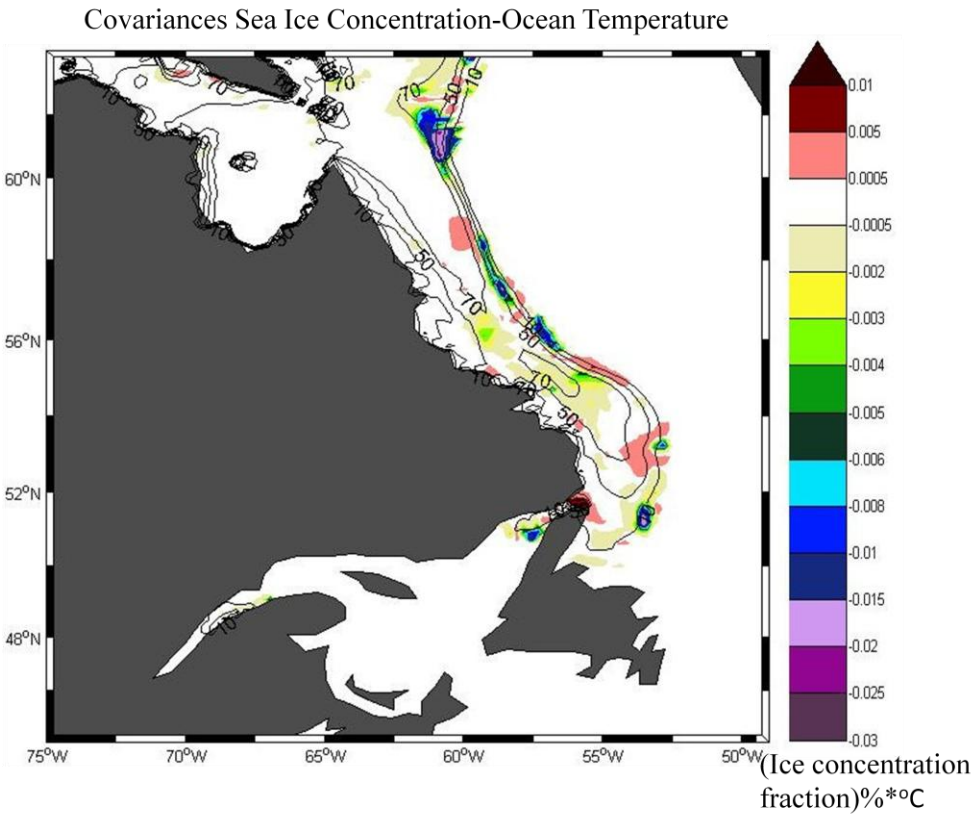

Figure 5.4: The sea ice concentration-ocean temperature covariances for the first 17 meters of the ocean. The contours represent the sea ice ocean concentrations. Attention should be paid to the nonlinearity of the colourbar.

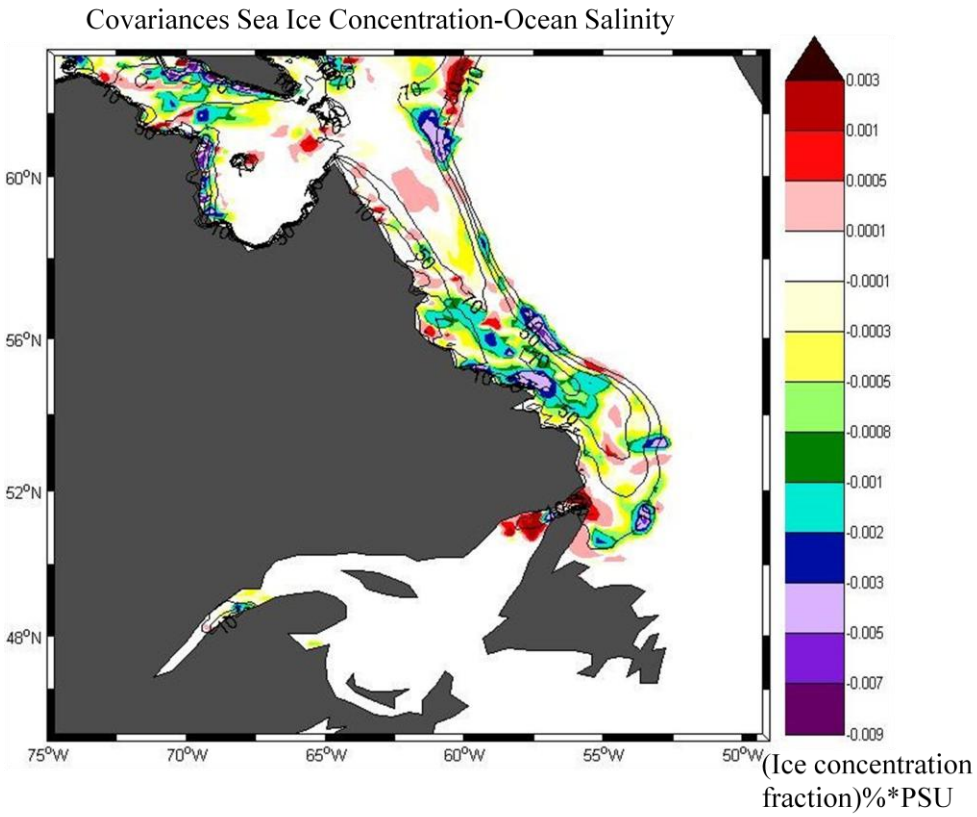

Figure 5.5: The sea ice concentration-ocean salinity covariances for the first 17 meters of the ocean. The contours represent the sea ice ocean concentrations. Attention should be paid to the nonlinearity of the colourbar.

5.2 1-D Data Assimilation Experiments Results

5.2.1 Details of the 1-D Data Assimilation Experiments

Results from the two 1-D data assimilation experiments are presented for January, February and March, where as the sea ice concentration is nudged towards the CIS sea ice concentration fields. The covariances for the first 15 days of January calculated in the above section are used to correct the sea ice thickness, the ocean salinity and the ocean temperature. A more accurate approach would be to use covariances regularly updated over the entire experiments, and not only based on the first 15 days of January. We chose this simple approach to reduce the computational cost. Also the behavior of sea ice and the physical processes associated with the sea ice are fairly constant within each season. Thus the

covariances for the first 15 days of January have been used for the winter (January, February and March) which is the season of our focus. The details of the two experiments are presented below

Table 5.2: The two 1-D data assimilation experiments details:

Experiment	**Years of Simulation**	**Nudging Coefficient**	**Assimilation Time Step**
Continuous 1-D	first 3 months of 2002	$1/(5*86400)$ sec^{-1}	Model's time step
Forecast 1-D	first 3 months of 2002	1/(sea ice model's time step) sec^{-1}	5 days

The same nudging coefficient and assimilation time step with the nudging experiments have been used to allow comparison of the 1-D experiments with the nudging experiments.

We have to mention that the two 1-D experiments were actually integrated for the first 6 months but since different processes are dominant during spring (April, May, June), we decided that using the same covariances (first 15 days of January) for spring and winter was inappropriate. Thus we only show results for the first 3 months (winter) for the 1-D experiments and ignored the following season here.

5.2.2 Sea Ice Edge

Figure 5.6 shows that the sea ice edges resulting from the two 1-D experiments are almost identical with the sea ice edges resulting from the two nudging experiments, for all three months. This was expected, since in both 1-D experiments sea ice concentration is nudged towards the CIS sea ice concentration fields exactly the same way as in the two nudging experiments. Figure 5.6 reveals that for January and specially February and March, the sea ice edge differences between the nudging and the 1-D experiments, when the experiments occur every 5 days, are slightly larger (green lines are starting to be more visible in the bottom

Figures) than the differences when the experiments occur every time step. This is associated with the different assimilation time scale of the experiments. In the forecast 1-D experiment, after the assimilation occurs, the coupled model evolves undisturbed for 5 days. Thus the impact of the underlying ocean and salinity corrections to the sea ice concentration is more profound in the forecast 1-D experiment.

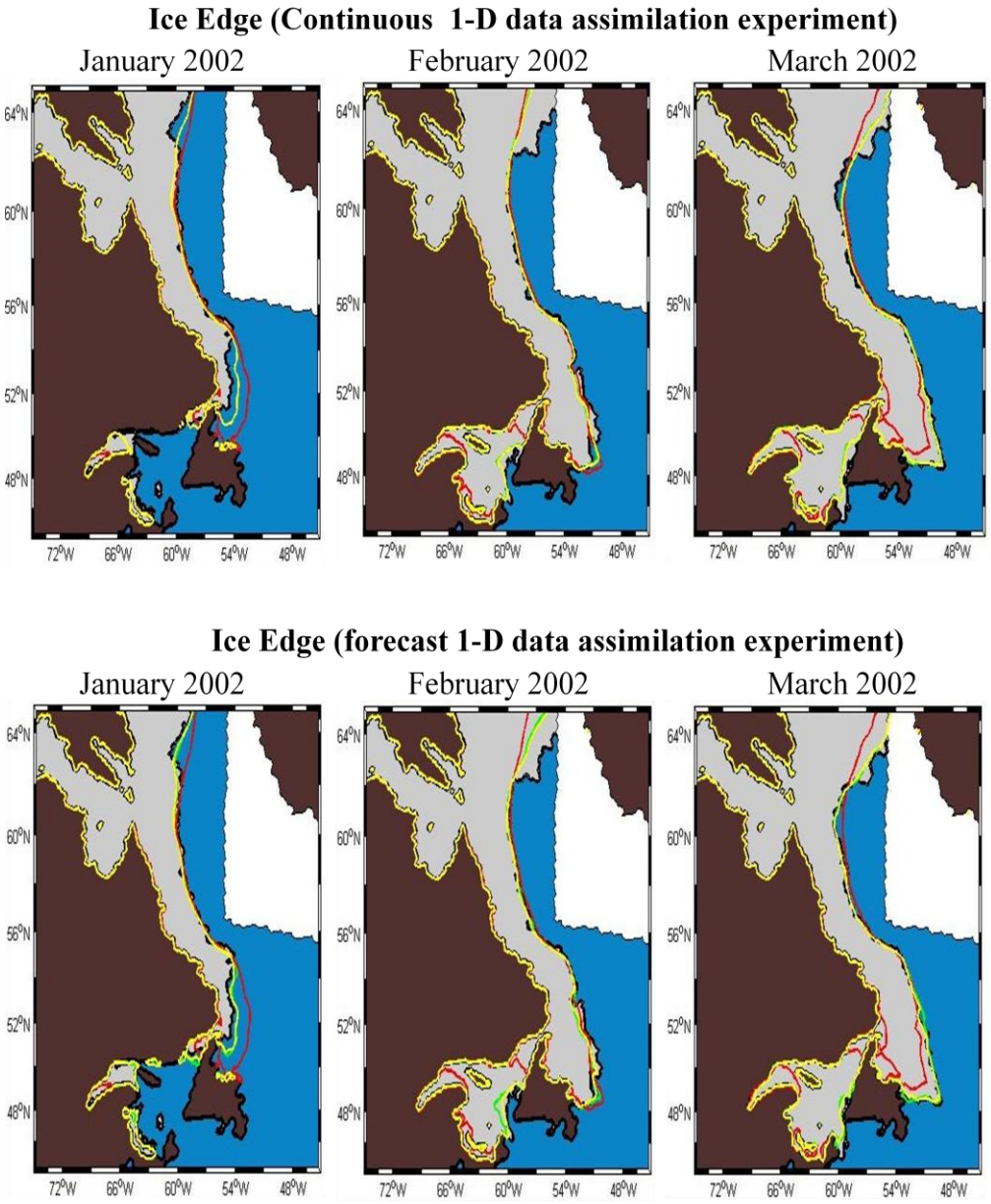

Figure 5.6: In the upper figures, the yellow lines indicate the continuous 1-D experiment sea ice edges and the green lines indicate the continuous nudging

experiments sea ice edges (not shown clearly because they are overlapped by the yellow lines). In the bottom figures, the yellow lines indicate the forecast 1-D experiment sea ice edges and the green lines indicate the forecast nudging experiments sea ice edges (not shown clearly because they are overlapped by the yellow lines). For all the figures, the red lines indicate sea ice edges resulting from the model's free run and the black lines indicate the sea ice edges produced by the Canadian Ice Service (CIS).Where the gray colour represents the region that the CIS indicates as covered by sea ice and where the white colour indicates that there are no CIS sea ice charts available.

5.2.3 Sea Ice Concentration

Figures 5.7 and 5.8 permit us to examine the sea ice concentration resulting from the forecast and the continuous 1-D experiments, correspondingly. For the middle figures, positive values indicate that the 1-D experiment overestimates the sea ice concentration, and negative values indicate that the 1-D experiment underestimates the sea ice concentration. For the right figures, positive values indicate that the 1-D experiment produces higher sea ice concentration values than the nudging experiment and negative values indicate that the 1-D experiment produces lower sea ice concentration values than the nudging experiment.

As can been seen by comparing Figures 5.7 and 5.8 with Figure 3.3, the big differences in sea ice concentration between the model's prognostic simulation results and the CIS ice fields, tend to be eliminated through the continuous and the forecast 1-D experiments. The differences in sea ice concentration between the continuous nudging and the continuous 1-D experiments (right figures) are smaller than 10%, for February and March and almost non-existent in January. This is related to the fact that the corrections that the continuous nudging imposes in January are smaller than in March and May. Thus the corrections that are imposed to the ocean fields are smaller since they are based on the changes of the sea ice concentration and as a consequence their "back influence" to the sea ice concentration will be smaller. On the other hand, Figure 5.8 reveals that the differences in sea ice concentration between the forecast nudging and the forecast

1-D data experiments are bigger (as big as 20% sea ice concentration). In the case of the forecast experiments, the discrepancies between the 1-D and the nudging experiments are of the same magnitude during all the months. This is related with the fact that the assimilation occurs every 5 days. Thus the ‘back influence” of the ocean state to the sea ice concentration is not only associated with the corrections imposed on the ocean state but with the changes that occurred to the ocean fields from the undisturbed evolution of the model, during the 5 days. For the same reasons, and in addition with the fact that the two nudging experiments result in different concentration fields (chapter 4), the spatial distribution of the sea ice concentration differences between the continuous experiments and between the forecast experiments is different.

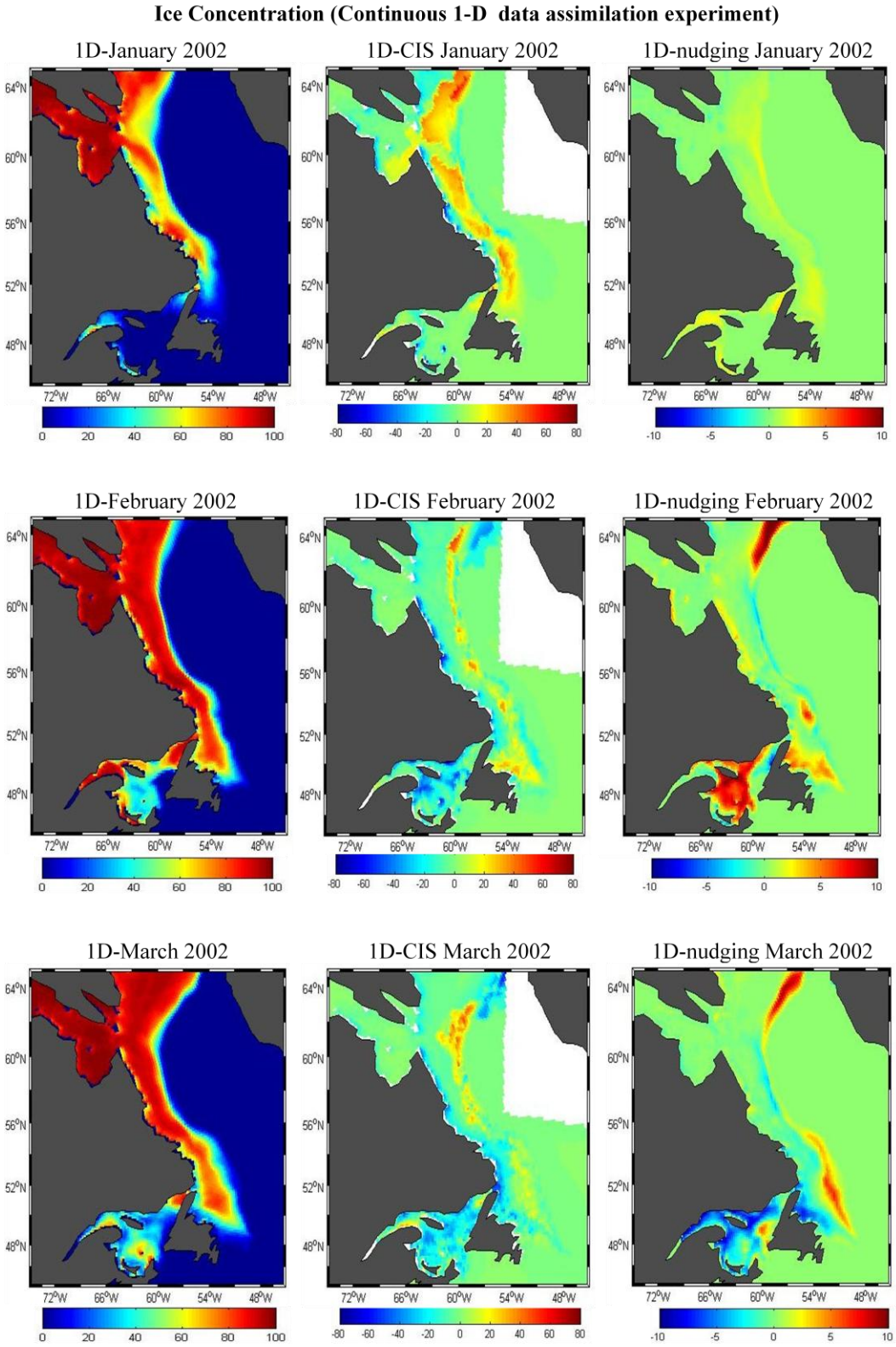

Figure 5.7: On the left, the sea ice concentration fields resulting from the continuous 1-D experiment, in the middle the sea ice concentration differences

between the continuous 1-D experiment and the CIS and on the right the sea ice concentration differences between the continuous 1-D and the continuous nudging experiments are presented for January, February and March of 2002.

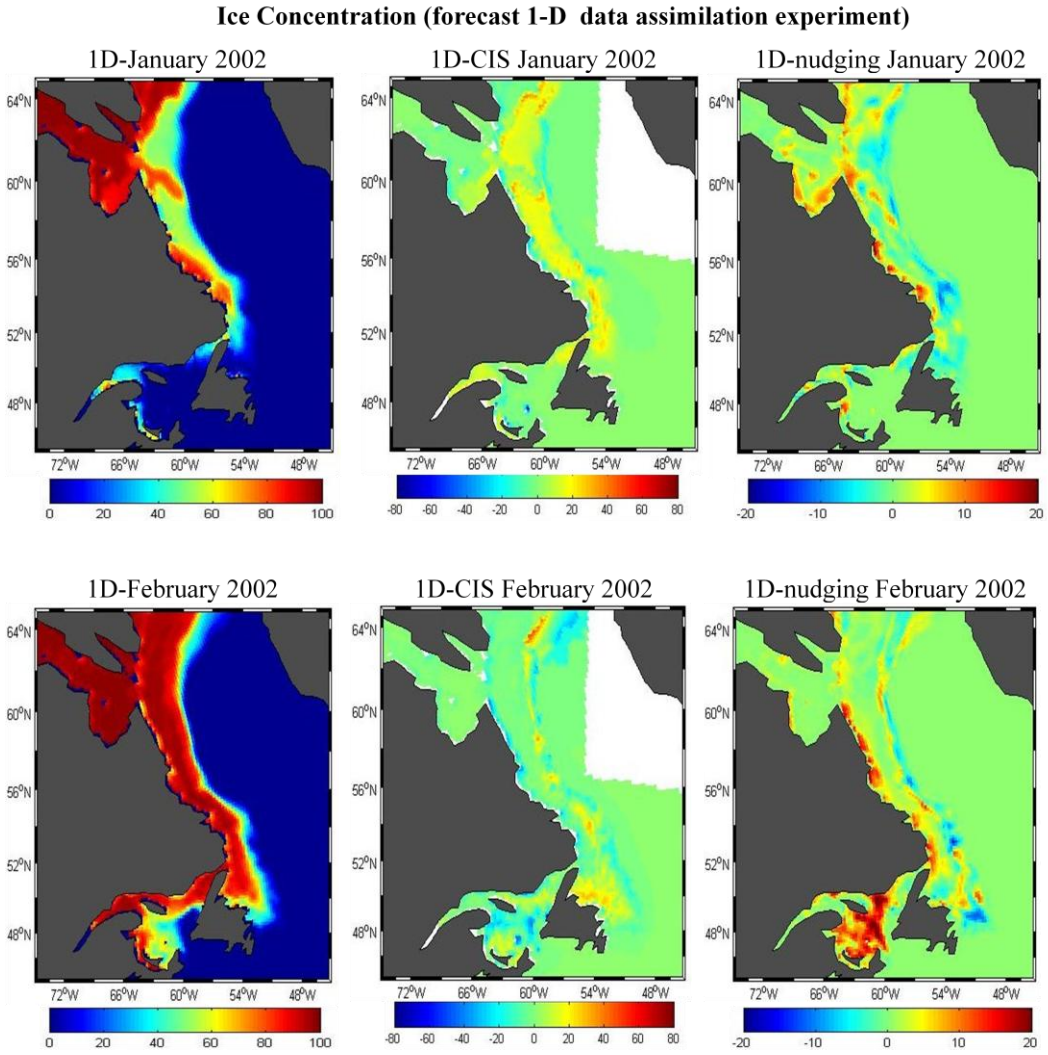

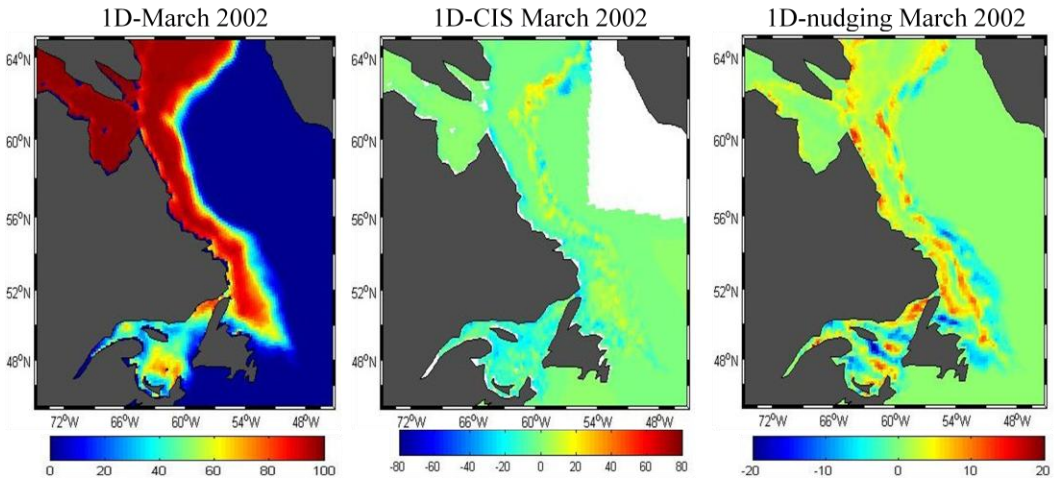

Figure 5.8: On the left, the sea ice concentration fields resulting from the weal 1-D experiment, in the middle the sea ice concentration differences between the forecast 1-D experiment and the CIS and on the right the sea ice concentration differences between the forecast 1-D and the continuous nudging experiments are presented for January, February and March of 2002.

5.2.4 Sea Ice Covered Area

Figure 5.9, upper picture, reveals that the sea ice covered area produced by the continuous 1-D experiment is in close agreement with the CIS sea ice covered area and almost identical with the sea ice covered area resulting from the continuous nudging experiment. The sea ice covered area absolute error figure indicates that the continuous 1-D sea ice covered area is general, in slightly better agreement (less than $5*10^3$ km^2) with the CIS data with some noticeable exceptions like the first days of February and March and the middle 15 days of January. The similarities between the sea ice covered areas, produced by the continuous 1-D and by the continuous nudging experiments, confirm that the sea ice concentration differences between the two experiments are very small, as was seen from the sea ice concentration fields comparison.

Figure 5.9, bottom picture, indicates that the sea ice covered area resulting from the forecast 1-D experiment is close to the sea ice covered area resulting from the forecast nudging experiment but their differences are more profound than those

between the continuous nudging and the continuous 1-D experiments. This is better seen through Figure 5.10, where the forecast 1-D experiment results generally in lower (as much as $2*10^4$ km^2) sea ice covered area absolute error than the forecast nudging experiment, while the sea ice covered area absolute error differences between the continuous experiments reach only as large as $5*10^3$ km^2. This confirms that the forecast 1-D experiment causes greater changes to the nudged field (sea ice concentration), than the continuous 1-D experiment, through the alteration of the underlying salinity and temperature. The fluctuations existing in the forecast nudging experiment tend to become smoother in the forecast 1-D experiment. Thus the forecast 1-D sea ice covered area generally drifts less from the CIS as can be seen in Figure 5.10. This leads us to the belief that in the forecast 1-D experiment the sea ice and the ocean fields are successfully balanced.

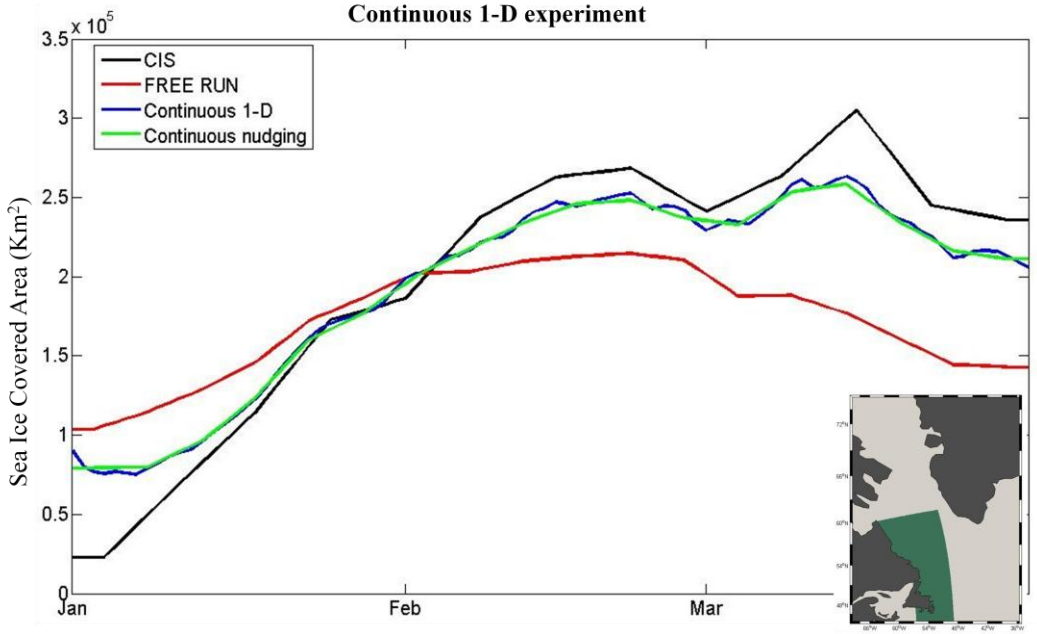

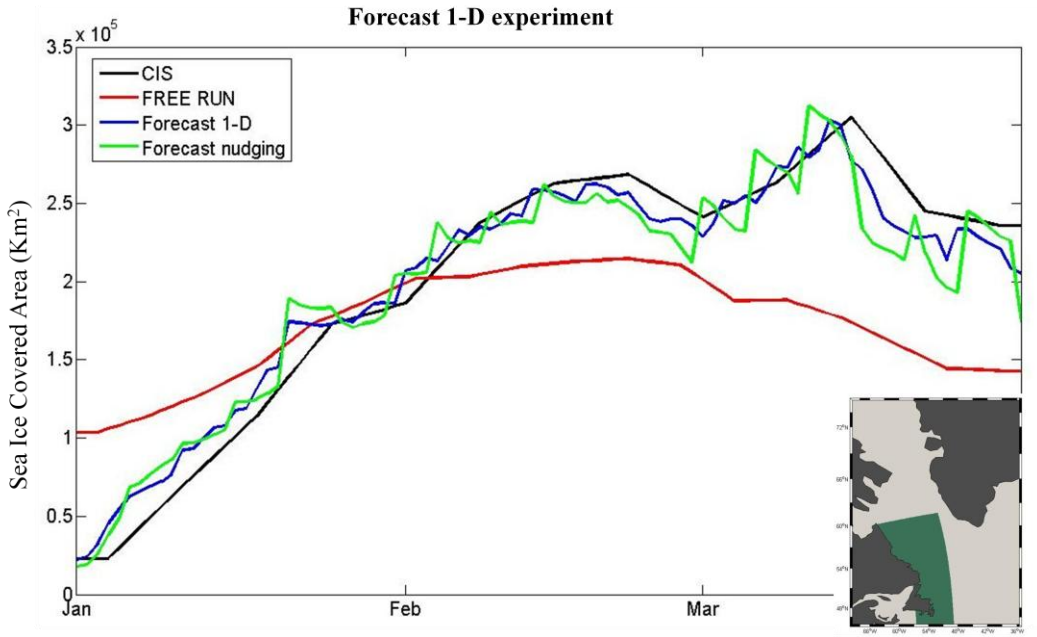

Figure 5.9: The time series of the sea ice covered area for the first 3 months of 2002. The sea ice covered area produced by the model's free run is represented with red, the sea ice covered area produced by the CIS is represented with black, the sea ice covered areas resulting from the 1-D experiments are represented with blue and the sea ice covered areas resulting from the nudging experiments are

represented with green. The upper picture is for the continuous experiments and the bottom picture is for the forecast experiments. All of the sea ice covered areas are computed for the region highlighted in green in the inset.

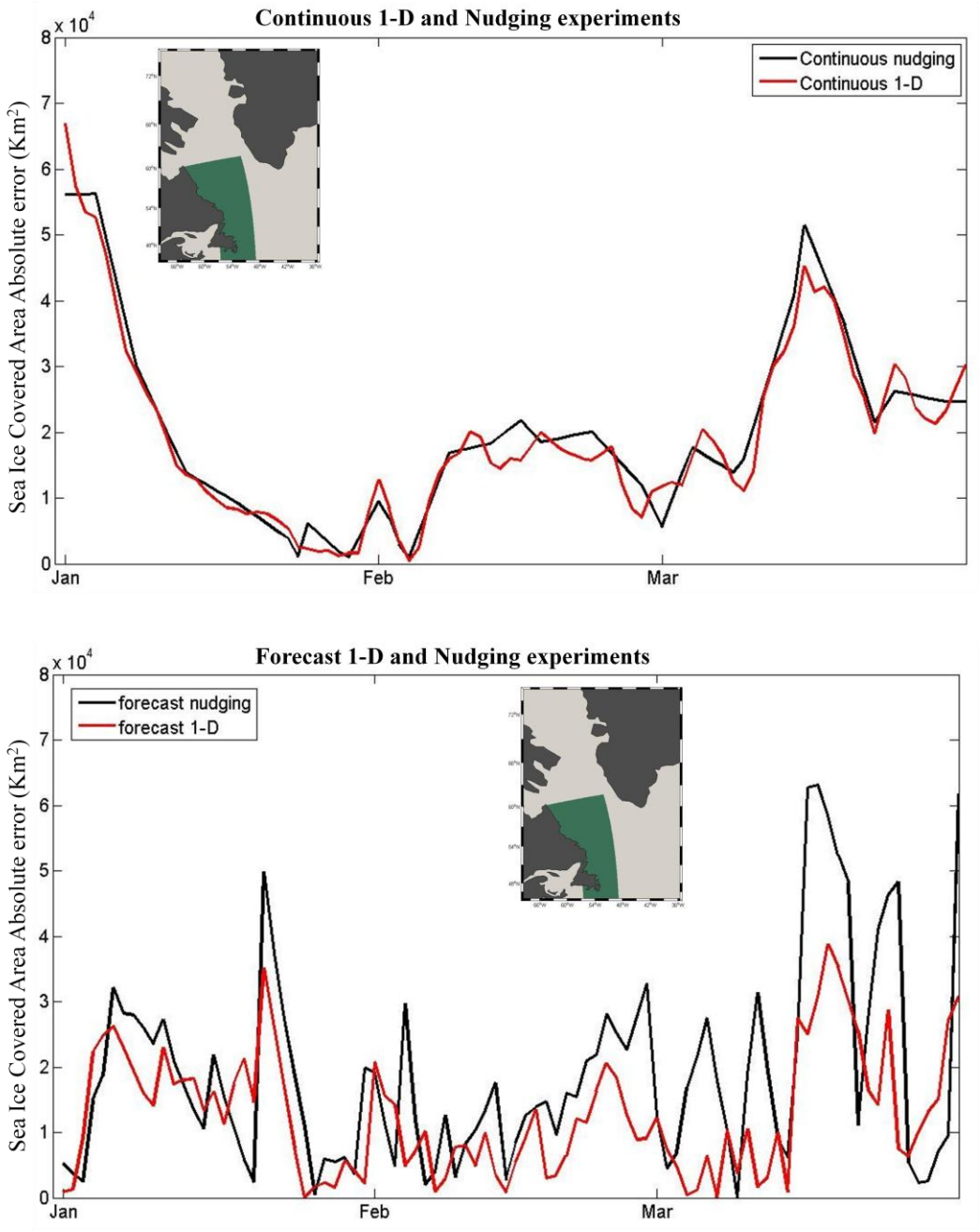

Figure 5.10: The time series of the sea ice covered area absolute error for the continuous nudging (black) and for the continuous 1-D (red) experiments are presented in the upper picture and the time series of the absolute error for the

forecast nudging (black) and for the forecast 1-D (red) experiments are presented in the bottom picture.

5.2.5 Sea Ice Thickness

The sea ice thickness fields produced by the continuous 1-D experiment (not shown) have the same structure as the sea ice thickness fields produced by the continuous nudging experiment. Differences are relative small (as much as 15 cm). These differences reflect the sea ice thickness corrections that were imposed in the continuous 1-D experiment and the influence from the corrections on the ocean state. In Figure 5.11, the sea ice thickness differences between the forecast 1-D data assimilation experiment and the forecast nudging experiment are presented (positive values indicate that the 1-D experiment results in higher values). The sea ice thickness differences, between the forecast experiments, reach 30 cm. Thus the sea ice differences between the forecast experiments are bigger than between the continuous experiments. This is associated with the fact that the sea ice thickness differences between the forecast experiments, are not only based on the sea ice thickness corrections (like the differences between the continuous experiments), but also on the forecast 1-D experiment's sea ice thickness different evolution from the forecast nudging experiment for 5 days, after the imposition of these corrections. In addition, the forecast 1-D experiment ocean fields (salinity and temperature) evolve differently than the forecast nudging experiment ocean fields, during the 5 days of free evolution, since their initial conditions are corrected and thus their impact on the sea ice thickness fields is different.

For January, along the sea ice edges, the forecast 1-D experiment results in 10 cm lower sea ice thicknesses than the forecast nudging experiment. Along the South Labrador coast and the path where the export of sea ice from the Hudson Bay takes place, the forecast 1-D experiment produces 10 to 20 cm thicker sea ice. For February, along the Labrador coast, the forecast 1-D experiment produced sea ice that is thicker by 5 to 10 cm and by 10 to 20 cm in the Newfoundland shelf. In the Gulf of Saint Lawrence and in the majority of the sea ice edge, the forecast 1-D

experiment sea ice is thinner by 10 to 15 cm and 5 cm, respectively. For March, in the Labrador and Newfoundland shelves, the forecast 1-D sea ice is 10 to 30 cm thicker. On the other hand, along the sea ice edge below the 54^{o} latitude and in the Gulf of Saint Lawrence, the sea ice is thinner by around 10 cm.

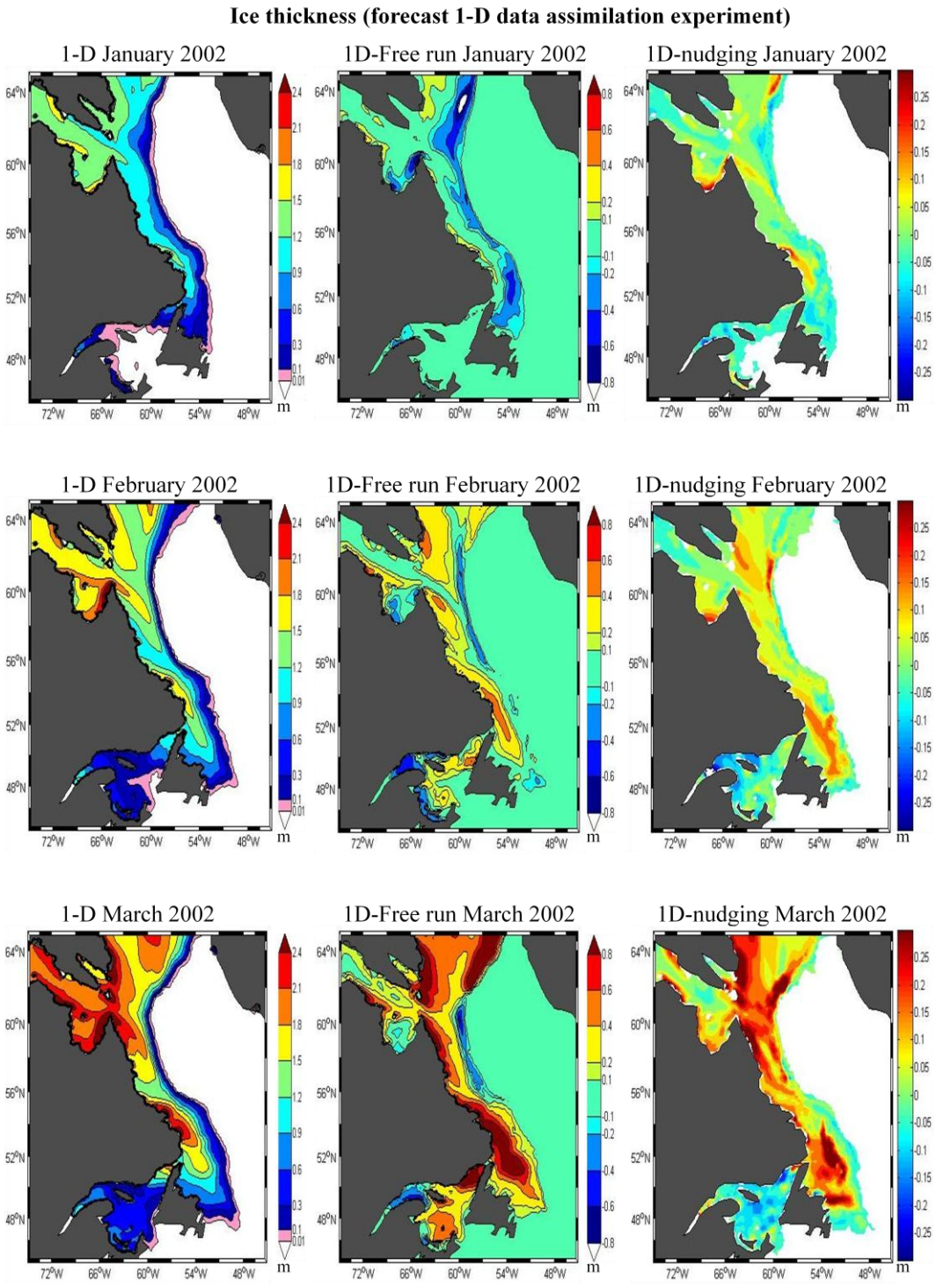

Figure 5.11: The sea ice thicknesses resulting from the forecast 1-D (on the left), the sea ice thickness differences between the forecast 1-D experiment and the model's prognostic simulation (in the middle) and the sea ice differences between

the forecast 1-D and the forecast nudging experiments (on the right), are presented for January, February and March of 2002.

5.2.6 Underlying Ocean Salinity and Temperature

The differences in ocean temperature and salinity, between the continuous nudging experiment and the continuous 1-D experiment (Figure 5.12 and 5.13), are small on the Labrador and Newfoundland shelves and exist mainly along the shelf breaks, where the sea ice edges lie. For January, the temperature and salinity differences are small. The forecast 1-D experiment produces 0.05 to 0.1 ^{o}C lower temperatures than the forecast nudging experiment along the North Labrador sea ice edge and 0.05 to 0.1 ^{o}C higher temperatures along the South Labrador sea ice edge. These temperature differences correspond to a $2*10^{9}$ J heat content increase in the areas where the temperature increased and to a $2*10^{9}$ J heat content decrease in the areas where the temperature decreased. The continuous 1-D experiment results in 0.02 to 0.03 PSU higher salinities than the continuous nudging experiment along the South Labrador shelf break, along the Newfoundland shelf break and along the coast of the Labrador Sea. The corresponding decrease in the fresh water content, in these areas, is 3 to 5 m^{3}. Along the North Labrador shelf, the forecast 1-D experiment salinities are 0.02 to 0.03 PSU lower than in the continuous nudging experiment, corresponding to around a 4 m^{3} increase in freshwater content.

In March, the salinity and the temperature differences between the two continuous experiments are larger than in January. In this month, the continuous 1-D experiment temperatures and salinities are 0.3 to 0.6 ^{o}C and 0.2 to 0.3 PSU lower, respectively, along the Labrador and Newfoundland shelf breaks. These differences in temperature and salinity correspond to a $0.5*10^{9}$ to $1*10^{9}$ J heat content loss and a 10 to 20 m^{3} freshwater content gain in the continuous 1-D experiment. During all the months, the temperature and salinity differences between the continuous 1-D and the continuous nudging experiments, match to some extent, the sea ice concentration differences (Figure 5.7), in the areas where sea ice exists. The salinity and temperature differences, in the South of the

domain where the Labrador Current meets the Gulf Stream, indicate a small dissimilarity in the mixing of those two waters between the continuous 1-D and the continuous nudging experiments.

Figures 5.14 and 5.15 reveal that the differences in the ocean's salinity and temperature, between the forecast 1-D and the forecast nudging experiments, are not the same as the differences between the continuous 1-D and the continuous nudging experiments. This is again based on the fact that in the forecast experiments, the assimilation occurs every 5 days and thus the ocean fields evolve dissimilarly. For January, the continuous 1-D experiment produces 0.2 to 0.5 ^{o}C higher temperatures and 0.1 to 0.2 PSU higher salinities along the North Labrador shelf break, in comparison to the forecast nudging experiment. The forecast 1-D experiment results in approximately 0.2 PSU higher salinities than the forecast nudging experiment along the Labrador coast. Due to the above differences in salinity and temperature, the forecast 1-D experiment results in a $0.5*10^{10}$ to $1*10^{10}$ J higher heat content and in a 10 m^3 lower freshwater content along the North Labrador shelf break, and in a 10 to 20 m^3 higher freshwater content along the Labrador coast.

For March, the forecast 1-D experiment produces 0.4 to 0.7 ^{o}C higher temperatures along the North Labrador shelf break and 0.2 to 0.3 ^{o}C lower temperatures along the South Labrador and the Newfoundland shelf breaks, in comparison to the forecast nudging experiment. These temperature differences correspond to a heat content loss, in the forecast 1-D experiment, between $0.5*10^{10}$ and $1.5*10^{10}$ J along the North Labrador shelf break and a heat content gain between $0.5*10^{10}$ and $1*10^{10}$ J along the South Labrador and the Newfoundland shelf breaks. The forecast 1-D experiment salinities are 0.1 to 0.4 PSU lower (correspond to a 10 to 60 m^3 gain in freshwater content) along the North Labrador shelf break and the Labrador coast and a 0.1 PSU higher (corresponding to a 15 m^3 loss of freshwater content) along the South Labrador and Newfoundland shelf breaks.

The temperature and salinity differences between the forecast 1-D and the forecast nudging experiments, match to some extent the differences in the sea ice concentration (Figure 5.7). The salinity changes are in better agreement with the sea ice concentration changes than the temperature changes. Again as we saw in chapter 4, this indicates that the salinity fields are more sensitive to the sea ice concentration changes. Again in the South of the domain, where the Labrador Current meets the Gulf Stream, the forecast 1-D and the forecast nudging experiments produce different salinities and temperatures. This indicates dissimilarity in the mixing of those two waters between the two forecast experiments.

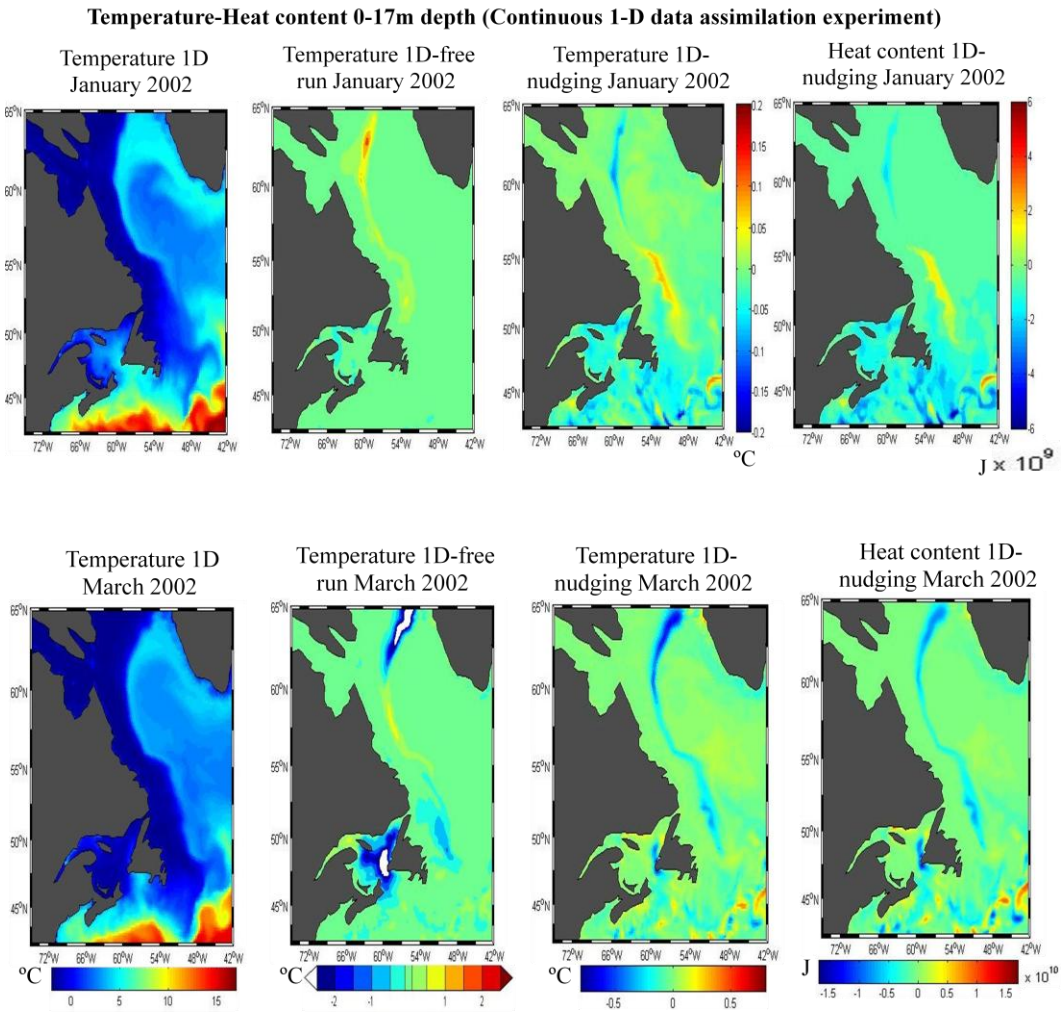

Figure 5.12: The ocean temperature, for the first 17 meters, resulting from the continuous 1-D experiment, the ocean temperature differences, for the first 17 meters, between the continuous 1-D experiment and the model's prognostic simulation and the ocean temperature and the heat content differences, for the first 17 meters, between the continuous 1-D and the continuous nudging experiments are presented, for January and March of 2002 (attention should be paid to the differences in the colour scale between January and March).

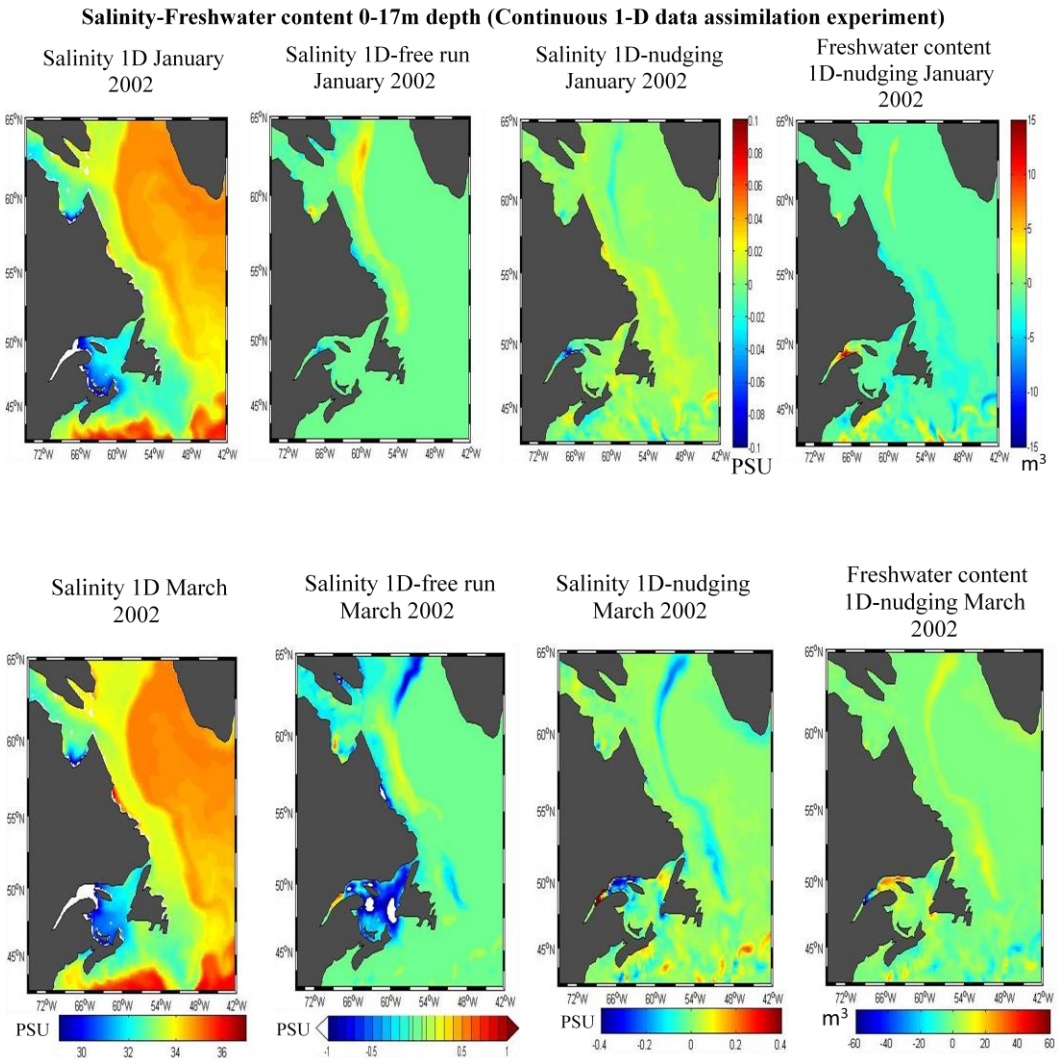

Figure 5.13: The ocean salinity, for the first 17 meters, resulting from the continuous 1-D experiment, the ocean salinity differences, for the first 17 meters, between the continuous 1-D experiment and the model's prognostic simulation and the ocean salinity and freshwater content differences, for the first 17 meters, between the continuous 1-D and the continuous nudging experiments are presented, for January and March of 2002 (attention should be paid to the differences in the colour scale between January and March).

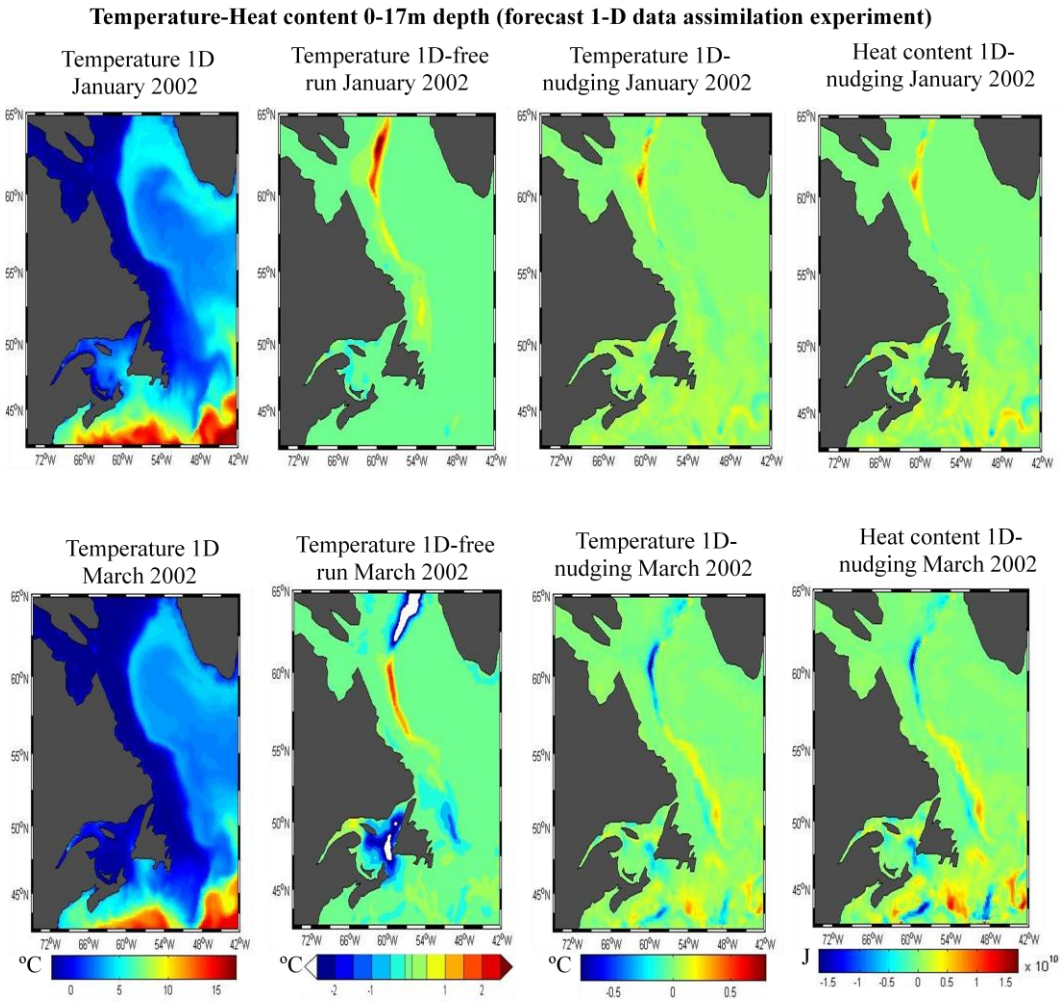

Figure 5.14: The ocean temperature, for the first 17 meters, resulting from the forecast 1-D experiment, the ocean temperature differences, for the first 17 meters, between the forecast 1-D experiment and the model's prognostic simulation, and the ocean temperature and heat content differences, for the first 17 meters, between the forecast 1-D and the forecast nudging experiments are presented, for January and March of 2002.

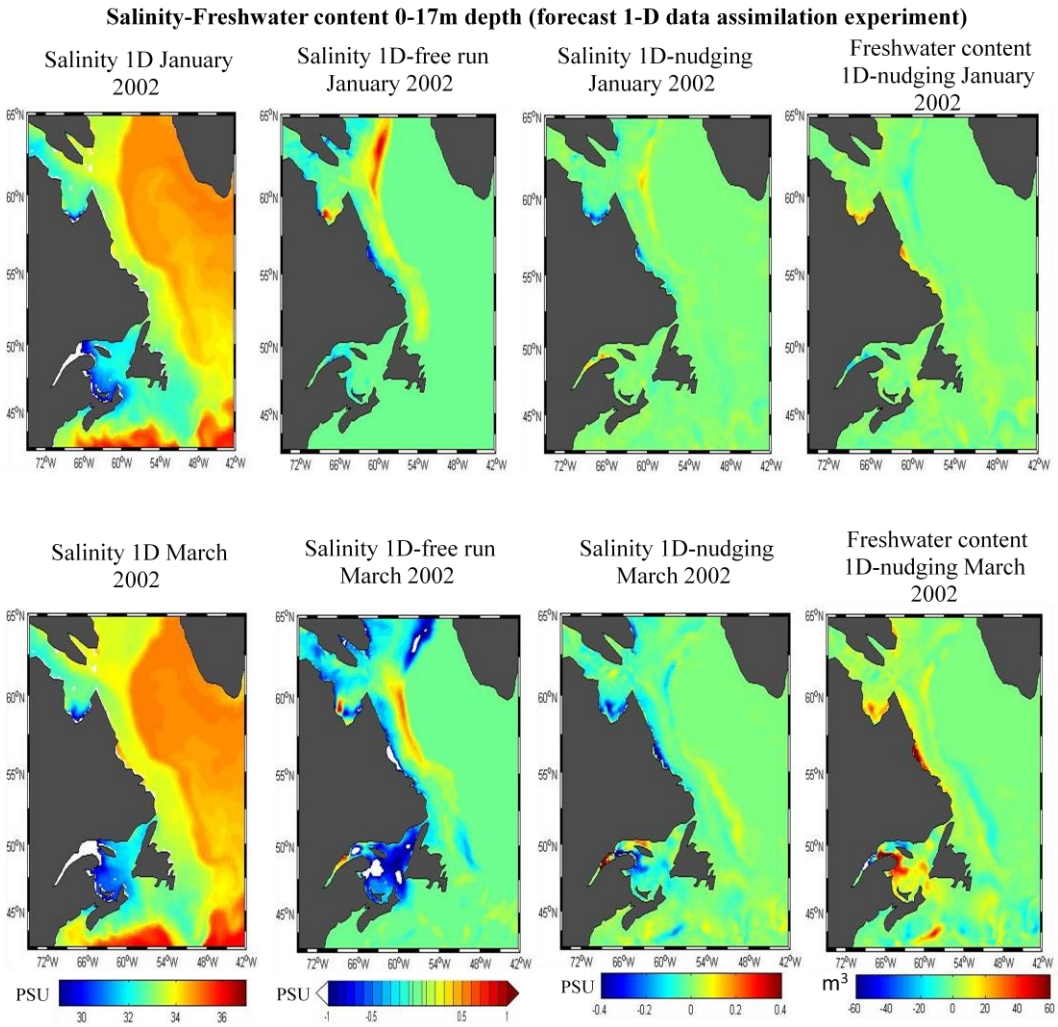

Figure 5.15: The ocean salinity, for the first 17 meters, resulting from the forecast 1-D experiment, the ocean salinity differences, for the first 17 meters, between the forecast 1-D experiment and the model's prognostic simulation, and the ocean salinity and freshwater content differences, for the first 17 meters, between the forecast 1-D and the forecast nudging experiments are presented, for January and March of 2002.

5.3 Evaluation of the Two 1-D Data Assimilation Experiments

In the continuous 1-D experiment, the resulting sea ice concentration fields have small discrepancies from the sea ice concentration fields resulting from the continuous nudging experiment, due to the corrections to the underlying salinity and temperature and the sea ice thickness fields. The differences in the sea ice

concentration fields, between the forecast 1-D and the forecast nudging experiments, are larger (as large as 10% sea ice concentration). This is due to the fact that, in the continuous 1-D experiment, the sea ice concentration is pushed towards the CIS fields in every time step, as the corrections occur to the underlying ocean. Thus the continuous 1-D experiment does not allow us to clearly see how the free evolution of the ocean state, after the corrections to salinity and temperature towards more appropriate conditions, is going to impact the sea ice and vice versa, which is the case in the forecast 1-D experiment. In the continuous 1-D experiment, by correcting the underlying ocean, the sea ice fields become somewhat better, as is shown in Figure 5.9, where the sea ice covered area resulting from the continuous 1-D experiment is generally in slightly closer agreement (less than 0.1 km^2), with the CIS sea ice covered area. This indicates that, to some extent, the balance between the sea ice fields and the ocean fields was achieved. The balance between the sea ice fields and the ocean fields becomes more profound in the forecast 1-D experiment. By looking Figure 5.9, it is clear that the sea ice covered area fluctuations are significantly smaller in the forecast 1-D experiment, than in the continuous nudging experiment. This is interpreted as: the sea ice concentration, in the forecast 1-D data assimilation experiment, is not allowed to drift as much away from reality (CIS) as in the forecast nudging experiment, during the 5 days period of the free model's evolution, but instead is always restrained closer to the CIS sea ice concentration fields through the ocean fields (salinity, temperature). The ocean fields' dissimilar evolution, during the 5 days period, between the forecast 1-D data assimilation experiment and the forecast nudging experiment, is associated with the initial conditions of salinity and temperature, before the start of the 5 days period of free evolution.

CHAPTER 6

Conclusions

In this study it was shown that the NEMO sea ice/ocean coupled model's sea ice results drift from the observations (Canadian Ice Service sea ice fields), for the region of the Canadian East coast, for the years of 2002 to 2005 (chapter 3). The sea ice concentration fields that resulted from the model's prognostic simulation had many discrepancies from the sea ice concentration fields produced by the Canadian Ice Service. The Canadian Ice Service sea ice fields are accepted as close representation of reality. On January 2002, the model overestimated by 20% to 50% the sea ice concentration in the Labrador and Newfoundland shelves and underestimated by 20% to 50% the sea ice concentration along the Labrador and Newfoundland coast and in the Gulf of Saint Lawrence. For March of 2002, this overestimation is present only along the North Labrador shelf break. In this month, the model underestimates by 20% to 80% the sea ice concentration in the South Labrador and Newfoundland shelves, along the coast of Labrador shelf and in the Gulf of Saint Lawrence. The big underestimation of the sea ice concentration in the Gulf of Saint Lawrence was due to the fact that the model indicated this area as ice free. For May 2002 the model overestimated by 20% to 70% the sea ice concentration offshore of the Labrador shelf and underestimated by 20% to 30% the sea ice concentration on the Newfoundland shelf. Overall the same was the case for all the years of the simulation. The model's prognostic

simulation generally underestimated the sea ice covered area for the Labrador and Newfoundland shelves, with the only exception being the period of the initiation of sea ice formation in the region (December-January). For the time period of maximum sea ice (around March) the underestimation was around $1*10^5$ km^2 for all the years except 2004 where the underestimation was only $0.4*10^5$ km^2. Although there are no direct measurements of sea ice thickness for the Canadian East coast, we used information provided by the Canadian Ice Service about the stage of sea ice development to validate the model's results. The comparison of these fields with the model's state of sea ice development fields revealed that they were in reasonable agreement, but small discrepancies were present. Thus the purpose of the study was to produce more accurate sea ice model fields by using data assimilation.

The two nudging experiments that were conducted for this study (chapter 4), brought desirable changes in the sea ice concentration fields for the Labrador and Newfoundland shelves. The continuous nudging experiment brought improvements in sea ice concentration with drift from reality less than 40%, for all of the year of 2002. The improvements using the forecast nudging were larger and led to differences around 30% with the CIS. On average both the experiments resulted in sea ice covered area very close to the CIS sea ice covered area. The improvement of sea ice covered area was clear during the maximum sea ice period. A closer look at the sea ice covered area resulting from the nudging experiments revealed that in the forecast nudging experiment the sea ice covered area is closer to the CIS than the continuous nudging experiment only during the days that nudging occurred. During the 5 days where the model was left to progress freely, the forecast sea ice covered area started to drift away from the CIS, until it was pushed back again after 5 days through nudging. The forecast experiment nudging coefficient is large, pushing the sea ice concentrations instantaneously to become almost equal to the CIS sea ice concentrations, before they start drifting during the 5 next days. The use of this large nudging coefficient is associated with the fact that the monthly sea ice concentration fields produced by the forecast nudging experiment are in better agreement with the reality.

The forecast nudging experiment is more practical, since the nudging occurred every 5 days. Thus the forecast nudging experiment effectively produces a 5 days ahead forecast. The sea ice thickness, the ocean salinity and temperature were indirectly altered though the sea ice-ocean coupled model physics in the two nudging experiments. These alterations did not help to keep the sea ice fields close to the CIS sea ice charts as it can be seen by the fluctuations in the forecast nudging experiment's sea ice covered area. Thus, one can understand that to suppress the drift, a balance between the sea ice and the ocean state should be attained.

To achieve that balance, we conducted two additional experiments (1-D experiments), where as the sea ice concentration was nudged, corrections occurred to the sea ice thickness and the ocean salinity and temperature (chapter 5). This is achieved by using cross-covariances, between the sea ice concentration and the sea ice thickness and between the sea ice concentration and the ocean salinity and temperature. These cross-covariances were obtained by random perturbation made to the forcing fields, following the approach of Robert and Alves, 2005. Thus, ten member ensembles with random perturbations to the atmospheric forcing fields were conducted and used to obtain the cross-covariances. The cross-covariance between the sea ice concentration and the sea ice thickness were generally positive, while the sea ice concentration-ocean salinity and sea ice concentration-ocean temperature cross-covariances were generally negative.

The continuous 1-D experiment appeared to result in slightly better sea ice fields than in the continuous nudging experiment. The sea ice edges where almost identical in both the continuous nudging and the continuous 1-D experiments, with the continuous 1-D experiment having small improvements. The continuous 1-D sea ice concentration improvements did not exceed 10%. The sea ice covered area comparison revealed that the continuous 1-D experiment was in slightly better agreement with the CIS charts than the continuous nudging experiment. The sea ice differences between the continuous nudging and the continuous 1-D

experiments reflected the differences in the ocean fields due to the corrections that they were applied to them. The impact of these corrections was understood through a forecast 1-D experiment, where the assimilation occurred every 5 days and thus the model had the opportunity to prognostically evolve for 5 days. This allowed us to see how the corrections of initial conditions of the ocean state impacted the short term sea ice concentration forecast of the model (5 days).

The sea ice edges resulting from the forecast 1-D experiment were slightly closer to the observations than in the forecast nudging experiment. The forecast 1-D experiments improved on the forecast nudging experiment sea ice concentration by 10 to 20%. The comparison of the sea ice covered area in the forecast 1-D experiment sea ice covered area with the forecast nudging experiment revealed that the drift (fluctuations) was suppressed in the forecast 1-D experiment. The above led to the conclusion that the corrections made to the ocean salinity, the ocean temperature and the sea ice thickness worked to achieve a balance between the sea ice state and the ocean state. This balance was the reason why during the 5 days of the model's free evolution, the forecast 1-D sea ice fields drifted less from the CIS charts than in the forecast nudging experiment. The above indicates that the method of using the ten member ensemble model results, with random perturbation to the forcing fields, is a useful way of creating covariances between relative fields (sea ice-ocean) and, based on them, correct these fields to achieve a better forecast.

Finally, at the end of this thesis, we would like to mention some additional results. The ideal approach would be to regularly compute and update cross-covariances over the entire experiments. In order to save computational time, cross-covariances between sea ice concentration and ocean salinity and ocean temperature, computed for a small time period of winter season (in our case the 15 first days of January) can be used for corrections to the entire season. On the other hand, it is not as efficient to use cross-covariances obtained from the winter season, for applying corrections to the spring season. The reasons are that during the winter season (January, February and March) in the Labrador and

Newfoundland shelves the sea ice has almost the same behavior. After the first appearance of sea ice during December in the area, the sea ice continues growing and advancing towards South until March, when the sea ice reaches its maximum growth and extent. Thus the corrections based only on the first 15 days of January cross-covariances for the entire winter season are realistic. In April the sea ice starts melting and retreating to the North, until it disappears completely from the domain by the end of June. Thus the behavior of the sea ice during spring (April, May, June) is different than in the winter, with melting being the dominant physical process. Therefore, in the spring the thermodynamic processes (melting) are responsible for the behavior of the sea ice. On the other hand, during winter, in addition to thermodynamic processes (formation), dynamic processes (the transportation of sea ice) are also responsible for the behavior of the sea ice and, in some areas, the dynamic effects dominate the thermodynamic effects. Thus the covariances computed for the first 15 days of January carry that information, for example salinity-sea ice concentration covariances, for most of the area, are negative, reflecting the dominant dynamic effects. The use of these covariances during spring is not realistic and does not lead to a balance between the sea ice state and the ocean state.

This study can be considered as the first step towards the exploration of the impact of sea ice data assimilation in a sea ice/ocean coupled model. In the future, it would be interesting to conduct a forecast assimilation experiment with corrections to the ocean salinity and temperature based on covariances calculated inside a radius of influence around each grid cell. Furthermore, this study focused only on the year 2002, a relatively high sea ice year. It would be interesting to explore the impact of sea ice data assimilation on a low sea ice year (e.g. 2004). To conclude, in the above study, in order to save computational time, we used cross-covariances obtain for the first 15 days of January for corrections over the winter months. In order to produce more accurate results, the corrections applied to the ocean fields can be based on covariances obtained for the entire time period of the simulation.

Bibliography

Aagaard, K. and E. C. Carmack (1989), The role of sea ice and other fresh water in the Arctic circulation, Journal of Geophysical Research, 94, 14,485-14,498.

Alves, O. and C. Robert (2005), Tropical Pacific ocean model error covariances from Monte-Carlo simulations, WMO International Symposium on Assimilation of Observations in Meteorology and Oceanography $N^0$4, Prague, Czech republic (18/04/2005), 131, 3643-3658.

Bouttier, F. and P. Courtier (1999), Data assimilation concepts and methods, ECMWF training notes.

Canadian Ice Service (http://ice-glaces.ec.gc.ca/)

Carrieres, T. (2000), Canadian Ice Service digital charts database, "History of data and procedures used in the preparation of regional ice charts".

Caya, A., M. Buehner and T. Carrieres (2010), Analysis and forecasting of sea ice conditions with three-dimensional variational data assimilation and a coupled ice-ocean model, Journal of Atmospheric and Oceanic Technology, 27, 353-369.

Cressman, G. P. (1959), An operational objective analysis system, Monthly Weather Review, 87, 367-374.

Cuny, J., P. B. Rhines and R. Kwork (2005), Davis Strait volume, freshwater and heat fluxes, Deep-Sea Research Part I, 52, 519-542.

Curry, R., B. Dickson and I. Yashayaev (2003), A change in the freshwater balance of the Atlantic ocean over the past four decades, Nature, 426, 224-232

Fichefet, T. and M. A. Morales Maqueda (1997), Sensitivity of a global sea ice model to the treatment of ice thermodynamics and dynamics, Journal of Geophysical Research, 102, 12,609-12,646.

Gandin, L.S (1963), Objective analysis for meteorological fields, Jerusalem, Israel, translation 1965.

Goose, H. and T. Fichefet (1999), Importance of ice-ocean interaction for the global ocean circulation: A model study, Journal of Geophysical Research, 104, 23,337-23,355.

Griffies, S. M., M. Winton and B. L. Samuels (2004), The Large and Yeager (2004) dataset and CORE, CORE dataset notes.

Hibler III W. D. (1979), A dynamic thermodynamic sea ice model, Journal of Physical Oceanography, 9, 815-846.

Ikeda, M. (1989), A review of sea ice and ocean modeling relevant to the Labrador and Newfoundland shelves, IEEE Transaction on Geoscience and Remote Sensing, 27, 535-540.

Lindsay, R. W and J. Zhang (2005), Assimilation of ice concentration in an ice-ocean model, Journal of Atmospheric and Oceanic Technology, 23, 742-749.

Lisaeter, K. A., J. Rosanova and G. Evensen (2003), Assimilation of ice concentration in a coupled ice-ocean model, using the Ensemble Kalman filter, Ocean Dynamics, 53, 368-388.

Madec, G., P. Delecluse, M. Imbard and C. Levy (1998) OPA 8.1 Ocean General Circulation Model reference manual.

Mertz, G., S. Narayanan and J. Helbig (1993), The freshwater transport of the Labrador current, Atmosphere-Ocean, CMOS publications, 31, 310205.

Myers, P. G. (2005), Impact of freshwater from the Canadian Arctic Archipelago on Labrador Sea water formation, Geophysical Research Letters, 32, L06605, doi:10.1029/2004GL022082.

Mysak, L. A, D. K. Manak and R. F. Marsden (1990), Sea-ice anomalies observed in the Greenland and Labrador Seas during 1901-1984 and their relation to an interdecadal Arctic climate cycle, Climate Dynamics, 5, 111-133.

Semtner A. J. (1976), A model for the thermodynamics growth of sea ice in numerical investigation for climate, Journal of Physical Oceanography, 6, 379-389.

Thompson, K. R., D. G. Wright, Y. Lu and E. Demirov (2006), A simple method for reducing seasonal bias and drift in eddy resolving ocean models, Ocean Modelling, 13, 109-125.

Timmermann, R., H. Goose, G. Madec, T. Fichefet, C. Ethe and V. Duliere (2005), On the representation of high latitude processes in the ORCA-LIM global coupled sea ice-ocean model, Ocean Modelling, 8, 175-201.

Visbeck M., Marshall J., T. Haine and M. Spall (1997), Specification of eddy transfer coefficients in coarse resolution ocean circulation models, Journal of Physical Oceanography, 27, 381-401.

Wadhams P. (2000), Ice in the ocean, Amsterdam, Gordon and Breach Science Publishers.

Wright, D. G., K. R. Thompson and Y. Lu (2006), Assimilating long-term hydrography information into an eddy-permitting model of the North Atlantic, Journal of Geophysical Research, 111, C09022, doi:10.1029/2005JC003200.

Zhang J. and W. D Hibler III (1997), On an efficient numerical method for modeling sea ice dynamics, Journal of Geophysical Research, 102, 8691-8702

APPENDIX A (Basic Linear Matrix Algebra)

A matrix is an array of numbers. An **A** *n* x *p* matrix contain *n* rows and *p* columns and its element can be denoted as $a_{i,j}$ for (*i=1:n* and for *j=1:p*), where *i* is the row index and *j* the column index. Specifically this matrix can be expressed as:

$$\boldsymbol{A} = \begin{bmatrix} a_{11} & a_{12} & \cdots & a_{1p} \\ \vdots & & \ddots & \vdots \\ a_{n1} & a_{n2} & \cdots & a_{np} \end{bmatrix}$$

-**Square matrix**: A matrix is called squared when the number of its rows is equal to the number of its columns.

-**Diagonal matrix**: A matrix is diagonal when all its non diagonal elements are equal to zero ($a_{i,j}=0,\ i\neq j$) and at least one of the diagonal elements is non zero. A diagonal matrix with all his diagonal elements equals to 1 is called the identity matrix **I**.

-**Size and equality:** Two matrices are the same size if they have the same number of columns and rows (same dimensions). Two matrices **A** and **B** are equal when they are same size and all their elements are equal ($a_{i,j}=b_{i,j}$ for every *i,j).*

-**Transpose**: A transpose of a *n* x *p* **A** matrix is a *p* x *n* matrix denoted as $\mathbf{A}^T$, whose every $a_{i,j}$ element is equal to the $a_{j,i}$ element of **A**. A matrix is characterized as symmetric if **A**= $\mathbf{A}^T$. From this one can understand that diagonal matrices are symmetric matrixes.

-**Summation:** The summation of two same size matrices **A** and **B**, gives a same size matrix **C**=**A**+**B**, with elements $c_{i,j}=a_{i,j}+b_{i,j}$. The addition is commutative i.e. **A**+**B**=**B**+**A**. As a rule: $(\mathbf{A}+\mathbf{B})^T=\mathbf{A}^T+\mathbf{B}^T$.

-**Multiplication**: A *n* x *p* matrix **A** times a scalar *c*, is defined as a same size matrix *c***A** with elements $ca_{i,j}$. Generally $(c\mathbf{A})^T=c\mathbf{A}^T$. Given two matrices **A** and **B**, the matrix multiplication is defined only when the number of the columns of **A** is equal to the number of the rows of **B**. The product between a *n* x *p* matrix **A** and a *p* x *q* matrix **B** is defined as a *n* x *q* matrix **C**=**AB** with elements $c_{i,j}$ given as:

$$c_{i,j} = \sum_{k=1}^{p} a_{i,k}\, b_{k,j}$$

As a rule: $\mathbf{AB} \neq \mathbf{BA}$, $\mathbf{A}(\mathbf{BC}) = (\mathbf{AB})\mathbf{C}$, $\mathbf{A}(\mathbf{B}+\mathbf{C}) = \mathbf{AB}+\mathbf{AC}$ and $(\mathbf{AB})^T = \mathbf{B}^T\mathbf{A}^T$

A special type of matrix multiplication that is called the Kronecker product, can be defined for matrices without size restrictions. For two matrices **A** (*n* x *p*) and **B** (*m* x *q*) the Kronecker product is defined as the *nm* x *pq* matrix:

$$\boldsymbol{A} \otimes \boldsymbol{B} = \begin{pmatrix} a_{11}\boldsymbol{B} & \cdots & a_{1p}\boldsymbol{B} \\ \vdots & \ddots & \vdots \\ a_{n1}\boldsymbol{B} & \cdots & a_{np}\boldsymbol{B} \end{pmatrix}$$

The Kronecker product is not commulative ($\mathbf{A}\otimes\mathbf{B} \neq \mathbf{B}\otimes\mathbf{A}$).

-**Invertible matrix**: A square *n* x *n* matrix **A** is invertible if a matrix *n* x *n* $\mathbf{A}^{-1}$, called inverse, exists by satisfying $\mathbf{A}^{-1}\mathbf{A} = \mathbf{A}\ \mathbf{A}^{-1} = \mathbf{I}$. As a rule: $(\mathbf{AB})^{-1} = \mathbf{B}^{-1}\mathbf{A}^{-1}$, $(\mathbf{A}^T)^{-1} = (\mathbf{A}^{-1})^T$.

-**Determinant** The determinant of an **A** square matrix, with $\mathbf{A}_{ij}$ denoting the sub-matrix obtained from **A** by deleting the i^{th} row and the j^{th} column; is defined as:

$$\det(\boldsymbol{A}) = \sum_{i=1}^{n} (-1)^{i+j} \det(\boldsymbol{A}_{ij})$$

The determinant of a 2 x 2 matrix **A** is simply $a_{11}a_{22}$-$a_{12}a_{21}$. A square matrix with a non-zero determinant is called nonsingular and a square matrix with a zero determinant is called singular.

- **Trace**: The trace of a square matrix is the sum of its diagonal elements and is defined as the scalar:

$$Tr(\boldsymbol{A}) = \sum_{i=1}^{n} a_{ii}$$

As a rule: $\mathrm{Tr}(\mathbf{AB}) = \mathrm{Tr}(\mathbf{BA})$, $\mathrm{Tr}(\mathbf{A}^T) = \mathrm{Tr}(\mathbf{A})$ and $\mathrm{Tr}(\mathbf{B}^{-1}\mathbf{AB}) = \mathrm{Tr}(\mathbf{A})$

-**Eigenvalues, eigenvectors**: For a square matrix **A**, if we have $\mathbf{Ax}=\lambda\mathbf{x}$ for a scalar λ and a non-zero vector **x**, then **x** is an eigenvector of **A** corresponding to the eigenvalue λ. The system $(\mathbf{A}-\lambda\mathbf{I})\mathbf{x}=0$ has a non trivial solution if, and only if, $det(\mathbf{A}-\lambda\mathbf{I})=0$ ($\mathbf{A}-\lambda\mathbf{I}$ is singular).

APPENDIX B (Covariances)

Let us assume that we have an X set, of n data. Then the *mean* of this set of data is:

$$\bar{X} = \frac{1}{n}\sum_{i=1}^{n} X_i$$

And the *standard deviation* of the data set is:

$$\sigma = \sqrt{\frac{\sum_{i=1}^{n}(X_i - \bar{X})^2}{(n-1)}}$$

The standard deviation of a data set is a measure of how spread out the data is. Another measurement of the spread of data and almost identical as the standard deviation is the *Variance* of the data set:

$$var(X) = \sigma^2 = \frac{\sum_{i=1}^{n}(X_i - \bar{X})^2}{(n-1)}$$

Standard deviation and variance operate only in 1-dimension. If we have a data set of 2-dimensions and more, we can only calculate independently the variance and the standard deviation of each dimension. In order to be able to see how much two dimensions (or two variables) change together we have to introduce another term, the covariance, which is measured between two dimensions (two variables). The variance is actually a special case of covariance where we find the covariance of a variable with itself. The formula for the *covariance* is:

$$cov(X,Y) = \frac{\sum_{i=1}^{n}(X_i - \bar{X})(Y_i - \bar{Y})}{(n-1)}$$

We can understand from the above formula that *cov(X,Y)=cov(Y,X)*. In a multidimensional system, a practical way to gather the covariances between each dimension is to put them all in a square matrix, the so called covariance matrix. If a vector has *n* dimensions (variables) then the covariance matrix will be an *n* x *n*

matrix, where its diagonal contains variances of each variable of the vector and its off-diagonal contains cross-covariances between each pair of variables of the vector. To make it more clear let us assume a 3-dimensional data set X of dimensions x, y and z (X(x,y,z)). The covariance matrix is illustrated as:

$$\boldsymbol{C} = \begin{bmatrix} cov(x,x) = var(x) & cov(x,y) & cov(x,z) \\ cov(y,x) & cov(y,y) = var(y) & cov(y,z) \\ cov(z,x) & cov(z,y) & cov(z,z) = var(z) \end{bmatrix}$$

The matrix is symmetrical about the main diagonal. The above lead us to the general definition of the covariance matrix of an X data set (where we have already subtracted the mean) as:

$$\boldsymbol{C} = \frac{1}{n-1} X^T X$$

The correlation coefficient between two random variables is very similar to the covariance. Its formula is:

$$\rho(x,y) = \frac{cov(x,y)}{\sqrt{\sigma(x)\sigma(y)}}$$

APPENDIX C (Model Further Details)

Tensorial formalism:

Let (*i,j,k*) be a set of orthogonal curvilinear coordinates on the sphere associated with the orthogonal set of vectors (***i,j,k***) defined in section 2.1.1 and in which the primitive equations of the model are represented. Then let us define (λ,φ,z) as the geographical coordinate system where $\lambda(i,j)$ is the longitude, $\varphi(i,j)$ is the latitude and $z(k)$ the altitude above the reference sea level. The distance from the center of the earth is represented as $a+z(k)$,where a represent the earth radius, but since we use thin layer approximation we can assume that $a+z(k)\approx a$. The transformation of the curvilinear coordinate system is given by the following scale factors (OPA 8.1 Reference manual, NEMO ocean engine):

$$e_1 = a\sqrt{\left(\frac{\partial\lambda}{\partial i}cos\varphi\right)^2 + \left(\frac{\partial\varphi}{\partial i}\right)^2}$$

$$e_2 = a\sqrt{\left(\frac{\partial\lambda}{\partial j}cos\varphi\right)^2 + \left(\frac{\partial\varphi}{\partial j}\right)^2}$$

$$e_3 = \frac{\partial z}{\partial k}$$

By using the above the primitive equations (2.1.1-2.1.6) can be rewrite in the tensorial form (OPA 8.1 Reference manual, NEMO ocean engine):

Momentum equation:

$$\frac{\partial u}{\partial t} = (\zeta + f)v - \frac{1}{e_3}w\frac{\partial u}{\partial k} - \frac{1}{2e_1}\frac{\partial}{\partial i}(u^2 + v^2) - \frac{1}{\rho_o e_1}\frac{\partial p_h}{\partial i} - \frac{1}{\rho_o e_1}\frac{\partial p_s}{\partial i} + D_u^U$$

$$\frac{\partial v}{\partial t} = -(\zeta + f)u - \frac{1}{e_3}w\frac{\partial v}{\partial k} - \frac{1}{2e_2}\frac{\partial}{\partial j}(u^2 + v^2) - \frac{1}{\rho_o e_2}\frac{\partial p_h}{\partial j} - \frac{1}{\rho_o e_2}\frac{\partial p_s}{\partial j} + D_v^U$$

Where $\zeta = \frac{1}{e_1 e_2}\left[\frac{\partial}{\partial i}(e_2 v) - \frac{\partial}{\partial j}(e_1 u)\right]$

And $\frac{1}{\rho_o e_1}\frac{\partial p_s}{\partial i} = \overline{M_u} + \frac{1}{He_2}\frac{\partial}{\partial j}\left(\frac{\partial \psi}{\partial t}\right)$, $\frac{1}{\rho_o e_2}\frac{\partial p_s}{\partial j} = \overline{M_v} + \frac{1}{He_1}\frac{\partial}{\partial i}\left(\frac{\partial \psi}{\partial t}\right)$ with

$$\frac{\partial}{\partial i}(e_2\overline{M_v}) - \frac{\partial}{\partial j}(e_1\overline{M_u}) = \frac{\partial}{\partial i}\left[\frac{e_2}{He_1}\frac{\partial}{\partial i}\left(\frac{\partial \psi}{\partial t}\right)\right] + \frac{\partial}{\partial j}\left[\frac{e_1}{He_2}\frac{\partial}{\partial j}\left(\frac{\partial \psi}{\partial t}\right)\right]$$

Vertical velocity and hydrostatic pressure:

$$\frac{\partial w}{\partial k} = -\chi e_3$$

$$\frac{\partial p_h}{\partial k} = -\rho g e_3$$

Where $\chi = \frac{1}{e_1 e_2}\left[\frac{\partial}{\partial i}(e_2 u) - \frac{\partial}{\partial j}(e_1 v)\right]$

Tracer equations:

$$\frac{\partial T}{\partial t} = -\frac{1}{e_1 e_2}\left[\frac{\partial (e_2 T u)}{\partial i} + \frac{\partial (e_1 T v)}{\partial j}\right] - \frac{1}{e_3}\frac{\partial (T w)}{\partial k} + D^T$$

$$\frac{\partial S}{\partial t} = -\frac{1}{e_1 e_2}\left[\frac{\partial (e_2 S u)}{\partial i} + \frac{\partial (e_1 S v)}{\partial j}\right] - \frac{1}{e_3}\frac{\partial (S w)}{\partial k} + D^S$$

$$\rho = \rho(T, S, z(k))$$

M*(M_u,M_v)* denotes the collected contributions of the non-linear, viscous, and hydrostatic pressure gradient terms with the overbar indicating the vertical average over the whole water column, from *z=-H to z=0*. Ψ represents the volume transport streamfunction, ζ the relative vorticity, χ represents the divergence of the horizontal velocity field and p_s the surface pressure ($p=p_s+p_h$).

Discretization and Numerical Methods (OPA model):

The C grid that the ocean model uses is presented in Figure C.1. At each grid cell center the scalar variables are defined (*T,S,p,etc...*). The vector variables (*u,v,w*) are defined at the center of each face of the grid cells. The time differencing schemes that are used, are the following:

- Leapfrog scheme with the use of Robert-Asselin time filter, for non-diffusive processes.
- Forward time differencing scheme for horizontal diffusive processes.
- Backward time differencing scheme for vertical diffusive processes.

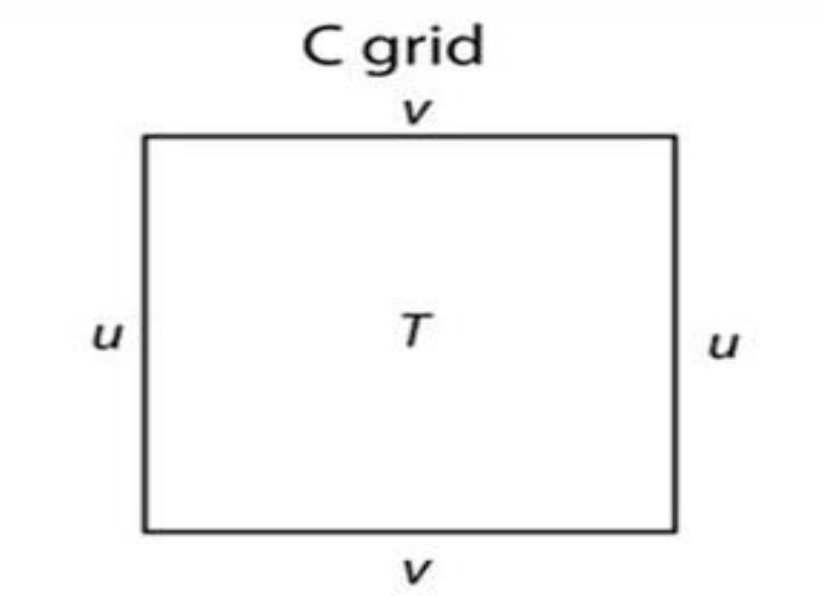

Figure C.1: Arrangement of variables in a C-grid

Discretization and Numerical Methods (LIM model):

The B-grid that the sea ice model uses is presented in Figure C.2. In each grid cell center the scalar variables are defined (*T*,*A*,*h*,etc…). The vector variables (velocities) are defined at the corners of each grid cell. The equations are solved by using the following difference techniques:

- The heat diffusion equation (eq. 2.2.1) is solved using a fully implicit numerical scheme.
- The fluxes balance equation (eq. 2.2.2) is solved using a Newton-Rapshon method.

- The ice momentum balance (eq.2.2.6) is treated following the approach of Hibler, 1979 with the two main differences being that the oceanic drag term is not linearized and a simultaneous underrelaxation technique is applied.
- The advective term of the continuity equation (eq 2.2.9) is computed using the forward time marching scheme of Prather, 1986.

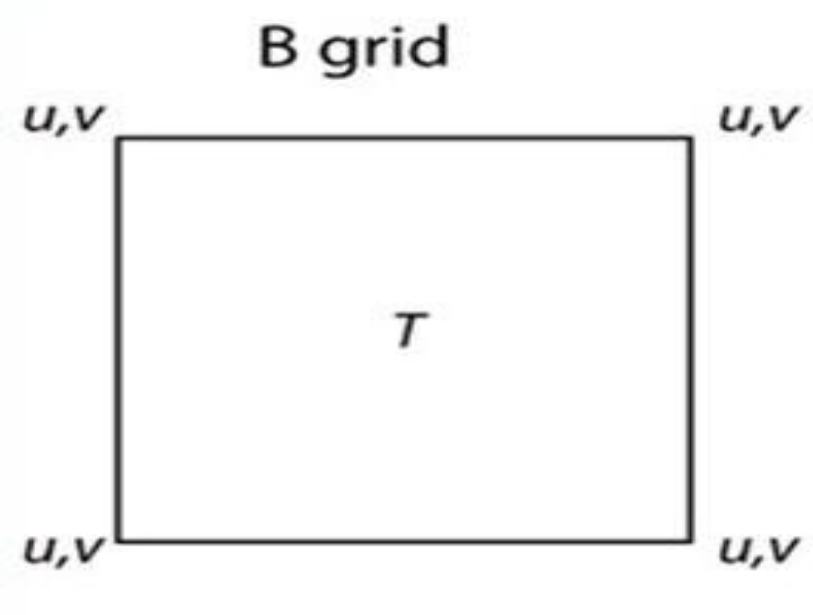

Figure C.2: Arrangement of variables in a B-grid

APENDIX D (Empirical Orthogonal Functions)

The Empirical Orthogonal Functions method (EOFs), also called the Principal Component Analysis method (PCA), is a method that transforms a large set of variables, possible correlated with each other, into a set of smaller number of variables, uncorrelated with each other. This is achieved by decomposing the set of data into orthogonal basic functions. Essentially, the EOFs method is a way to break the spatial variability in a time evolving field into patterns (modes of variability) and time series correspond to each pattern, which shows how each pattern evolves in time. These patterns are often called EOFs and their time evolutions are presented by the so called expansion coefficients. The way of performing the EOF method is presented below (H. Bjornsson & S. A. Venegas):

Assuming we have an F data set in which the time mean has already been removed, we first form the covariance matrix C as

$$C = F^T F$$

Then we solve the eigenvalue problem

$$CE = E\Lambda$$

Λ is a diagonal matrix containing the eigenvalues λ_i of the covariance matrix C and E is a matrix which contains the column vectors $\boldsymbol{e_i}$ which represent the eigenvectors that correspond to each eigenvalue. These eigenvectors are our EOFs. The eigenvalues show the fraction of the total variance explained by each EOF, thus the EOFs are ordered based on the size of their corresponding eigenvalue. For example, the EOF_1 which correspond to the highest eigenvalue accounts for the largest variability etc. The EOFs, since they are uncorrelated to each other, they are uncorrelated over space. In order to find how each EOF is evolving in time, we can calculate the expansion coefficient that corresponds to each EOF as the projection of the data set matrix F onto each EOF:

$$\boldsymbol{a}_i = F \otimes EOF_i$$